IMAGING THE UPPER MANTLE BENEATH TURKEY AND SURROUNDING REGIONS

by

Ahu Kömeç Mutlu

B.Sc., Geophysical Engineering, İstanbul University, 2000
M.Sc., Geophysical Engineering, Boğaziçi University, 2005

Submitted to the Kandilli Observatory and
Earthquake Research Institute in partial fulfillment of
the requirements for the degree of
Doctor of Philosophy

Graduate Program in Geophysics Department
Boğaziçi University
2012

IMAGING THE UPPER MANTLE BENEATH TURKEY AND SURROUNDING REGIONS

APPROVED BY:

Prof. Dr. Hayrullah Karabulut ....
(Thesis Supervisor)

Prof. Dr. Niyazi Türkelli ....

Assoc. Prof. Dr. Nurcan Meral Özel …........................

Assist. Prof. Ali Özgün Konca ....

Prof. Dr. Argun Kocaoğlu ....
(İ.T.U.)

DATE OF APPROVAL: 16.02.2012

To my father İlker Kömeç,

ACKNOWLEDGEMENTS

I would like to express my appreciation to my academic advisor Prof. Hayrullah Karabulut for his guidance and encouragement. I am grateful to him for his endless support and patience during my PhD study. It is always pleasure to be one of his students and work with him.

Thanks to the Kandilli Observatory and Earthquake Research Institute, National Earthquake Monitoring Center (KOERI-NEMC), International Seismological Centre (ISC), European–Mediterranean Seismological Centre (EMSC), Incorporated Research Institutions for Seismology (IRIS) and GEOFON Seismic Network for providing earthquake catalog and seismic data. I would like to thank the Department of Geophysics for providing environment for education and research.

Thanks also to Dr. Anne Paul from the Institute des Sciences de la Terre (France) for providing the SIMBAAD data (funded by ANR France, contract 06-BLAN-0317). She also provided guidance on shear wave splitting analysis. I would like to thank Dr. Andreas Wüstefeld for his MATLAB interface, which facilitates the processing of shear wave splitting observations. I would like to thank Prof. Thomas M. Hearn for providing P_n tomography code.

I would like to thank Esen Arpat for discussions on the geology and tectonic of the study area. Thanks to Assoc. Prof. Serdar Özalaybey for his guidance and comments on shear wave splitting analysis. I would like to thank my colleague and my friend Dr. Musavver Didem Cambaz for her support.

I would like to thank to my spouse Bülent Kemal Mutlu. He turned my dreadful times to feast with his limitless tolerance and patience. I would like to thank to my sons Kuzey and Çınar. I was discharged at the end of a wearing day by spending time with them. I would like to thank to my mother Asuman Kömeç, my sister Didem Kubat and to my huge family for supporting me with full faith and credit during my life time.

ABSTRACT

IMAGING THE UPPER MANTLE BENEATH TURKEY AND SURROUNDING REGIONS

This study includes two interdependent sections. The first section presents an analysis of P_n travel times to determine P_n velocity, P_n anisotropy and crustal thickness variations beneath Turkey and surroundings. Between 1999 and 2010, more than 50 000 P_n arrivals are compiled from 700 regional earthquakes by 832 stations of permanent and temporary networks operated in the study area. A regularized least squares inversion method is used to estimate crustal thickness variations and image velocity perturbations in the uppermost mantle. The results reveal features that correlate well with the surface geology and the active tectonics of the region.

The P_n velocities show very fast (> 8.4 km s^{-1}) and very slow (< 7.6 km s^{-1}) anomalies indicating a heterogeneous lithospheric structure. The average velocity of 8.0 km s^{-1} is determined from a linear fit to P_n travel times. Relatively uniform P_n velocities (7.9-8.1 km s^{-1}) are observed in the Western Turkey. Large velocity contrasts are located at subduction and suture zones. A sharp transition in the central Anatolia is apparent from the uniform P_n velocities in the west to lowest velocities (< 7.6 km s^{-1}) in the east. The lowest velocities coincide with the volcanics of the easternmost Anatolia and the Central Anatolian Volcanic Zone. Beneath the Dead Sea Fault Zone and Dinarides-Hellenides, the upper mantle velocities are also low (< 7.8 km s^{-1}). High P_n velocities are observed beneath oceanic lithosphere such as Mediterranean Basin (> 8.3 km s^{-1}), western Black Sea basin (> 8.3 km s^{-1}), Adriatic Sea (> 8.3 km s^{-1}), and Zagros suture zone (> 8.3 km s^{-1}). Large velocity contrasts are observed at subduction, suture zones and across the North Anatolian Fault.

P_n anisotropy has maximum amplitude of ± 0.8 km s^{-1} in the study area corresponding to 10 per cent anisotropy. The coherent and largest anisotropic anomalies are observed in the western Anatolia, Aegean Sea, and Cyprian Arc. A significant anisotropic pattern is observed in the Cyprian Arc region. P_n anisotropy in western Anatolia, Aegean Sea and Greece correlate well with the present state of tectonic deformation and GPS velocities. The Dinarides-Hellenides exhibit arc-parallel anisotropy. In Western Anatolia, anisotropy is aligned in N-S direction along the major principal strain orientation. Along the North Anatolian Fault, the anisotropy directions are E-W, aligned with the fault geometry in the western part while no correlation is observed on the central and eastern parts of the fault. Anisotropy in Eastern Anatolia is complex and the directions are varying strongly in the region of low P_n velocities. The absence of anisotropy is apparent in an area dominated by the neogene volcanism. Low P_n velocities and absence of clear anisotropic pattern beneath Eastern Anatolia may have resulted from thermal anomalies in the uppermost mantle possibly due to delamination processes.

Large positive station delays are observed along the southern coast of Anatolia, Eastern Anatolia and beneath Dinarides-Hellenides while large negative station delays are observed in Western Anatolia and the Marmara Region. The majority of the stations in Central Anatolia show small station residuals indicating the average crustal thickness of 35±2 km. Western Anatolia and the Aegean Sea have crustal thicknesses between 28±2 and 33±2 km. In Greece, the crustal thicknesses are increasing from 33±3 km from the western coast to a maximum of 48±3 km beneath Dinarides-Hellenides. The large crustal thicknesses (40-48 km) are also observed along southern coast of Anatolia. In eastern and Southern Anatolia the average crustal thicknesses are 40 km and 36 km, respectively.

In the second section of this study, shear wave splitting on records of core-refracted (SKS) phases are obtained. Waveform data from 850 teleseismic earthquakes occurred between 1999-2010 at epicentral distances between 84° and 130° with magnitudes greater than 6.0 are analyzed. A total number of 4163 splitting measurements are obtained from 217 broadband seismic stations located in and around Turkey.

The anisotropy parameters measured from SKS are consistent with the results of similar studies conducted in North-Central Anatolia, Eastern Anatolia and Aegean. Fast direction polarizations are dominantly in NE-SW direction in the Eastern Anatolia. In the Marmara Region, fast polarization directions are in NNE-SSW direction with greater lag times. There is a relatively sharp change in the fast polarization directions form NE-SW to

NW-SE at the Antalya Bay, Isparta Angle Region (~30°E). SKS measurements are non-uniform in Central and Northern Greece. There are progressive changes in the fast splitting directions as well as delay times from Eastern Turkey to the Aegean. The change in the fast splitting directions from NNE-SSW in the eastern Anatolia to N-S in the Aegean may be the result of the retreat of the Hellenic slab. Through the North Anatolian Fault, shear wave splitting directions are aligned NE-SW.

ÖZET

TÜRKİYE VE ÇEVRESİ ÜST MANTO YAPISININ GÖRÜNTÜLENMESİ

Bu çalışma iki ayrı bölümden oluşmaktadır. İlk bölümde P_n hızlarını, P_n yön bağımlılığını ve kabuk kalınlığı değişimlerini elde etmek için P_n varış zamanlarının analizi yapılmıştır. Çalışma bölgesi Türkiye ve çevresi olarak seçilmiştir. Bu bölgede 1999-2010 yılları arasında meydana gelmiş 700 adet depremden elde edilen 50 000 den fazla P_n varışı, analizlerde kullanılmıştır. Bunun için bölgede bulunan farklı ağlara ait sabit ve geçici 832 adet istasyona ait verilerden yararlanılmıştır. Üst mantodaki hız dağılımını ve kabuk kalınlığını belirlemek için, en küçük kareler ters çözüm yöntemi kullanılmıştır. Sonuçlar bölge jeolojisi ve aktif tektoniği uyumluluklar göstermektedir.

P_n hızları, tekdüze olmayan bir litosfer yapısını işaret eden çok yüksek (> 8.4 km s^{-1}) ve çok düşük (< 7.6 km s^{-1}) anomaliler göstermiştir. P_n varış zamanlarından en küçük kareler yöntemi ile elde edilen ortalama P_n hızı 8.0 km s^{-1} dir. Türkiye'nin batısında homojen P_n hızları (7.9-8.1 km s^{-1}) ölçülmüştür. Dalma-batma ve bindirme bölgelerinde yüksek P_n hız değişimleri saptanmıştır. Batıdaki homojen P_n hızlarından, doğudaki en düşük hızlara (< 7.6 km s^{-1}) doğru Orta Anadolu'da keskin bir geçiş göze çarpmaktadır. En düşük hızlar Doğu Anadolu ve Orta Anadolu volkanizması ile uyumluluk göstermektedir. Ölü Deniz Fay hattı ve Dinarit-Helenik zonu altında üst manto hızları düşüktür (< 7.8 km s^{-1}). P_n hızları Akdeniz (> 8.3 km s^{-1}), Karadeniz'in batısı (> 8.3 km s^{-1}), Adriyatik Denizi (> 8.3 km s^{-1}) ve Zagros bindirme hattı (> 8.3 km s^{-1}) gibi okyanusal litosfer altında yüksektir. Dalma-batma, bindirme bölgelerinde ve Kuzey Anadolu Fay Hattı boyunca yüksek hız farklılıkları gözlenmiştir.

Çalışılan bölgede en yüksek P_n yön bağımlılık değeri ±0.8 km s^{-1} dir ve yüzde 10 yön bağımlılığa karşılık gelmektedir. En büyük ve tutarlı yön bağımlılık farklılıkları Batı Anadolu, Ege Denizi ve Kıbrıs Yayı'nda ölçülmüştür. Batı Anadolu, Ege Denizi ve

Yunanistan'daki P_n yön bağımlılığı, GPS hızları ile elde edilen lithosferik deformasyonlar ile uyumludur. Dinarit-Helenik zonunda yaya paralel yön bağımlılık görülmektedir. Batı Anadolu'da yön bağımlılık, en büyük gerilme doğrultusu boyunca K-G yönelimlidir. Kuzey Anadolu Fay Hattı boyunca yön bağımlılık fayın batısında fay geometrisiyle uyumlu ve D-B uzanımlıdır. Fayın orta bölümünde ve doğusunda fay geometrisi ile yön bağımlılık arasında uyumluluk gözlenmemiştir. Doğu Anadolu'da yön bağımlılık karmaşıktır ve yönler düşük P_n hızlı bölgelerde ani değişimler göstermektedir. Doğu Anadolu'nun altında ki P_n hızları ve yön bağımlılık gözlenmemesi, üst mantoda meydana gelen sıcaklık değişimlerinden kaynaklanıyor olabilir.

Anadolu'nun güney sınırı, Doğu Anadolu ve Dinarit-Helenik zonu boyunca büyük pozitif istasyon gecikmeleri, Batı Anadolu ve Marmara Bölgesi'nde büyük negatif istasyon gecikmeleri elde edilmiştir. Orta Anadolu'daki istasyonların büyük çoğunluğu 35±2 km ortalama kabuk kalınlığına işaret eden küçük istasyon gecikmeleri göstermektedir. Batı Anadolu ve Ege Denizi'nde kabuk kalınlıkları 28±2 ve 33±2 km arasında değişmektedir. Yunanistan'da, kabuk kalınlıkları batı sınırında 33±3 km'den Dinarit-Helenik zonu altında 48±3 km'ye ulaşır. Güney Anadolu'da yüksek kabuk kalınlıkları (40-48 km) elde edilmiştir. Doğu ve Güneydoğu Anadolu'da ortalama kabuk kalınlıkları sırasıyla 40 km ve 36 km'dir.

Çalışmanın ikinci bölümünde, çekirdekten kırılan fazlar (SKS) kullanılarak kesme dalgası ayrımlanması elde edilmiştir. Sayısal veri için 1999-2010 yılları arasında meydana gelen 850 adet uzak deprem kullanılmıştır. Büyüklükleri 6.0 ve üstü olan bu depremlerin istasyonlara olan uzaklıkları uzaklıkları 84° ve 130° den arasındadır. Türkiye ve çevresinde bulunan 217 adet geniş bantlı sismometre kullanılarak toplamda 4163 tane ayrımlanma ölçümü yapılmıştır.

SKS kullanılarak elde edilen yön bağımlılık parametreleri, Kuzey-Orta Anadolu, Doğu Anadolu ve Ege'de yapılan benzer çalışmaların sonuçları ile uyumluluk göstermiştir. Doğu Anadolu'da hızlı polarlanma yönü KD-GB baskındır. Marmara Bölgesi'nde hızlı polarlanma yönleri daha büyük gecikme zamanlı ve KKD-GB'dir. Antalya Körfezi ve Isparta Açısı Bölgesi'nde (~30°E) hızlı polarlanma yönünde KD-GB'den KB-GD'ye nispeten keskin bir geçiş ölçülmüştür. Orta ve Kuzey Yunanistan'da SKS ölçümleri tutarlı değildir. Doğu Anadolu'dan Ege Bölgesi'ne doğru hem hızlı polarlanma yönlerinde hem de gecikme zamanlarında aşamalı değişimler elde edilmiştir. Hızlı polarlanma yönünde Doğu Anadolu'da gözlenen KKD-GGB doğrultunun Ege'deki K-D'ya değişiminin Helenik dilimin çekmesinin bir sonucu olabileceği düşünğlmektedir. Kuzey Anadolu Fayı boyunca kesme dalgası ayrımlanması yönleri KD-GB uzanımlıdır ve fayın güneyinden kuzeyine değişim göstermemektedir..

TABLE OF CONTENTS

LIST OF FIGURES

LIST OF SYMBOLS

Δ_{es}	Horizontal distance between source and receiver
C_{ijkl}	Stiffness
ε_{ij}	Strain tensor
τ_e	Event time term
τ_{es}	Travel time between station and event
τ_s	Station time term
V	P or S wave velocity
σ_{ij}	Stress tensor
δt	Delay time
θ	Incidence angle
φ	Fast polarization direction

LIST OF ACRONYMS/ABBREVIATIONS

Ab	Antalya Basin
APM	Absolute Plate Motion
AsS	Assyrian Suture
A-T	Anatolide-Tauride Block
BZS	Bitlis-Zagros Suture
CAVZ	Central Anatolia Volcanic Zone
CMB	Core Mantle Boundary
CNAFZ	Central North Anatolian Fault Zone
DSF	Dead Sea Fault
EAF	East Anatolian Fault
EAP	Eastern Anatolia Plateau
EBsB	Eastern Black Sea Basin
EMSC	European-Mediterranean Seismological Centre
ETSE	Eastern Turkey Seismic Experiment
GPS	Global Positioning System
GSRM	Global Strain Rate Map
IA	Isparta Angle
IAES	Izmir-Ankara-Erzincan Suture
IRIS	Incorporated Research Institutions for Seismology
ISC	International Seismological Centre
IZ	Istanbul Zone
KOERI	Kandilli Observatory and Earthquake Research Institute
LN	Lycian Nappes
LPO	Lattice Preferred Orientation
LVZ	Low Velocity Zone
MM	Menderes Massif
NAF	North Anatolian Fault
NEIC	National Earthquake Information Centre
ORFEUS	Observatories and Research Facilities for European Seismology

PPF	Paphos Transform Fault
PREM	The Preliminary Reference Earth Model
PT	Pontides
qP	Quasi-P Wave
qSH,qSV	Quasi-S Waves
RC	Rotation-Correlation Technique
RS	Rhodope-Strandja Basin; SulF, Sultandağ Fault
SC	Minimum Energy Technique
SIMBAAD	Seismic Imaging Beneath Aegean-Anatolia Domain
SPO	Shape Preferred Orientation
SZ	Sakarya Zone
ThB	Thrace Basin
WASRE	Western Anatolia Seismic Recording Experiment
WBsB	Western Black Sea Basin
WNAFZ	Western North Anatolian Fault Zone

1. INTRODUCTION

1.1. Outline

To better understand the geodynamic behavior of the lithosphere, it is important to know composition and thermal state of the Earth's mantle. Seismic velocities have been used for decades to determine the physical parameters of mantle and how they are affected by the mantle composition. In this work P_n velocity variations are used to study the uppermost mantle and infer the state of the lithosphere beneath Turkey and adjacent regions. In order to fully characterize the influence of upper mantle on the active tectonic, shear wave splitting measurements which provide reliable measurements on anisotropy of the upper mantle are also investigated. Two observations provide more complete view of the upper mantle.

In this work seismic data from various networks between 1999 and 2010 are used for the analysis. More than 50 000 P_n arrivals from 700 earthquakes and 832 stations and 4163 shear wave splitting measurements from 217 seismic stations are obtained. P_n velocity and crustal thickness variations, anisotropy of upper mantle are determined from P_n travel times and SKS observations.

The geology and tectonic settings of Turkey and surrounding regions are presented in Section 1.2. Section 1.3 summarizes the previous studies on P_n velocity variations, P_n anisotropy and shear wave splitting measurements in the region. A general review of mineralogy, composition and structure of Earth’s mantle are presented in Section 1.4. In Section 1.5 the origin and types of anisotropy are presented and how anisotropy varies with depth, temperature and pressure is discussed.

Chapter 2 provides analysis and discussions on the tomographic P_n velocity and P_n anisotropy structure beneath Turkey and surrounding regions. The fundamentals of P_n travel time tomography used in this study are introduced in Section 2.2. The data and processing are presented in Section 2.3, the resolution and error analyses are discussed in Section 2.4. Inversion results are discussed in Section 2.5 with discussions in Section 2.6.

Shear wave splitting method is presented in Chapter 3 with brief introduction and methodologies to analyze shear wave splitting observations. The details of the computation and data processing with the obtained results are also provided in Chapter 3.

The conclusions are presented in Chapter 4.

1.2. Geology and Tectonic Settings

Turkey is an east-west trending segment of the Alpine-Himalayan orogenic belt and can be thought of as a collage of different pieces of ancient continental and oceanic basins named as Tethys Ocean stuck together by younger igneous, volcanic and sedimentary rocks (Şengör *et al.*, 1981; Göncüoğlu *et al.*, 2000; Okay, 2008). The geometry and evolution of the Tethys Ocean is still in debate. On the other hand there is a consensus regarding the presence of two mechanisms called Paleotethys and Neotethys located on the south and on the north respectively both rifted from Gondwana margin (Stampfli, 2000). Two major E-W trending ophiolite belts were stated with the closure of Neotethys and while southern branch of it parted Arabian Platform in the south from Anatolide-Tauride Platform in the north, the northern branch was located between the Anatolide-Tauride Platform and Sakarya continent in the north (Okay, 2008) (Figure 1).

During Early Miocene – Late Oligocene in Central East, Bitlis-Pontid suture zone occurred as a result of Arabian-Eurasian collision (Faccenna *et al.*, 2006). This collision leads to formation of 2 km high plateau in the eastern Anatolia (Keskin, 2003). The northward motion of Arabia gave rise to the westward escape of the Anatolian block with the effect of the uplift of the Turkish-Iranian plateau. There are longitudinal mountain ranges extending along Black Sea and Mediterranean shores in the Northern and Southern Turkey. High Anatolian plateau is located between these mountains. North Anatolian Fault Zone (NAFZ), which is a right-lateral fault zone, lies in the Northern Turkey as one of the major neotectonic structures that form the northern boundary of the Anatolia-Eurosia plates. NAFZ runs for about 1500 km from Eastern Anatolia and splits branches in the Aegean Sea (Barka and Kadinsky-Cade, 1988; Şengör *et al.*, 2005). The tectonic regime along the fault chanhes from east to west; collision zone of Bitlis-Zagros produced by northward movement of Arabian Plate with respect to Eurasia, Aegean extension procured by Hellenic trench rollback (Faccenna *et al.*, 2006). NAF accommodates most of the present day motion of Anatolia with respect to Eurasia (Reilinger *et al.*, 1997; McClusky *et al.*, 2000). The East Anatolian Fault (EAF) is a major left lateral strike-slip fault activated during the Late Miocene that extends from the northern end of the Dead Sea Fault (DSF) to the eastern end of the NAF (Arpat and Şaroğlu, 1971).

While the continental collision was active in the east, extension was taking place in the Eastern Mediterranean Region. In the middle to late Miocene (13-10 Ma) (Le Pichon and Angelier, 1981; Jackson, 1994) extension behind Aegean subduction system began and affected in N-S direction (Mckenzie, 1978). Crustal thickening and subsequent extension and magmatism followed the closure and the destruction of the Neotethyan oceans (Taymaz *et al.*, 2007). This rapid extension has thinned the crust from 45-50 km down to 28-32 km (Şengör, 1993; Yılmaz, 1997; Saunders *et al.*, 1998). The major factors on the distribution of deformation in the region have been the Hellenic and Cyprian trenches. Not only westward motion of Turkey with respect to Eurasia but also southeastward motion of the Aegean with respect to Eurasia, governs the large-scale deformation. Overall velocity field of the Anatolian-Aegean block relative to Eurasia accelerates toward the Hellenic Arc as a result of subduction roll-back. The subduction slab from Hellenic to Bitlis lost its continuity to the depths of least several hundred kilometers and was almost totally consumed on the east of Cyprus (Wortel and Spakman, 2000; Piromallo and Morelli, 2003; Faccenna *et al.*, 2006; Biryol *et al.*, 2011). Presently northern Aegean is extending to ~31ºE within the Anatolian plate. In the south, the African oceanic lithosphere subduction beneath Hellenic Arc is retreating. Extension in Aegean dies out in the ~42ºN in Bulgaria and Northern Greece (Al-lazki *et al.*, 2004).

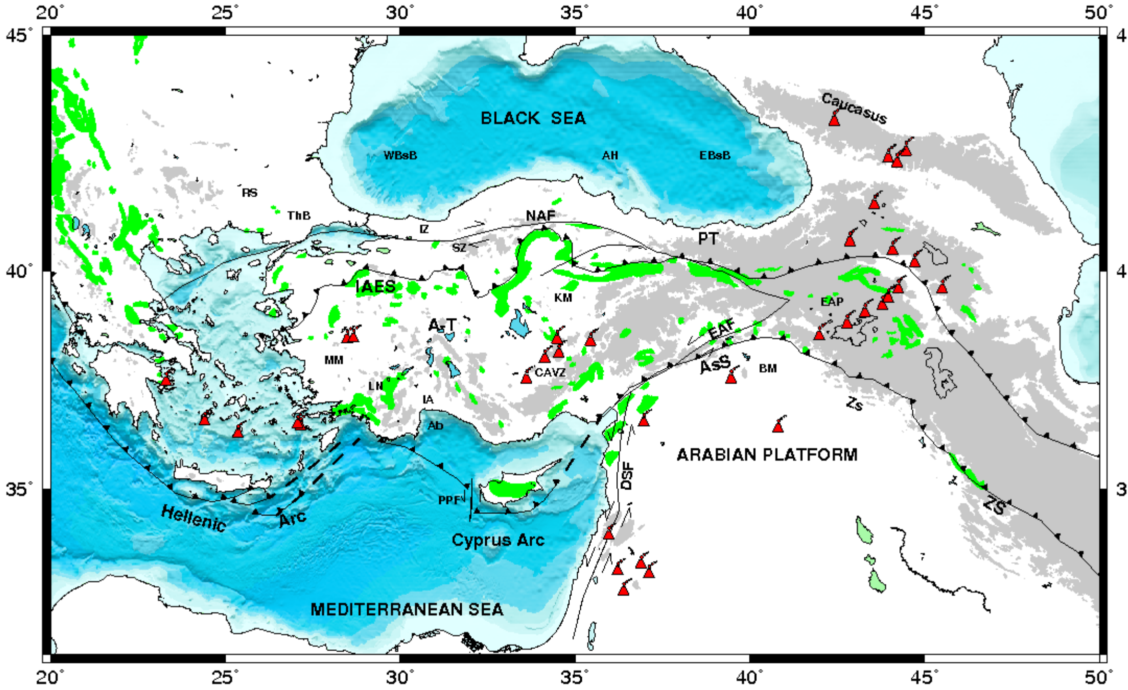

Figure 1.1. Tectonic map of the study area. Ab: Antalya Basin; A-T, Anatolide-Tauride Block; AsS, Assyrian Suture; BZS, Bitlis-Zagros Suture; EAF, East Anatolian Fault; EAP, Eastern Anatolia Plateay; DSF, Dead Sea Fault; IA, Isparta Angle; IAES,Izmir-Ankara-Erzincan Suture; IZ, Istanbul Zone; MM, Menderes Massif; LN, Lycian Nappes; NAF, North Anatolian Fault; PT, Pontides; PPF: Paphos Transform Fault; RS, Rhodope-Strandja Basin; SulF, Sultandağ Fault; SZ, Sakarya Zone; ThB, Thrace Basin; WBsB, Western Black Sea Basin; EBsB, Eastern Black Sea Basin;. Gray shaded area shows topography higher than 1500m. Green and light green units represent the ophiolites and ophiolitic mélanges, respectively. Red volcano signs show neogene and quaternary volcanism. Black triangles show the sutures and subduction zones. Black lines indicate the major faults. Bathymetry and Topography of the region derived from ETOPO5 and GTOPO30 (Okay and Tüysüz, 1999; Wessel and Smith, 1998; Yılmaz *et al*, 1998; Cambaz and Karabulut, 2010)

The western part of the Anatolian Plate is dominated by E-W trending horst and graben structures (Stampfli, 2000). The central Anatolia forms a broad transitional tectonic zone between the extensional tectonic regime of the western Anatolia and the strike slip tectonic regime of the Eastern Anatolia (Koçyiğit *et al.*, 2000). The Central Anatolia is also a continental back-arc of the north dipping Hellenic-Cyprus subduction zone. Most of the geological structures of Central Anatolia and the Taurides, including Isparta Angle, is a result of the tectonic and magmatic events related to this active convergent plate boundary (Glover and Robertson, 1998; Koçyiğit *et al.*, 2000). The region is also characterized by ~13 Ma to recent post-collision related volcanism (Notsu *et al.*, 1995).

1.3. Previous Studies

The first study on the use of P_n velocities is performed by Hearn and Ni (1994) on the Turkish-Iranian Plateau. The aim of their study was to determine the effect of subduction and continental collision on the upper mantle structure beneath the plateau using regional earthquakes. First arrival times were selected for distances between 200 km and 1223 km of the event depth (< 30 km), event size (> 25 arrivals recorded) and residual (< 9 s). After these selections 70 755 P_n first arrivals were used for analysis. They observed P_n velocity variations from 7.6 km s^{-1} to 8.2 km s^{-1}, low P_n velocities (< 7.9 km s^{-1}) beneath most of the Turkish-Iranian Plateau and high P_n velocities (> 8.1 km s^{-1}) beneath Black Sea and southern Caspian Sea. Average P_n velocities (8.0-8.1 km s^{-1}) beneath south western Mediterranean were observed.

A tomographic study by Papazachos *et al.* (1995) revealed strong variations on the velocity and crustal thickness. Permanent stations in south east Europe (16°E-31°E, 34°N-43°N) between the years 1971-1987 were used in the study. From 4229 earthquakes, more than 100 000 P arrivals were used to determine detailed structure of the crust and the upper mantle. They presented P wave velocities for different depth ranges (0-10 km, 10-20 km, 20-30 km, 30-40 km, 40-60 km, 60-90 km, 90-120 km, 120-160 km). P wave velocities beneath northern and southern Aegean vary between 7.5-7.9 km s^{-1} for the depths between 30 km to 40 km. P_n tomography presented by Hearn (1999) beneath the European Region covered part of the Aegean Sea. In their study ISC (International Seismological Centre) data between the years 1960-1987 were used for regional events with first arrivals between 200 km and 1221 km. The study showed lower seismic velocities (7.6-8.1 km s^{-1}) beneath tectonically active mantle of Southern Europe than the more stable mantle of the sub-African Plate of Adriatic Sea (8.3 km s^{-1}). Al-Lazki *et al.* (2004) obtained the variations of P_n velocities and anisotropy at the junction of the Arabian, Eurasian and African plates. For the study, 64 seismic stations were used from different networks. 166 000 P_n first arrivals out of 8944 events were used in the analysis. They observed broad scale (~500 km) low P_n velocity structures (< 8 km s^{-1}) underlying the Anatolian plate. Smaller scale (~200 km) very low P_n anomalies (< 7.8 km s^{-1}) were also observed in Central Turkey and Isparta Angle. The most recent study that images high resolution velocity structure beneath Central Turkey was done by Gans *et al.* (2009). 39 broad band seismic stations were located in the central North Anatolian Fault. They observed very low P_n velocities (< 7.8 km s^{-1}) beneath east of the Central Anatolian Fault Zone and high P_n velocities (> 8.1 km s^{-1}) beneath west of the fault.

Azimuthal variations of P_n velocities have been observed in both oceanic and continental upper mantle. Detection and interpretation of seismic anisotropy is one of the ways to image deformation beneath continents. Direct estimate of seismic anisotropy in the uppermost mantle can be done by P_n anisotropy analysis. On the other hand, tradeoff between anisotropy due to aligned fabric and apparent anisotropy due to seismic velocity heterogeneity is one of the limitations of P_n anisotropy analysis. Hearn (1999) observed very low velocities and arc-parallel anisotropy beneath Mediterranean. Al-lazki *et al.* (2004) presented anisotropy from P_n analysis beneath Anatolian plateau. Orientations within the Anatolian plate and along the NAF vary from E-W in the center to N-S in the western parts. They observed largest anisotropy values in Aegean Sea (~0.6 km s^{-1}) and smaller (~0.2 km s^{-1}) in the Arabian Plate and eastern zone of the Arabian Plate.

Shear wave splitting is the most commonly used method to investigate mantle anisotropy. Hatzfeld *et al.* (2001) studied seismic anisotropy of the upper mantle from SKS splitting measurements from 25 seismic stations located in the Aegean. They observed large delay times and concluded their study by suggesting that the crust and upper mantle deform similarly beneath Aegean. Sandvol *et al.* (2003) performed shear wave splitting analysis for Eastern Turkey. In this study, shear wave fast polarization directions and delay times were computed for young continent-continent collision zone by using data from Eastern Turkey Seismic Experiment (ETSE) broadband experiment. 29 broad band seismic stations across the collision zone of the Arabian, Eurasian and Anatolian plates were used for the computations. They observed that the fast polarization directions are relatively uniform and exhibit primarily NE-SW orientations with average 1.0 second delay times.

Mainly sub-parallel fast polarization directions to the Anatolian, Arabian and Eurasian plates are observed. The more recent study was done by Biryol *et al.* (2010) in order to determine mantle anisotropy along the NAFZ by using the splitting of SKS and SKKS phases. Biryol *et al.* (2010) used array data from 39 seismic stations located that crossed the NAFZ. They interpreted the measurements with a single layer sub-horizontal anisotropic model. This model reveals fairly uniform NE-SW trending anisotropy directions with decreasing delay times from west to east. Evangelidis *et al.* (2011) studied shear wave anisotropy beneath Aegean and focused in the back-arc and near-trench areas of the Hellenic Arc. They used 54 seismic stations for splitting measurements. They observed trench perpendicular fast anisotropy directions in the back-arc area and trench parallel fast directions near the trench. There is no consistency observed between anisotropy and the GPS velocity or strain field in the Southern Aegean.

Studies summarized above are performed for specific geographical areas with datasets at limited durations. In this study 10 years of seismic data collected from temporary and permanent stations were merged to cover a greater area of Turkey and surrounding regions. As a result a higher resolution analysis of P_n velocity, P_n and SKS anisotropy is obtained.

1.4. An Overview of Mantle Structure

Mantle is the most massive and viscous part of the Earth located between Core below and Crust above. Based on the seismological observations during the last century the mantle structure could be resolved into several layers as upper mantle (from Moho at around 7 to 35 km, downward to 410 km depth), transition zone (between 410 km and 660 km depth) and D'' layer (~200 km thickness in average).

With the observations of plate tectonics, the mantle convection theory has been developed in the late 1970s. Mantle convection occurs at the transition zone in a solid-solid phase transformations and the result of the temperature difference between outer core and Earth’s surface. Hot mantle material up-wells and cooling material sinks downward. At the spreading centers warm mantle material up-wells then transfer its heat to the ocean and cools. As a result of this cooling mantle below separates mechanically in two layers. The layer above is called lithosphere with average thickness about 40 km under oceans and 150 km under continents. The layer below that reaches down to approximately 700 km depth is called asthenosphere. When oceanic lithosphere moves away from the ridge, it gets cold, dense and eventually reaches to the unstable gravity. Lithosphere reaches the subduction zone, it descends and sinks back to the mantle.

Observations show that the mantle structure varies with depth with the increase in temperature. The temperature beneath the crust is low (500-900º C) reaches to highest (4000º C) where the heat-producing core contact with the mantle material. The geothermal gradient is the main cause along with the increasing pressure with depth to separate mantle in two main layers as upper mantle and lower mantle. The rocks are cooler and more brittle in the upper mantle and hot and soft in the lower mantle.

The lithosphere is underlain by asthenosphere extending from the base of lithosphere to the 700 km discontinuity. Lithosphere is divided into plates and the plates move on top of the asthenosphere which is a semi-fluid layer with plastic-like materials. Rocks become ductile as a result of interaction between pressure and temperature. Asthenosphere is composed of iron-magnesium silicates while lithospheric materials contain more silica, less aluminum, sodium and potassium. When compared to the lithosphere, asthenosphere has relatively low density and seismic waves travel slowly through the asthenosphere.

The most abundant rock in the continental lithospheric mantle is peridodite. Peridotite, includes magnesium-rich silicates, olivine and orthopyroxene dominantly, and aluminium rich minerals. Peridotites are mainly composed of olivine between 40 per cent and 95 per cent. Secondary abundant rock is xenolith which includes eclogite. Eclogites are deep metamorphosed rocks under basaltic composition with high seismic velocities. The basaltic composition contains pyroxene and garnet dominantly. The mantle rocks shallower than 410 km consist of olivine, garnet, pyroxene. Olivine is orthorhombic and anisotropic mineral which is the combination of magnesium iron silicate. Under high temperature and pressure olivine transforms from α to β spinels. Upper mantle includes 57 per cent of olivine, 17 per cent of orthopyroxene, 12 per cent of clinopyroxene and 14 per cent garnet (Ringwood, 1979). Kimberlites, explosive volcanic rocks, bring mantle material to the surface and give information about mantle. These mantle materials called xenolith which tells about composition, physical structure and temperature of the continental crust.

1.5. An Overview of Anisotropy

Anisotropy can be explained within the context of Hooke's law relating stress and strain through stiffness tensor. The stress is related to internal forces acting on the volume of material which is called body forces. Strain is related to deformation in the volume of material under the effect of external forces, or contact forces. Body forces depend on the volume and density of the medium while contact forces proportional to the surface area of material. External forces deform the medium as they are applied both in shape and size and involve small elastic deformations or strains. Internal forces give response to this deformation which is called stress. Stress tensor "σ_{ij}" is defined as force acting on "i" plane and oriented in "j" direction. Stress at any point can be described with the nine independent parameters of stress tensor.

$$\sigma_{ij} = \begin{bmatrix} \sigma_{11} & \sigma_{12} & \sigma_{13} \\ \sigma_{21} & \sigma_{22} & \sigma_{23} \\ \sigma_{31} & \sigma_{32} & \sigma_{33} \end{bmatrix} \quad \text{with i, j = 1, 2, 3} \qquad (1.1)$$

An elastic body deforms under stress. This deformation is called strain "ε_{ij}" which is dimensionless. Strain tensor written as below,

$$\varepsilon_{ij} = \begin{bmatrix} \varepsilon_{11} & \varepsilon_{12} & \varepsilon_{13} \\ \varepsilon_{21} & \varepsilon_{22} & \varepsilon_{23} \\ \varepsilon_{31} & \varepsilon_{32} & \varepsilon_{33} \end{bmatrix} \quad \text{with i, j = 1, 2, 3} \qquad (1.2)$$

Relationship between applied force resulted with deformation is depicted by Hooke's Law (Love, 1927) which assumes sufficiently small strain and stress.

$$\sigma_{ij} = C_{ijkl}\varepsilon_{kl} \text{ with i, j, k, l = 1, 2, 3} \qquad (1.3)$$

C_{ijkl} is stiffness tensor which describes the elastic properties of the medium. Due to the symmetry considerations ($C_{ijkl} = C_{jikl} = C_{ijlk} = C_{klij}$) Hooke's Law is simplified. This symmetry decreases the number of independent parameters from 81 to 21. The most general form of anisotropy has 21 independent parameters. The number of the independent parameters decreases with the increasing symmetry in the structure. For the orthorhombic medium nine independent constants, for the hexagonal medium five independent constants exist. This hexagonal symmetry anisotropy is known as transverse isotropy. Solids with a special direction are called transversely isotropic which is a common form of anisotropy. Another common form of anisotropy is azimuthal anisotropy. In this form velocities change as a function of horizontal direction and specified by seven independent constants. A preferred orientation of the olivine crystals which is the most abundant mineral in the upper mantle is often thought as the cause of azimuthal anisotropy (Silver, 1996).

Thin layered isotropic materials with different velocities (Backus, 1965), fluid-filled aligned cracks and orientation of anisotropic minerals (LPO) may be the cause of anisotropy. The horizontal layering and aligned cracks and anisotropic mineral orientation in the medium are the cause of anisotropy. Under high strain, olivine fast axis aligns through the strain direction. Strain ellipse axis and olivine crystal orientations are correlated with each other. During the deformation, slow axis of the olivine orients with the short axis of strain, while vice versa is valid. Greater than 20 per cent difference in velocity between fast and slow axis of the olivine mineral may exist (Montagner, 1998).

Mapping the seismically fast direction gives the relationship between plate movement and material flow in depth. Although crystal structure of the olivine is homogeneous, it acts like anisotropic due to its acoustic properties. These properties change with direction according to the crystal lattice, which is called lattice-preferred orientation (LPO). When fast S-wave polarized along the strike of cracks shape preferred orientation (SPO) occurs as a result of fast and slow orientation of seismic wave propagation effect. Different mechanisms at different depths arouse seismic anisotropy.

Orientation of the minerals is affected by high temperature and high pressure. Under constant pressure, anisotropy increases with the increasing temperature although minerals lose their anisotropy with partial melt and deformed olivine crystals cannot be reoriented easily. Partial melt increases the preferred orientation of the mineral which enlarges the grain size. The alignment increases with the bigger grain size which cause increase in anisotropy.

P and S waves propagate in an isotropic medium while quasi-P (qP) and two quasi-S (qSH, qSV) waves propagate in a weakly anisotropic medium. These waves propagate faster through the long axis of cracks than the short axis of cracks. Particle motion of the P and S waves are linear in an isotropic medium, while S wave particle motion is elliptical in an anisotropic medium. Anisotropy is generally expressed as the percentage difference between fastest and slowest oriented velocities;

$$\mathrm{A} = (\mathrm{V}_{max} - \mathrm{V}_{min})/\mathrm{V}_{average} \tag{1.4}$$

V represents either P or S wave velocity. Anisotropy in the crust varies between 1.5 per cent and 4 per cent while it increases to 6-7 per cent along fault zones. It is approximately 4-5 per cent in lithosphere up to 100 km depth and decreases to 0.5 per cent in asthenosphere between 100 and 400 km depth (Marone and Romanowicz, 2007).

Seismic anisotropy can be related to mantle deformation. Relevant movement between mantle and overlying plate in the asthenosphere is the cause of this deformation. It has been indicated from body and surface waves data that anisotropy in the continental lithosphere changes over short length scales (Helffrich *et al.*, 1994; Montagner *et al.*, 2000; Conrad *et al.*, 2007) while anisotropy in the oceanic upper mantle appears to be uniform (*e.g.* Montagner, 2002; Behn *et al.*, 2004).

2. ANISOTROPIC P_n TOMOGRAPHY OF THE UPPERMOST MANTLE

2.1. Introduction

The Earth surface is covered by several rigid plates that move along the surface. The plate motion induces tectonic activities such as mountain building, earthquakes and magmatism mostly at plate boundaries, and the plate interiors are tectonically rather stable. Plate tectonics is a striking feature of the Earth mantle convection. The chemically differentiated mantle makes up to 82 per cent of the volume of the earth and 65 per cent of its mass with major discontinuities at depths of 410 km, 660 km and significant lateral heterogeneities (Chakrabarti *et al.*, 2011).

Constraints on the variation of temperature in the Earth's mantle are critical for our understanding of Earth's convective behavior and mantle flow. A precise estimate of the mantle flow and its relationship with the surface velocity field is a key in order to understand the kinematics and dynamics of continental deformation. The best constraints on temperature in the deeper parts of the mantle obtained from seismic studies, particularly from tomographic studies. Tomographic imaging has been successful in understanding the mechanism of subducting slab, magmatism, and process in the deep structure of the Earth. Since the first global isotropic tomographic models of the mantle were published in 1984 (Woodhouse and Dziewonski, 1984; Dziewonski, 1984), many new tomographic models was developed, and a large number of techniques used for various seismic observations was made available. The tomographic images of the Earth interior completely renewed our vision of upper mantle dynamics, made it possible to relate surface geology and plate tectonics to the mantle convection, and to map the depth of geological objects such as continents, mountain ranges, slabs, ridges, and plumes.

The sensitivity of seismic velocities to mantle composition is investigated by several laboratory studies (Karato and Jung, 1988; Sato *et al.*, 1989; Karato, 1995; Watanabe, 1993; Carlson *et al.*, 2005) as well as observations from different tectonic regimes (Wagner, *et al.*, 2008, Eberhart-Phillips *et al*., 2006; Rossi and Abers, 2006; Zheng and Lay, 2006). Low and high seismic velocity anomalies were reported and interpreted in terms of tectonic processes. These variations mainly result from changes in upper mantle temperature, composition, presence of water and other volatiles. It is generally accepted that olivine rich ultramafic minerals are the main constituents of the upper mantle and the most important representatives of these minerals are peridoties, pyroxenites and eclogites (Babuska and Cara, 1991). The laboratory studies on dry peridodite samples at high pressure and temperature indicate that seismic velocities show a rapid decrease with increasing temperature (Sato *et al*., 1989). Small quantities of water can significantly lower the solidus temperature within the mantle and contribute to the creation of partial melt (Karato, 1995; Karato and Jung, 1988). Such melting is enhanced by the presence of water and carbon dioxide that has percolated into the mantle wedge from the slab beneath (Hearn and Ni, 1994; Karato, 1995). Tectonic activities, *e.g.* subduction, volcanism, rifting, significantly change upper mantle composition, through the changes of temperature and water content as well as the flow of material from asthenosphere. As the low velocities observed in the upper mantle can be attributed to increasing temperature. Both the laboratory and theoretical studies indicate that eclogite can have P wave velocities as large as 8.5 km s^{-1} or greater. However, the amount of eclogite present in the upper mantle is proposed to be less than 1 per cent.

A major change on the structure in the Earth takes place on crust-mantle boundary, which was identified early in 20th century. It was recognized on the earthquake records at regional distances by a Croatian geophysicist, Andrija Mohorovičić. It is one of the most distinct manifestations of Earth, with major changes in petrology, mineralogy, chemistry, seismic wave velocity, density and rheology. The compressional wave velocity increases rapidly and/or discontinuously to a value between 7.6 and 8.6 km s^{-1}. A distinct phase, P_n that is a compressional wave travels through the Moho discontinuity. P_n velocities changes from ocean to continent. It is high in oceanic lithosphere, reaches up to 8.4 km s^{-1} while depends on the rheology of the crust and mantle boundary in continental lithosphere. In the continental lithosphere tectonically stable mantle lid shows higher P_n velocities (> 8.0 km s^{-1}) while very low P_n (< 7.8 km s^{-1}) velocities indicate partial melt in general (Hearn, 1999; Calvert *et al*., 2000). In order to investigate the upper mantle velocity and anisotropic structure at local and regional scales, P_n tomography has been proven to be very useful (Hess 1964; Backus 1965; Hearn and Ni, 1994; Hearn 1996; Hearn 1999).

The uppermost mantle structure beneath the Anatolian-Aegean domain has a complex geological history, having experienced convergence, subduction, collision, slab break-off and extension since Cretaceous time (Hinsbergen *et al*., 2010). The forces driving the deformation are still discussed: basal drag by mantle flow, edge forces (Arabia pull and Hellenic slab pull) or body forces (gravitational potential energy differences) (*e.g.* Jolivet *et al*., 2009). Therefore, it is of great interest to determine the detailed structure of upper mantle of a region which contains the major questions posed by the deformation of continents.

A study was done by Hearn and Ni (1994) in order to determine the subduction and continental collision effects on the upper mantle structure beneath Turkish-Iranian Plateau. They obtained P_n velocities varying between 7.6 km s^{-1} to 8.2 km s^{-1}. Low P_n velocities (< 7.9 km s^{-1}) beneath most of the Turkish-Iranian Plateau, high P_n velocities (> 8.1 km s^{-1}) beneath Black Sea and southern Caspian Sea were observed. Average P_n velocities beneath southwestern Mediterranean were obtained as 8.0-8.1 km s^{-1}. A tomographic study by Papazachos *et al*. (1995) revealed strong velocity variations and crustal thickness beneath Aegean. They presented P velocities for different depth ranges. P velocities beneath northern and southern Aegean vary between 7.5-7.9 km s^{-1} for the depth of 30 km to 40 km. Hearn (1999) computed P_n velocity distribution beneath the European Region and part of the Aegean Sea. Beneath tectonically active mantle of southern Europe, he obtained much lower seismic velocities (7.6-8.1 km s^{-1}) than the more stable mantle of the sub-African plate of Adriatic Sea (8.3 km s^{-1}).

Al-Lazki *et al*. (2004) obtained the variations of the P_n velocities and anisotropy at the junction of Arabian, Eurasian and African plates. They observed a broad scale (~500 km) low P_n velocity structures (< 8.0 km s^{-1}) underlying the Anatolian plate and smaller scale (~200 km) very low P_n anomalies (< 7.8 km s^{-1}) beneath Central Turkey and Isparta Angle. They associated low and very low P_n velocities with active volcanism since Late Miocene beneath Eastern Turkey, Northeastern Iran and the Caucasus. These low velocity zone may be the result of subducted Tethys oceanic lithosphere. The most recent study is done by Gans *et al*. (2009) relatively smaller area and dataset in Central Turkey. The obtained high P_n velocities (> 8.1 km s^{-1}) on the western part of the NAF and very low velocities (< 7.8 km s^{-1}) on the eastern part of the fault.

Other tomographic studies at various scales and resolutions were also computed in region (Karagianni *et al.*, 2005; Pasyanos, 2005; DiLuccio and Pasyanos, 2007; Cambaz and Karabulut, 2010).

P_n phase velocities also changes with direction which can be used to characterize anisotropy. The anisotropy then can be related to the deformation of the lithosphere. Previous studies based on P_n data observed anisotropy in both oceanic and continental crust (Backus, 1965). Most of the anisotropy was observed beneath the upper mantle (Beghoul and Barazangi, 1990).

Sudden anisotropy changes are detected along plate boundaries by Al-Lazki *et al.* (2004) beneath Anatolia. Fast axis of anisotropy predominantly observed east-west in the east, north-south in the center and east-west in the west. There is anisotropy fast axis oriented NE-SW beneath southern part of the DSF and changes to E-W beneath north of the DSF observed. As a result of this study they basically obtained anisotropy orientations along easternmost segment of the NAF zone. These orientations are possibly sampling a large scale asthenospheric anomaly beneath a thin to absent mantle lid.

In this study, an analysis of P_n travel times is presented to determine P_n velocity, P_n anisotropy and crustal thickness variations beneath Turkey and surroundings. The recent improvements on the number and quality of seismic stations in Turkey and surrounding regions have provided high quality seismic data and improved coverage of Anatolian and Aegean domain. Improved data quality and coverage have provided a better potential to obtain finer details beneath the region. The approach in this work is similar to Hearn (1996), Hearn (1999) and Al-lazki *et al.* (2004) but benefits from the improved coverage of stations and data quality. In this work, a total of 700 earthquakes with magnitudes greater than 4.0 which occurred between 1999 and 2010 are selected. The first arrivals between 180 and 1500 km distance range are defined as P_n arrivals. More than arrivals recorded to study P_n velocity and anisotropy beneath the region. For tomographic 50 000 images 832 seismic stations were used. Tomographic inversion of regional P_n travel time residuals used to image lateral variations of seismic velocity within the uppermost mantle of region is determined. Both isotropic and anisotropic velocity distributions and estimated variations of the crustal thickness computed. P_n velocities are found to be highest in the Eastern Mediterranean Sea and Zagros Suture (> 8.3 km s^{-1}) and lowest in Eastern Turkey (< 7.6 km s^{-1}). An anomalous low velocity zone is obtained in central Anatolia.

The tomographic method of Hearn *et al.* (1999) is applied to determine P_n velocities, anisotropy and station delays. Large P_n anisotropy is observed in the Aegean, central Anatolia, along the southern coast of Anatolia. The result of the geodetic measurements and N-S aligned shear wave slitting directions in the extensional regime of Western Anatolia are consistent with the direction of the anisotropy in the Aegean. The station delays are found to be proportional to the crustal thickness. Large crustal thicknesses are observed along the Dinarides-Hellenides and along the southern coast of Anatolia.

A number of checker board tests were used to investigate the resolving power of the tomographic system and Bootstrap method is used to calculate standard deviation of P_n velocities, anisotropy and station delays. The previous P_n travel time tomography and anisotropy results discussed.

2.2. Time Term Method

Time term method has been widely used in the seismic refraction studies. This method is a simple travel-time inversion which was formulated and developed by Scheidegger and Willmore (1957) and Willmore and Bancroft (1960). Reitter (1970) developed time term method completely dependent upon the refraction structure and the angles of dip involved. An expanded form of this method has been used by Hearn (1984) in order to determine lateral velocity variations, delay times and regional anisotropy. By using this method, it is possible to study the effects of a vertical and lateral velocity variations and effect of a dipping interface.

The method assumes that there are three segments of a P_n ray path: the ray path from the source to the mantle, the ray path through the upper mantle, and the ray path from the mantle to the receiver (Figure 2.1). The ray mainly travels below the Moho discontinuity with wave velocity characteristic of the upper mantle. As a consequence, tomographic imaging of P_n travel times yields the lateral distribution of wave velocity in the uppermost mantle.

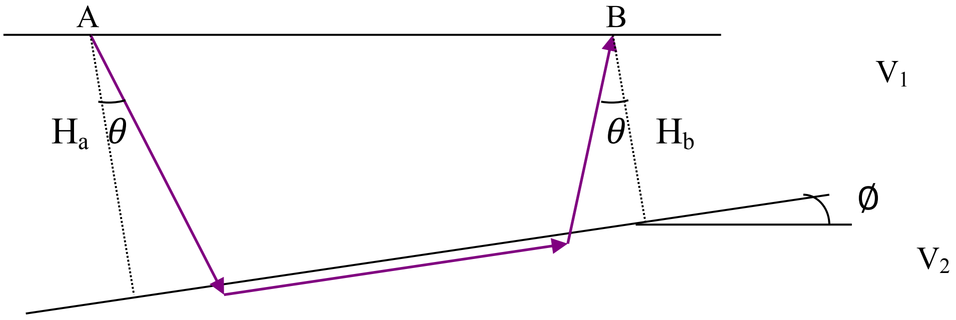

Figure 2.1. P_n ray paths from a dipping layer medium (Adapted from Scheidegger and Willmore, 1957)

The equation of the travel time of a seismic wave between two materials separated by a plane interface is given as below,

$$t = \frac{H_a}{\cos\theta V_1} + \frac{H_b}{\cos\theta V_1} + \frac{\Delta\cos\emptyset - H_a\tan\theta - H_b\tan\theta}{V_2} \tag{2.1}$$

where H_a and H_b (if source is assumed as a shot point $H_b = H_a - \Delta\sin\emptyset$ represents the perpendicular distances drawn from the source A to receiver B to the interface. V_1 and V_2 are the velocities of layers $\sin\theta = V_1/V_2$. Δ is distance between source and receiver. $\emptyset$ is the angle between AB and the interface. θ is the incidence angle of the refracted wave, which is also the critical angle (Figure 2.1).

The main idea beneath time term method is to calculate travel time for a refracted ray between source and receiver. That may be written as;

$$t = \frac{(H_a + H_b)\cos\theta}{V_1} + \frac{\Delta\cos\emptyset}{V_2} \tag{2.2}$$

In order to simplify the equations $\cos\emptyset$ assumed to equal one. This assumption increases the error in $H_a + H_b$ which depends on the interface between two medium. If the interface is not a plane, errors may arise. Travel time roughly presented as;

$$t = a + b + \frac{\Delta}{V_2} \tag{2.3}$$

a and b represent time terms of source A and receiver B.

Hearn (1984) wrote that basic form of the time term approach as the travel time between event (e) and station (s) for horizontal upper mantle layer is,

$$t_{es} = \Delta_{es}S + \tau_e + \tau_s \tag{2.4}$$

where S refers to the slowness of the uppermost mantle, Δ_{es} refers to the horizontal distance between station and event, and τ_e and τ_s are event and station time terms.

These time terms, or delay times, can be written as,

$$\tau_s = \int_0^h (S(z)^2 - S^2)^{1/2} dz \tag{2.5}$$

$$\tau_e = \int_z^h (S(z)^2 - S^2)^{1/2} dz \tag{2.6}$$

where h is the Moho depth, z is the event depth and S(z) is the crustal slowness profile. Delay times are effected by P_n velocity and crustal slowness. For a constant velocity crust, delay times are related to the crustal thickness.

In order to compute lateral velocity variations and anisotropy, travel time equation can be linearized with respect to slowness.

$$t_{es} = \Delta_{es}S_0 + \tau_e(S_0) + \tau_s(S_0) + \left[\Delta_{es} + \frac{\partial\tau_s}{\partial S} + \frac{\partial\tau_e}{\partial S}\right]_{S=S_0} \delta S(x.y.\emptyset) \tag{2.7}$$

Hearn (1984) expressed the event and station offset distances by F_e and F_s. The horizontal path that ray travels from source to Moho or Moho to receiver is called "Offset Distance".

Equation 2.7 may be written as;

$$t_{es} = \Delta_{es} S_0 + \tau_e(S_0) + \tau_s(S_0) + [\Delta_{es} - F_e - F_s]\delta S(x.y.\emptyset) \tag{2.8}$$

The horizontal offset distances for station and event are written as;

$$F_e = \int_z^h [\frac{S}{(S(z)^2 - S^2)^{1/2}}]\, dz \tag{2.9}$$

$$F_s = \int_0^h [\frac{S}{(S(z)^2 - S^2)^{1/2}}]\, dz \tag{2.10}$$

These offset distances depend on P_n velocity, crustal velocity, Moho depth and event depth which are all unknowns. Accordingly, by assuming F as constant, Equation 2.8 may be written as;

$$t_{es} = \Delta_{es} S_0 + \tau_e(S_0) + \tau_s(S_0) + [\Delta_{es} - 2F]\delta S(x, y, \emptyset) \tag{2.11}$$

The travel time of the ray passing through each cell might be written as;

$$t_{es} = \tau_e(S_e) + \tau_s(S_s) + \sum_{i=0}^{n} \Delta_i S_i \tag{2.12}$$

where S_e is P_n velocity at the event location, S_s is P_n velocity at the station location, Δ_i is the horizontal distance that ray travels through the cell "i", S_i is the slowness of cell "i". The time term equation is;

$$t_{es} = \tau_e(S_0) + \tau_s(S_0) + \sum_{i=0}^{n} \Delta_i S_i - F\delta S_e - F\delta S_s \tag{2.13}$$

where S_0 is the mean slowness, δS_e and δS_s are the slowness perturbations at event and station. In order to compare time terms with each other $\tau_e(S_0)$ and $\tau_s(S_0)$ has to be calculated instead of $\tau_e(S_e)$ and $\tau_s(S_s)$. Travel time equation solved for the relevant parameters is;

$$t_{es} = (\tau_e(S_0) + 2FS_0) + \tau_s(S_0) + \textstyle\sum_{i=0}^{n} \Delta_i S_i \tag{2.14}$$

$$\text{where } \Delta_i' = \begin{Bmatrix} \Delta_i \text{ if } i \neq e \text{ and } i \neq s \\ \Delta_i' \text{ if } i = e \text{ or } i = s \end{Bmatrix}$$

Δ_i' is the distance along the Moho in each cell that the ray travels. Unknowns $(\tau_e(S_0) + 2FS_0)$, $\tau_e(S_0)$, S_0 and mean P_n slowness for each cell be calculated.

Due to the mantle anisotropy or horizontal variations beneath isotropic mantle and crust, P wave velocity is depends on the azimuthal angle $\emptyset$. A weak anisotropy perturbation described by $2\emptyset$ azimuthal variations (Backus, 1965; Crampin, 1977).

$$\delta V_p^2 = A + B\cos 2\emptyset + C\sin 2\emptyset + D\cos 4\emptyset + E\sin 4\emptyset \tag{2.15}$$

where $\emptyset$ is the direction of maximum velocity. A, B, C, D and E are the constants which are related to the elastic tensor components and they are functions of the anisotropic elasticity of the upper mantle.

Hearn (1996) simplified P_n travel time problem by assuming a transverse anisotropy. By using magnitude of anisotropy and the direction of the fastest wave propagation, azimuthal P_n travel time variations can be simply described. Hearn (1996) formulated P_n travel time equation as;

$$t_{es} = \tau_e(S_e) + \tau_s(S_s) + \textstyle\sum_{i=0}^{n} \Delta_i (S_i A_i \cos 2\emptyset + B_i \sin 2\emptyset) \tag{2.16}$$

$\emptyset$ is the back azimuth angle. Time terms for station and event (τ_e, τ_s), mantle slowness (S_i), and anisotropy coefficients (A_i, B_i) are unknowns.

Magnitudes of anisotropy for cell i;

$$(A_i^2 + B_i^2)^{1/2} \tag{2.17}$$

and, direction of fastest wave propagation is given by;

$$\frac{1}{2}\arctan(\frac{B_i}{A_i}) \tag{2.18}$$

In order to obtain slowness, anisotropy and station and event delays the set of equations solved by least-squares QR factorization algorithm for all source-receiver pairs (Hearn 1996). Assume waves from “n” sources observed by “m” stations. With many of source- receiver couples a linear system can be solved.

$$Ax = t \tag{2.19}$$

t is observed travel times and x is station delays, event delays and slowness. Unknown “x” might be computed as;

$$x = (A^T A)^{-1} A^T t \tag{2.20}$$

A has linearly independent columns. It has QR decomposition. Since the columns of Q are orthonormal and R is an invertible matrix $Ax = t$ can be written as;

$$Rx = Q^T t \tag{2.21}$$

Since R is the upper triangular matrix system will be solved by using Gram-Schmidt process.

Solution of the inverse problem controls the trade-off between errors and resolution. Trade-off between the velocity and anisotropy is computed for each inversion.

2.3. Data Processing

A waveform database from 1999 to 2010 is formed from the permanent and temporary stations operated in the region (Figure 2.2). The main source of the data is the National Network of Turkey operated by Kandilli Observatory and Earthquake Research

Institute (KOERI-NEMC). The network has been continuously upgraded since 2004 and the total number of broadband stations has exceeded 130 in 2010. Supplementary data are obtained for the permanent stations from IRIS and ORFEUS in the region. The data from Eastern Turkey Seismic Experiment (ETSE) (Sandvol *et al*., 2003), Western Anatolia Seismic Recording Experiment (WASRE) (Akyol *et al*., 2006), Seismic Imaging beneath Aegean-Anatolia Domain (SIMBAAD) (Paul *et al*., 2008), the temporary networks, are also included in the analysis. The observations from several local and aftershock studies are added in the analysis (*e.g*, Karabulut *et al*., 2011).

The station spacing is not regular with greater density in the Marmara and Aegean Region and relatively less densely in the Central and Eastern Anatolia. The earthquake distribution is not uniform either. The majority of the earthquakes are located along the active seismic zones such as North Anatolian Fault (NAF), East Anatolian Fault (EAF) and Aegean. Few earthquakes were included from Caucasus and Iran.

KOERI-NEMC, International Seismological Centre (ISC) and European-Mediterranean Seismological Centre (EMSC) bulletins were compiled for initial P_n tomography catalogue. A total of 700 earthquakes with magnitudes $Ml > 4.0$ were re-located. Waveform database was constructed for the selected events (Figure 2.3). With the available waveform data more than 50 000 P_n arrival times recorded at 832 seismic stations were manually picked. P_n arrivals are defined as the first arrivals between 180 km and 2000 km. The data quality was generally good and only clear P_n arrivals were picked. Figure 2.4 shows an earthquake gather constructed from the stations sited between 27.5°E and 28.5°E for an earthquake approximately located in the middle of the profile.

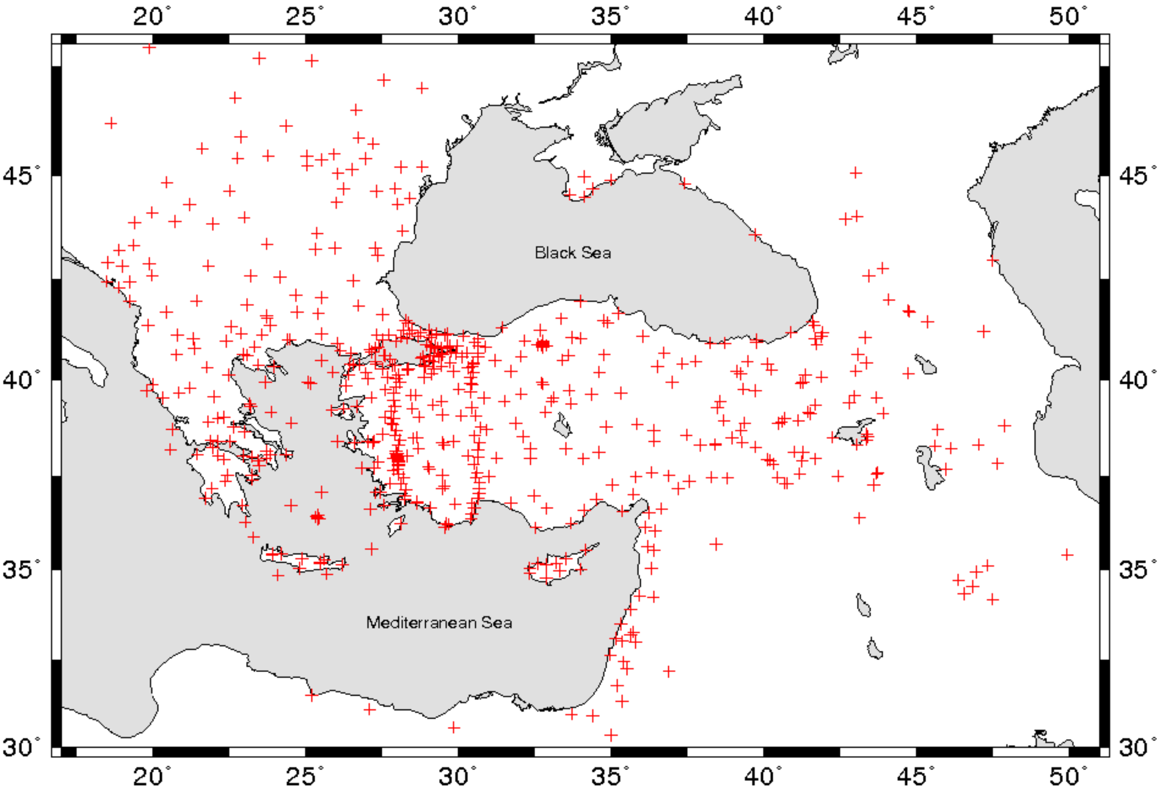

Figure 2.2. Seismic stations (+) used for P_n tomography. A total of 695 stations are displayed from both permanent and portable deployments operated between the years 1999-2010

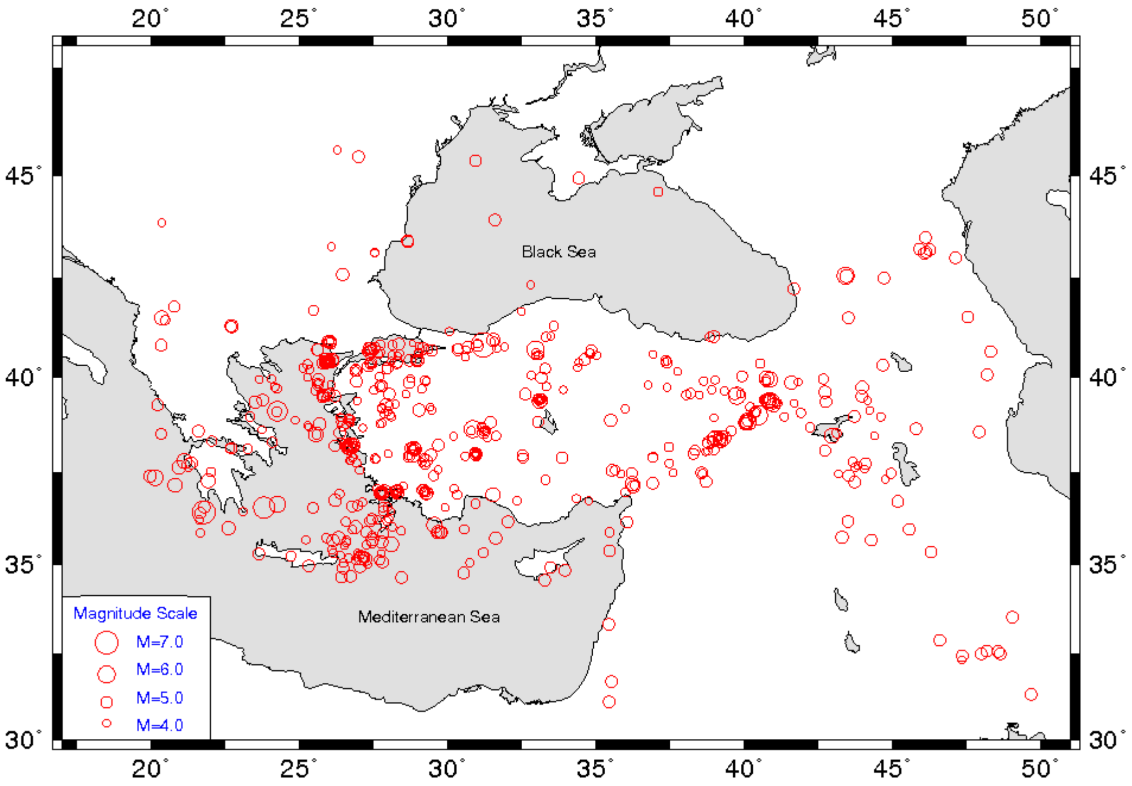

Figure 2.3. Selected 596 earthquakes (o) for the P_n analysis with magnitudes greater than 4.0 between the years 1999 and 2010

Manually picked P and S arrivals at distances smaller than 180 km, are used to improve the locations of the selected earthquakes. Regional velocity models are constructed using Velest inversion code (Kissling *et al.*, 1994). Hypocenter code (Lienert *et al*, 1986) is used to compute the locations of the earthquakes. The events with location errors more than 5 km and hypocentral depths greater than 40 km are discarded. Stations recorded less than 10 events and earthquakes with fewer than 10 P_n arrivals are also eliminated. Travel time residuals greater than 8 seconds are ignored as the residuals greater than 8 seconds are significantly larger than the data scatter. As a result, 596 of the relocated earthquakes and 695 stations are selected for the analysis and 40 826 first arrival phases used for iterations.

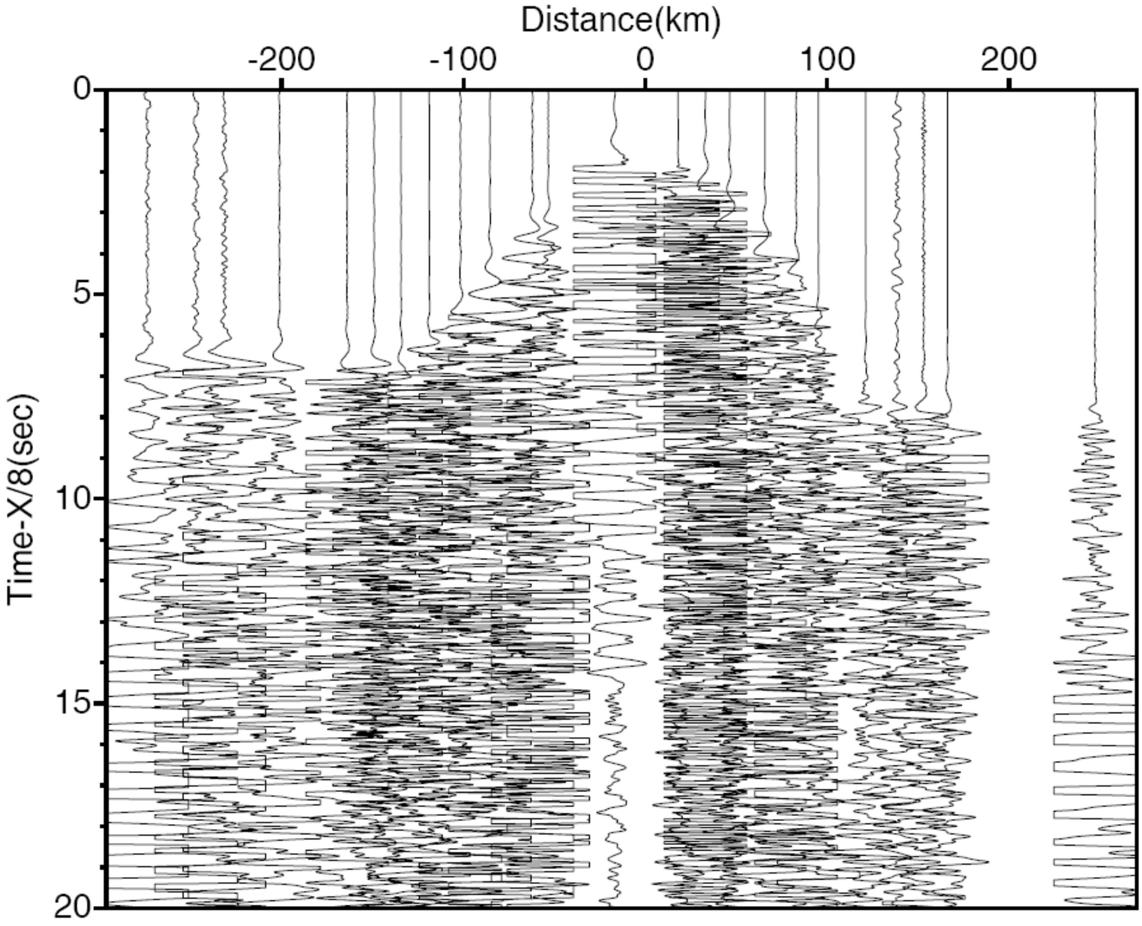

Figure 2.4. Recordings of an earthquake in Western Anatolia. The stations are located between 27.5°E and 28.5°E. The traces are normalized with their maximum amplitudes and plotted with a reducing velocity of 8.0 km s^{-1}

Average P_n velocity and crustal delay for the data set by a least squares fit is determined as 8.0 km s^{-1} for P_n velocity. An average crustal velocity of 6.3 km s^{-1} and crustal thickness of 35 km are obtained from the slope of the Pg travel times and intercept time, respectively. Lateral variations of P_n velocity are imaged as perturbations from the average velocity of 8.0 km s^{-1}. Topography corrections at the station sites are applied assuming a constant velocity of 5.5 km s^{-1}. These initial estimates are used as the starting model for the subsequent tomographic inversion. The reduced travel times with a reducing velocity is depicted in Figure 2.5. The travel time residuals vary between ±10 seconds. P_g and P_n branches of the travel times are clearly visible. The critical distance for the dataset is observed at ~180 km. At distances greater than 800 km there is a sharp decrease on the number of observations (Figure 2.5).

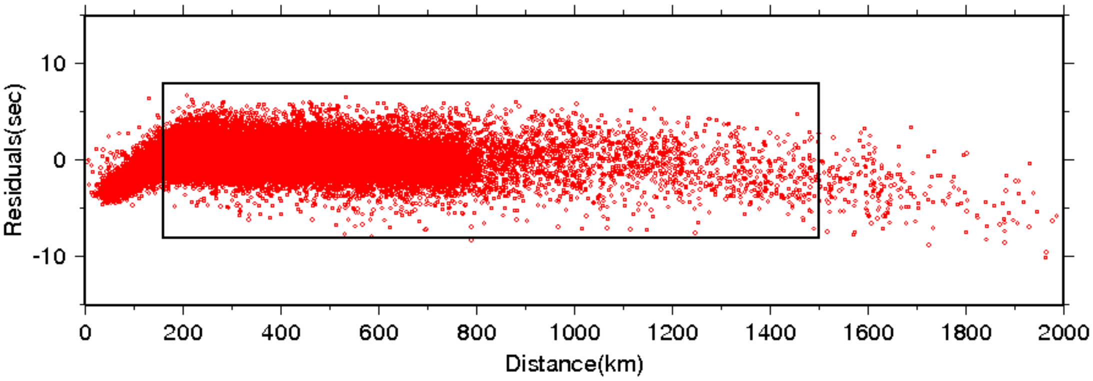

Figure 2.5. Travel time observations at epicentral distances smaller than 2000 km. A reducing velocity of 8.0 km s^{-1} is used. The crossover distance is ~180 km. The box shows the range of the observations used in tomography

A total of 36 290 ray paths between events and stations are shown in Figure 2.6. A total of 532 earthquakes and 695 stations are used to compute ray paths. Each ray path passes through at least a single 0.5°x0.5° square cell. The ray paths provide a good coverage of the study area. Dense path coverage exists in the central and Eastern Anatolia and relatively high coverage exist in the Northwestern Turkey and Aegean region. The coverage is poor in the Black sea, Caucasus and Southern Mediterranean.

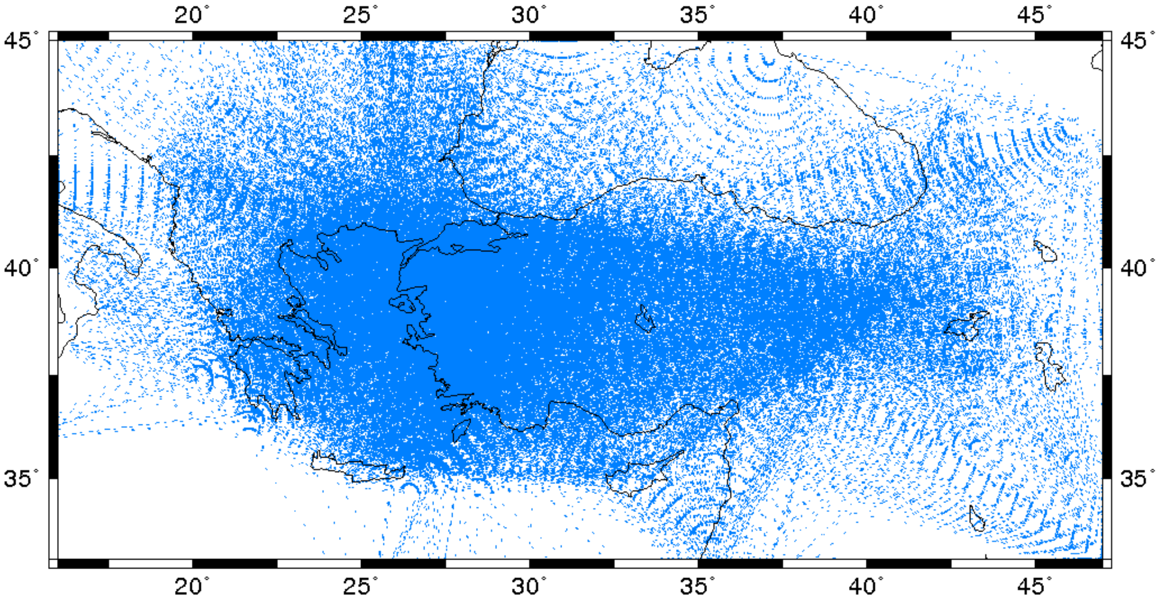

Figure 2.6. P_n ray paths for tomographic inversion

2.4. Resolution and Error Analysis

One of the main problems at the tomographic studies is to determine the quality of the results. Tomographic results are affected by not only velocity perturbations but also data errors, ray path geometry and model parameters. Checkerboard test is a way to check the resolution of the final model by using source-receiver configuration with different damping constants. This is a widely used method to evaluate the solution quality, ray coverage effect, parameterization of the model space and damping factors (Zelt, 1988).

Before to select the optimum cell size, smoothing and weighting parameters, a number of analyses are performed using both real and synthetic data. Same source-receiver configurations are used both on observations and checkerboard tests. Tests are performed with alternating input velocity patterns. Optimum damping parameters are determined as a result of checkerboard tests. The criterion for selecting optimum parameters is to obtain high level of resolution in which both magnitude and shape of the anomalies are preserved.

The initial checkerboard model for velocity contains alternating values of ±0.5 km s^{-1} for low and high velocity regions with 1°, 2°, 3° and 4° pattern sizes (Figure 2.7). For anisotropy tests, input is a model with 5 per cent variations with fast directions perpendicular in adjacent cells (Figure 2.8). The tests are performed by using various damping factors (200, 400, 600 and 800) for both velocity and anisotropy. Figure 2.7 presents the checkerboard tests on velocity only. In order to determine the effect of path coverage on various pattern sizes, a damping factor of 400 used for these tests. Figure 2.8 shows the tests on velocity only using fixed pattern size 2^o with varying damping parameters (200, 400, 600 and 800). Figure 2.9 shows the tests on anisotropy (without velocity) with constant damping factor as 400 and various pattern sizes as 1°, 2°, 3°, 4°. Figure 2.10 shows the fixed pattern size of 2^o and varying damping factors (200, 400, 600 and 800) of anisotropy tests without velocity. Checkerboard tests were performed for anisotropy with included velocity variations depicted in Figure 2.11 (constant damping factor (400) and varying pattern sizes (1°, 2°, 3°, 4°)) and Figure 2.12 (constant pattern size as 2° and varying damping factors (200, 400, 600, 800)). Figure 2.13 shows the P_n anisotropy magnitude checkerboard tests (without velocity) performed for fixed damping factor (400) with varying pattern size (1°, 2°, 3°, 4°). Figure 2.14 shows fixed pattern size of 2° and various damping factors (200, 400, 600 and 800) for magnitude of anisotropy without velocity.

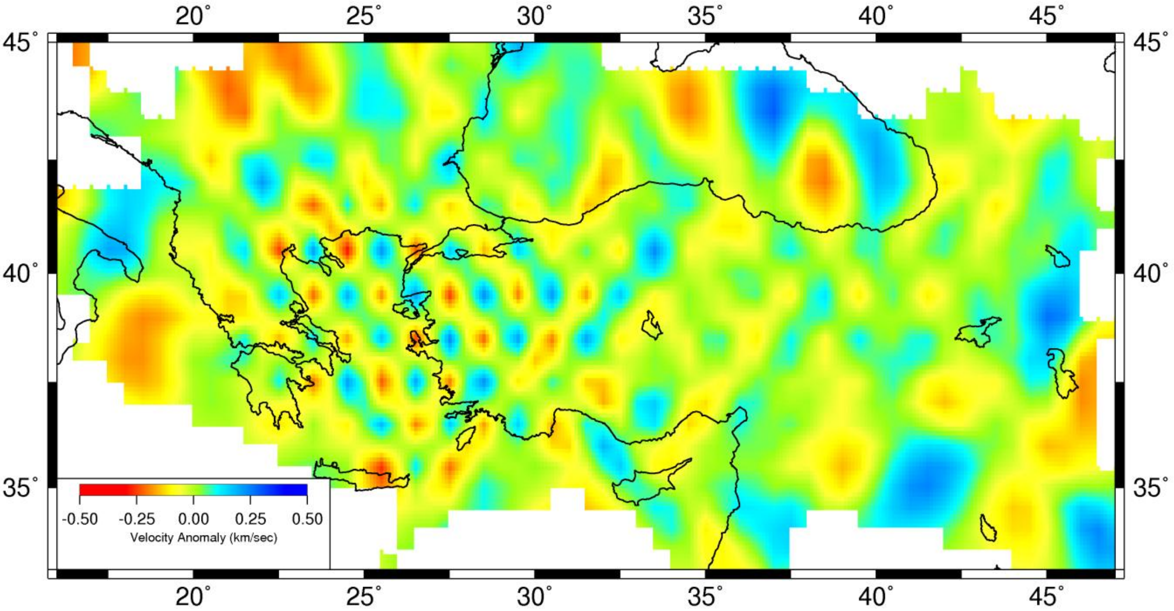

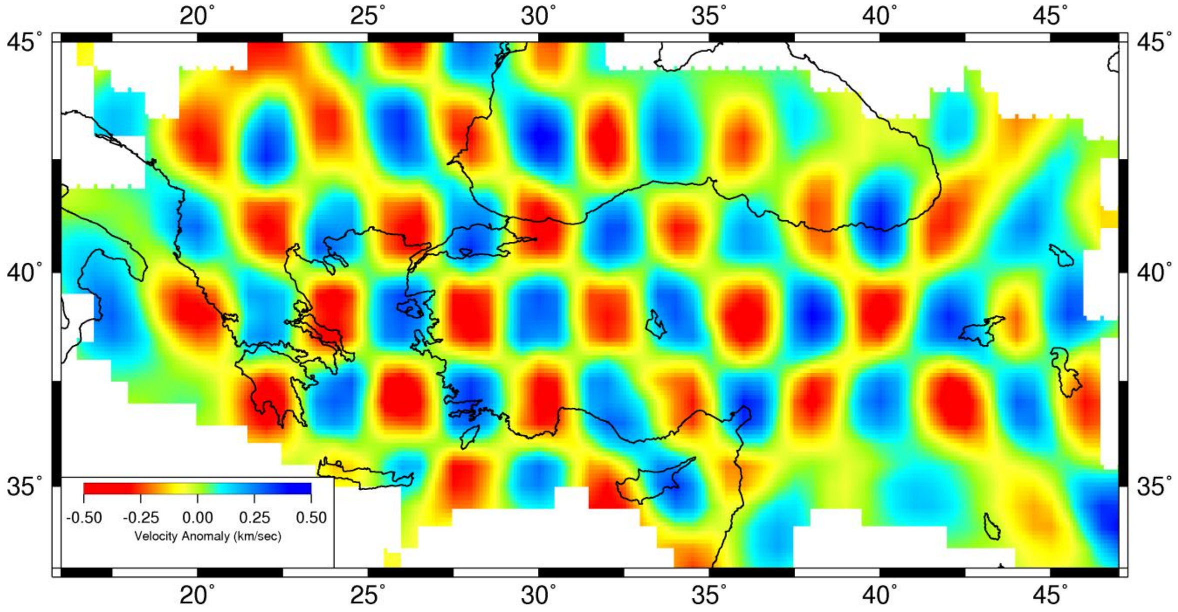

Figure 2.7. P_n velocity checkerboard tests. Synthetic data are generated with ±0.50 km s^{-1} isotropic velocity perturbations. Recovered isotropic model: starting from top to bottom, input pattern sizes are 1°, 2°, 3° and 4°. The damping parameter is assumed as 400.

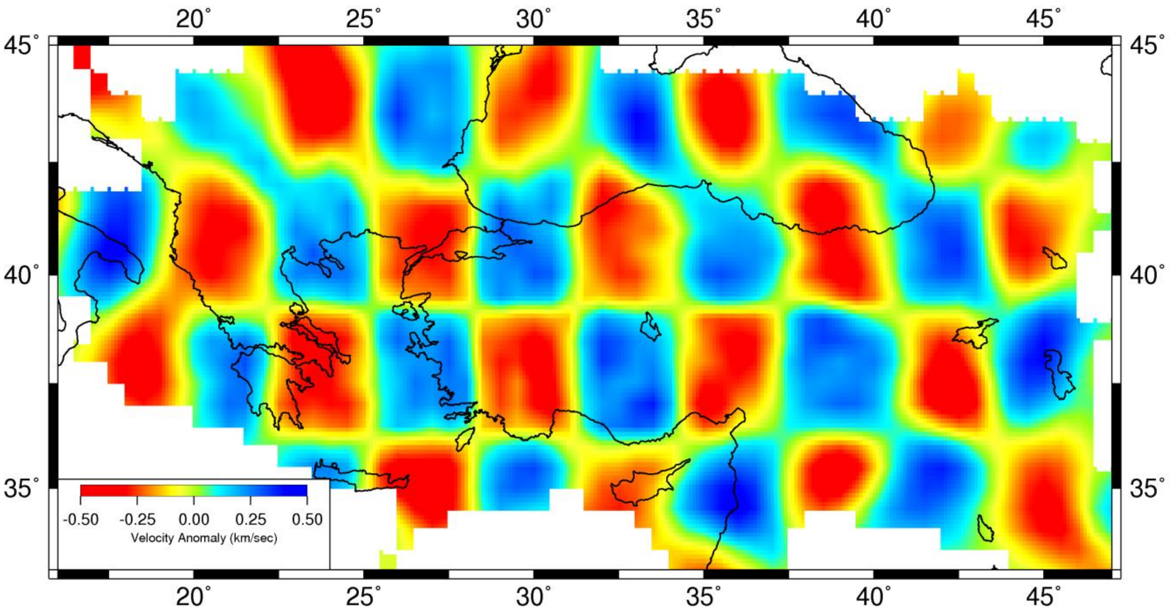

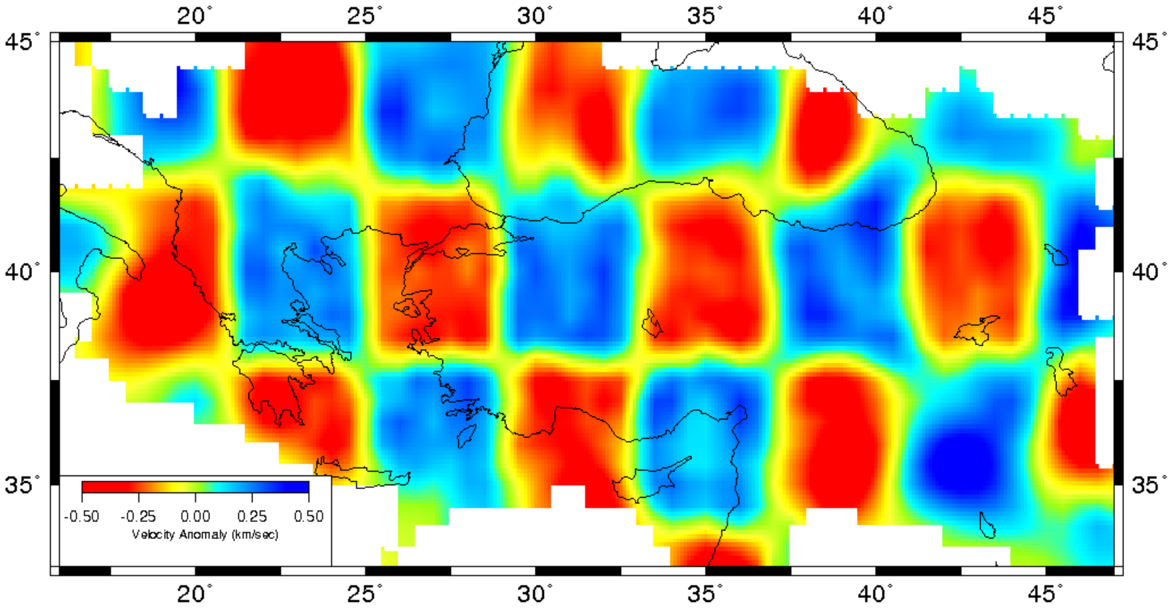

Figure 2.7. Cont.

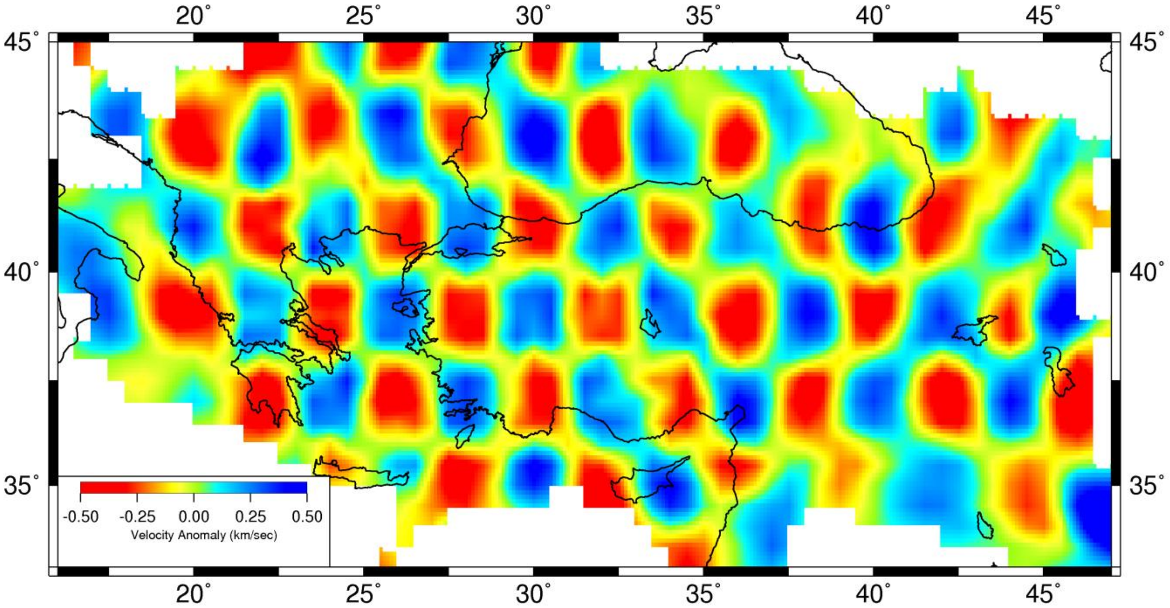

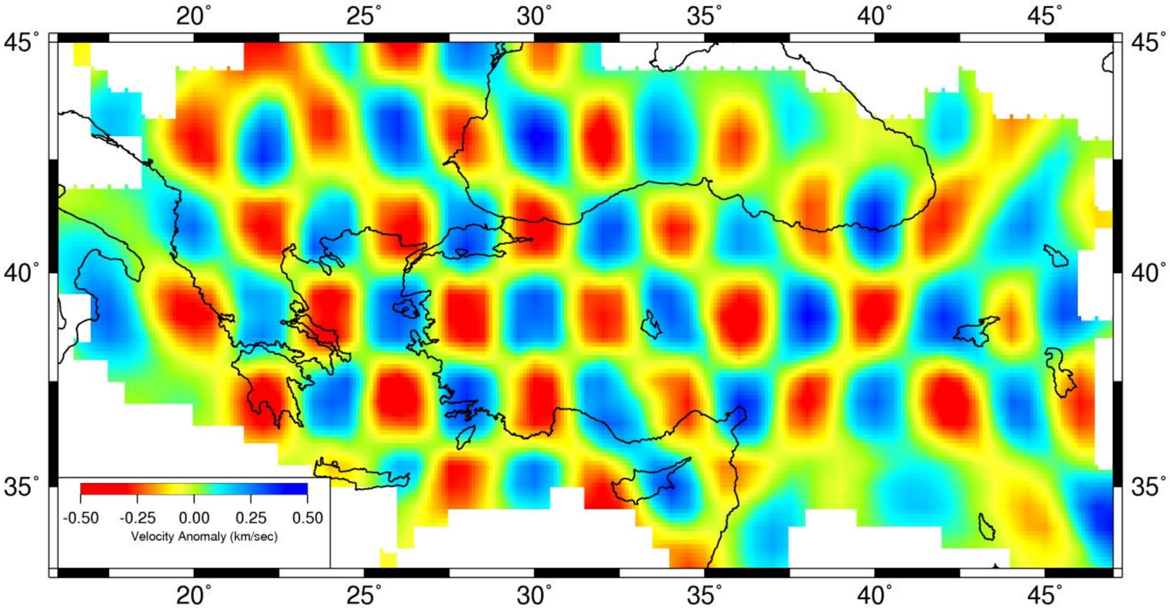

Figure 2.8. P_n velocity checkerboard tests. Synthetic data are generated with ±0.50 km s^{-1} isotropic velocity perturbations. Recovered isotropic model: starting from top to bottom, damping parameters are 200, 400, 600, 800. The input pattern size is assumed as 2°

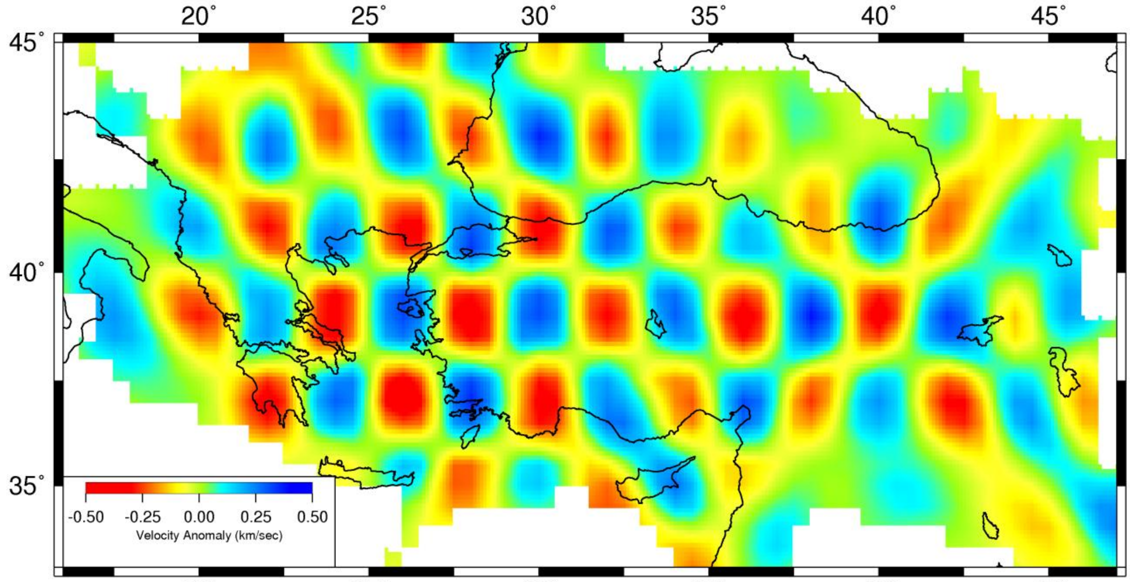

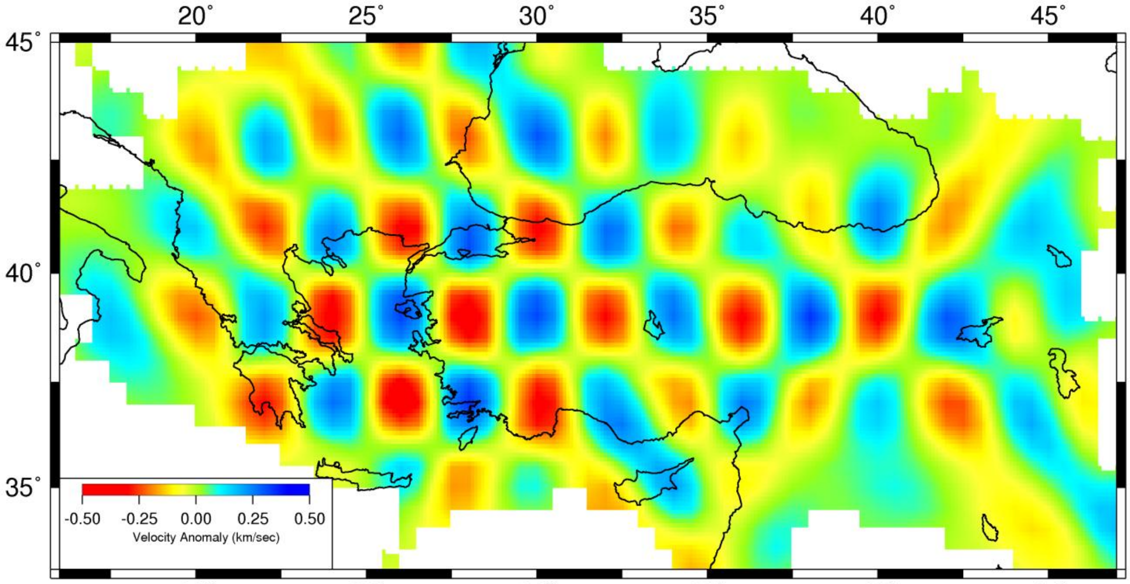

Figure 2.8. Cont.

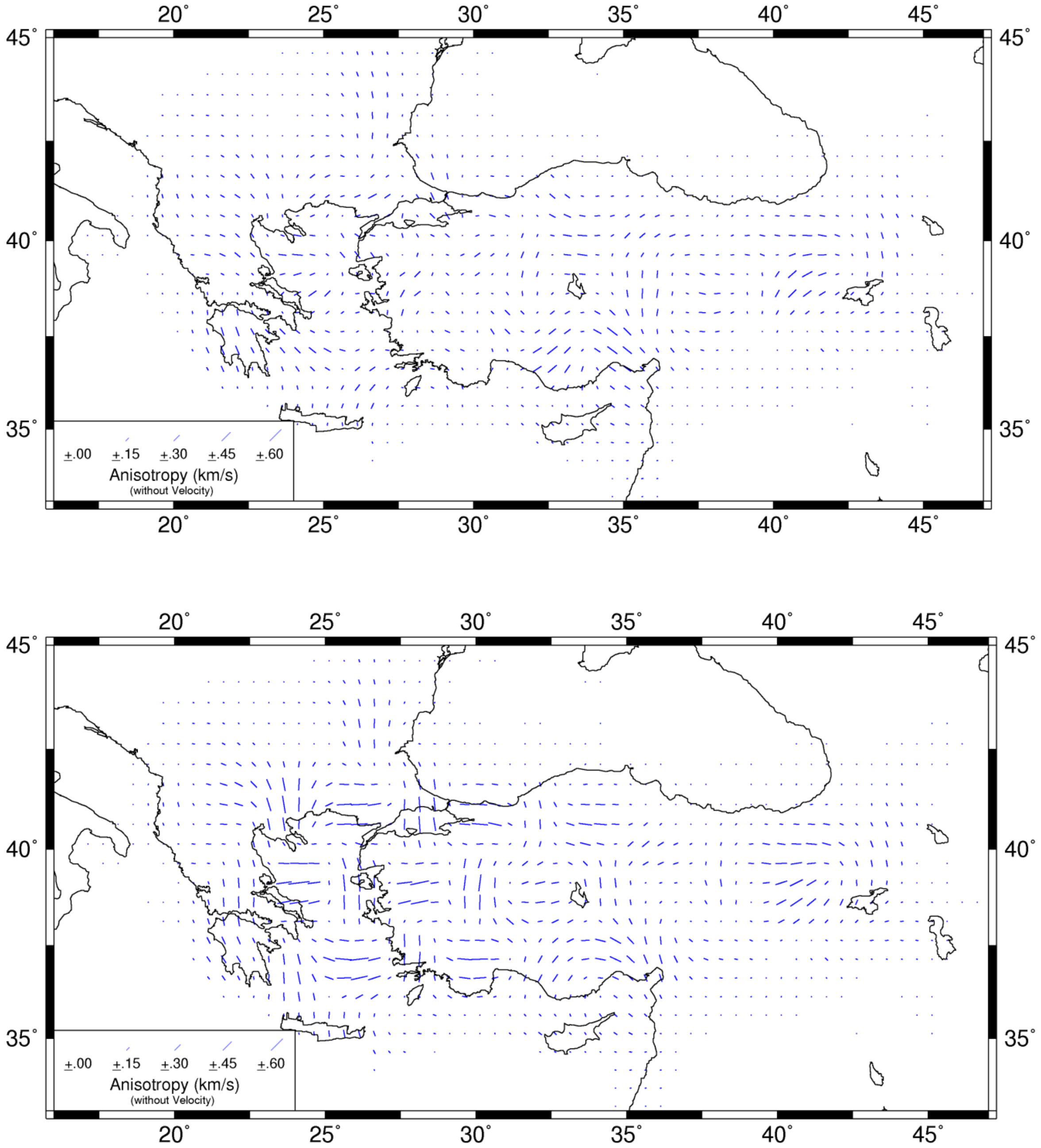

Figure 2.9. P_n anisotropy checkerboard test (without velocity): Synthetic data are generated with 5 per cent anisotropy. Anomalies change between ±0.50 km s^{-1} with a constant damping parameter of 400. Starting from top to bottom, pattern sizes are 1°, 2°, 3° and 4°

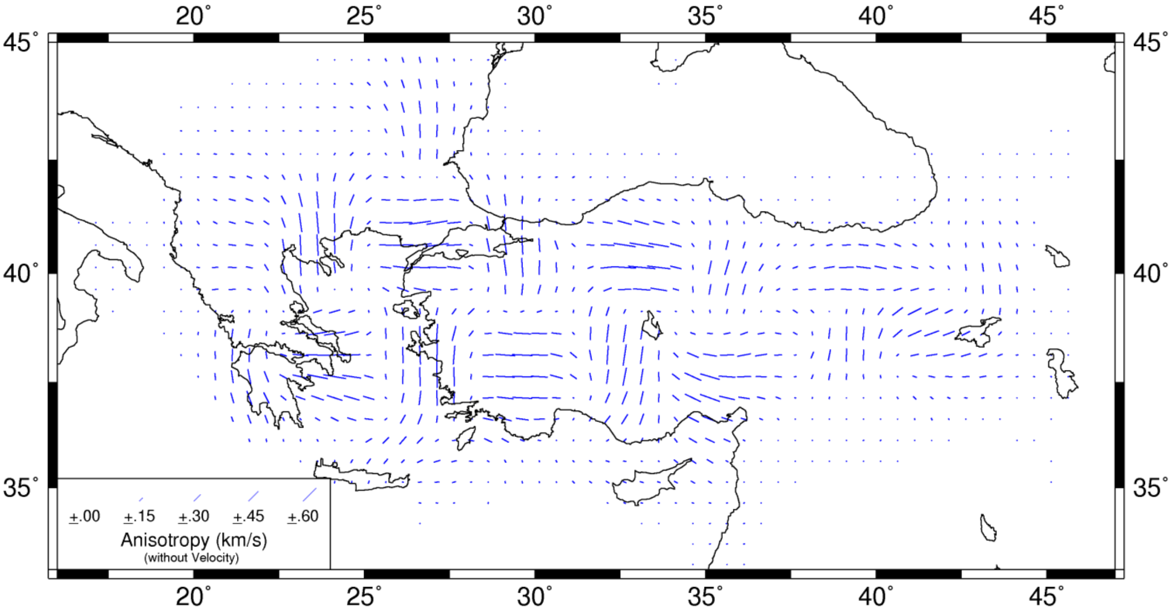

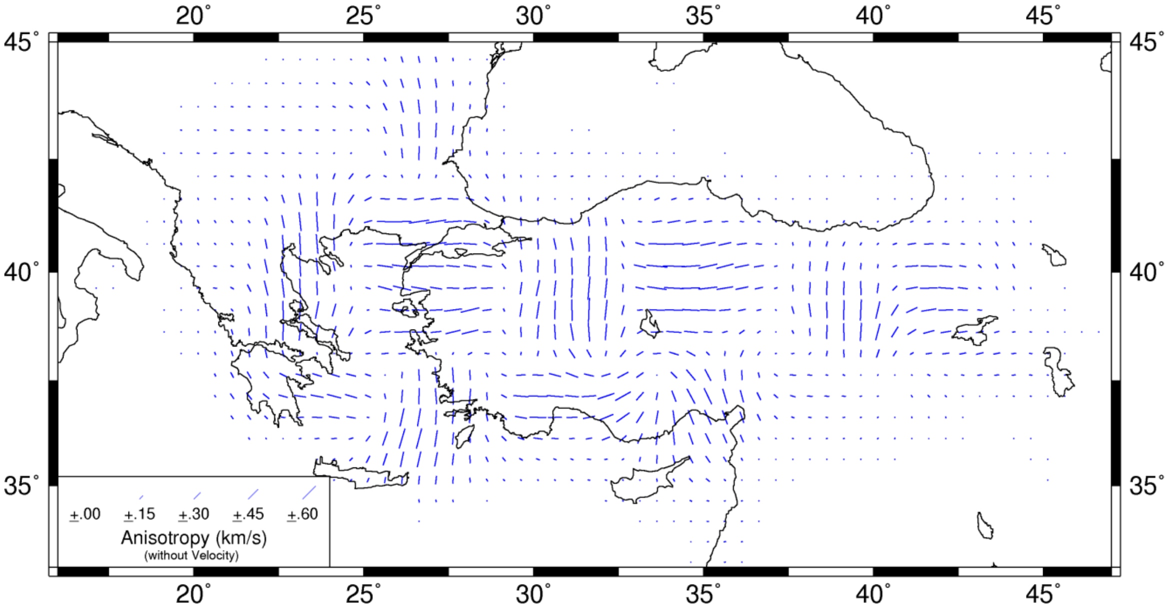

Figure 2.9. Cont.

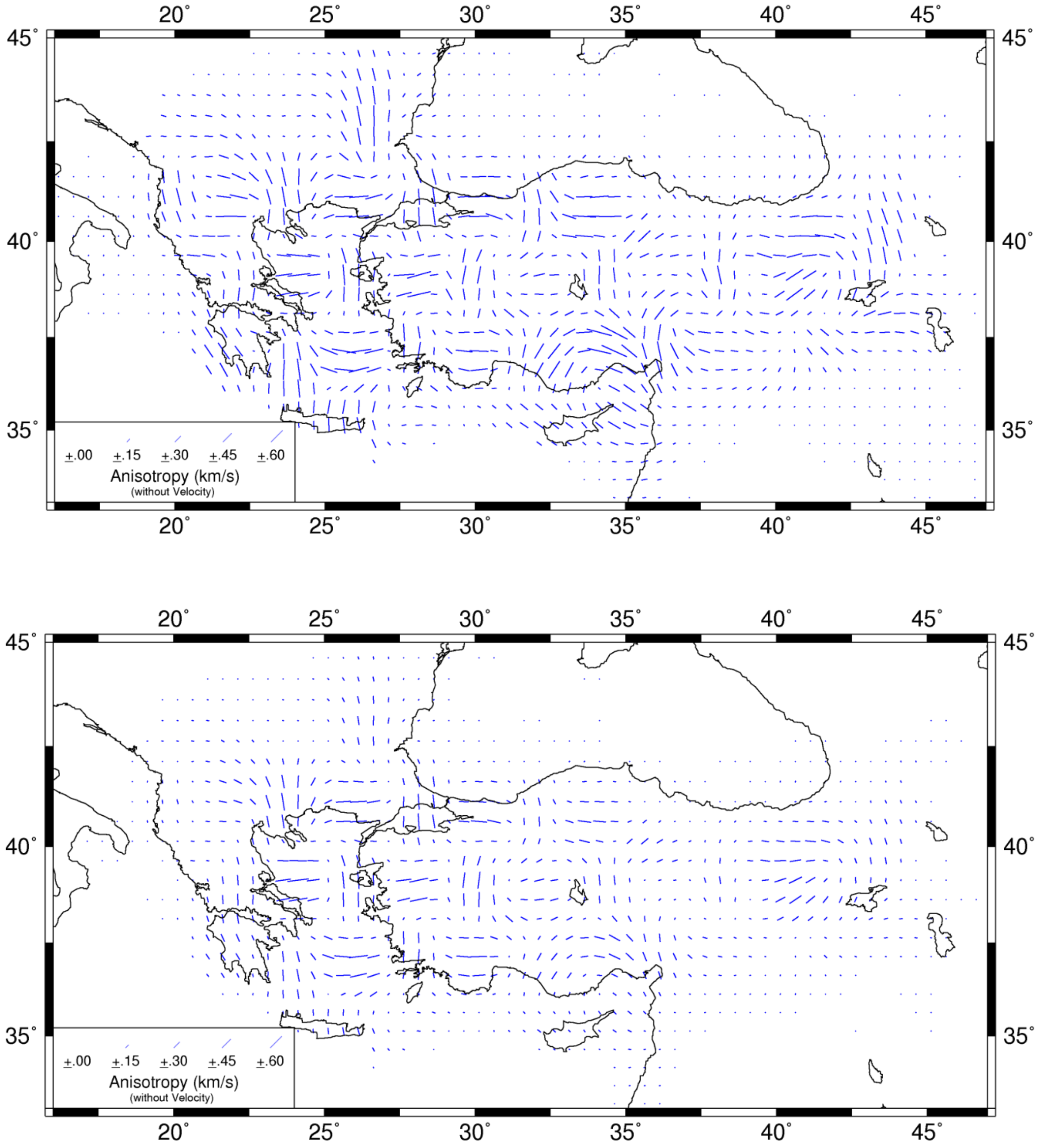

Figure 2.10. P_n anisotropy checkerboard test (without velocity): Synthetic data are generated with 5 per cent anisotropy. Anomalies change between ±0.50 km s^{-1} with a pattern size of 2°. Starting from top to bottom, damping parameters are 200, 400, 600, 800

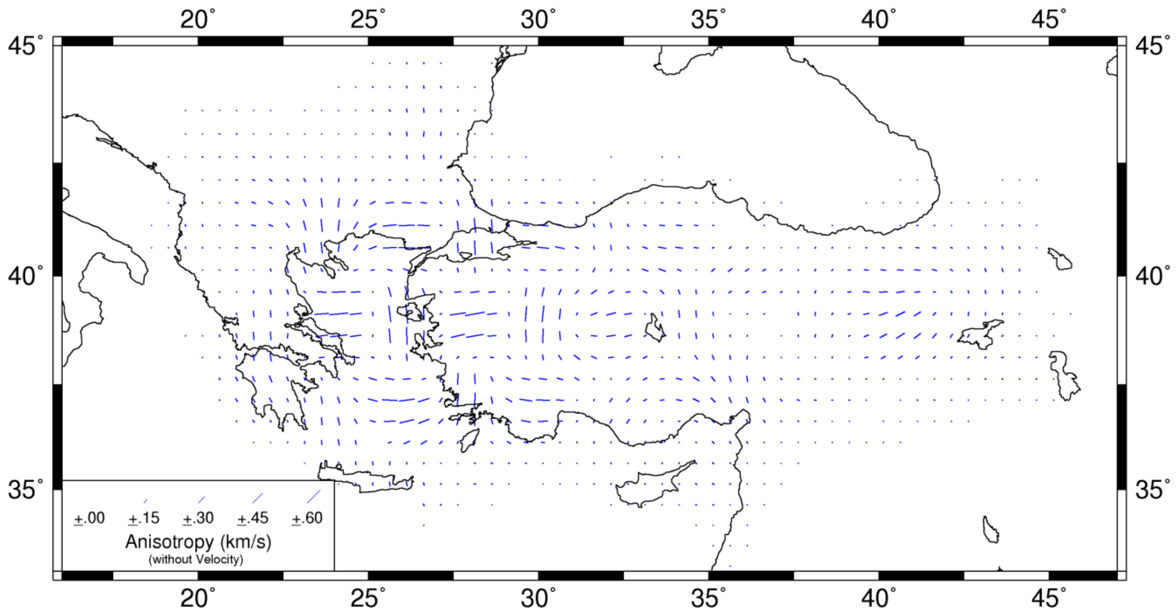

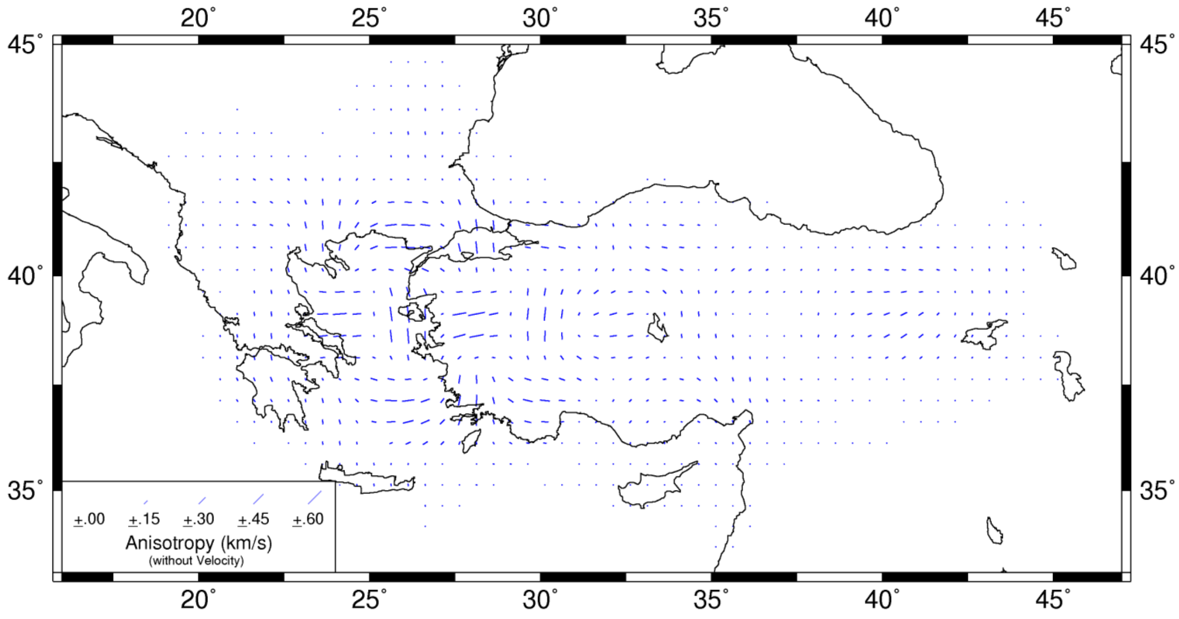

Figure 2.10. Cont.

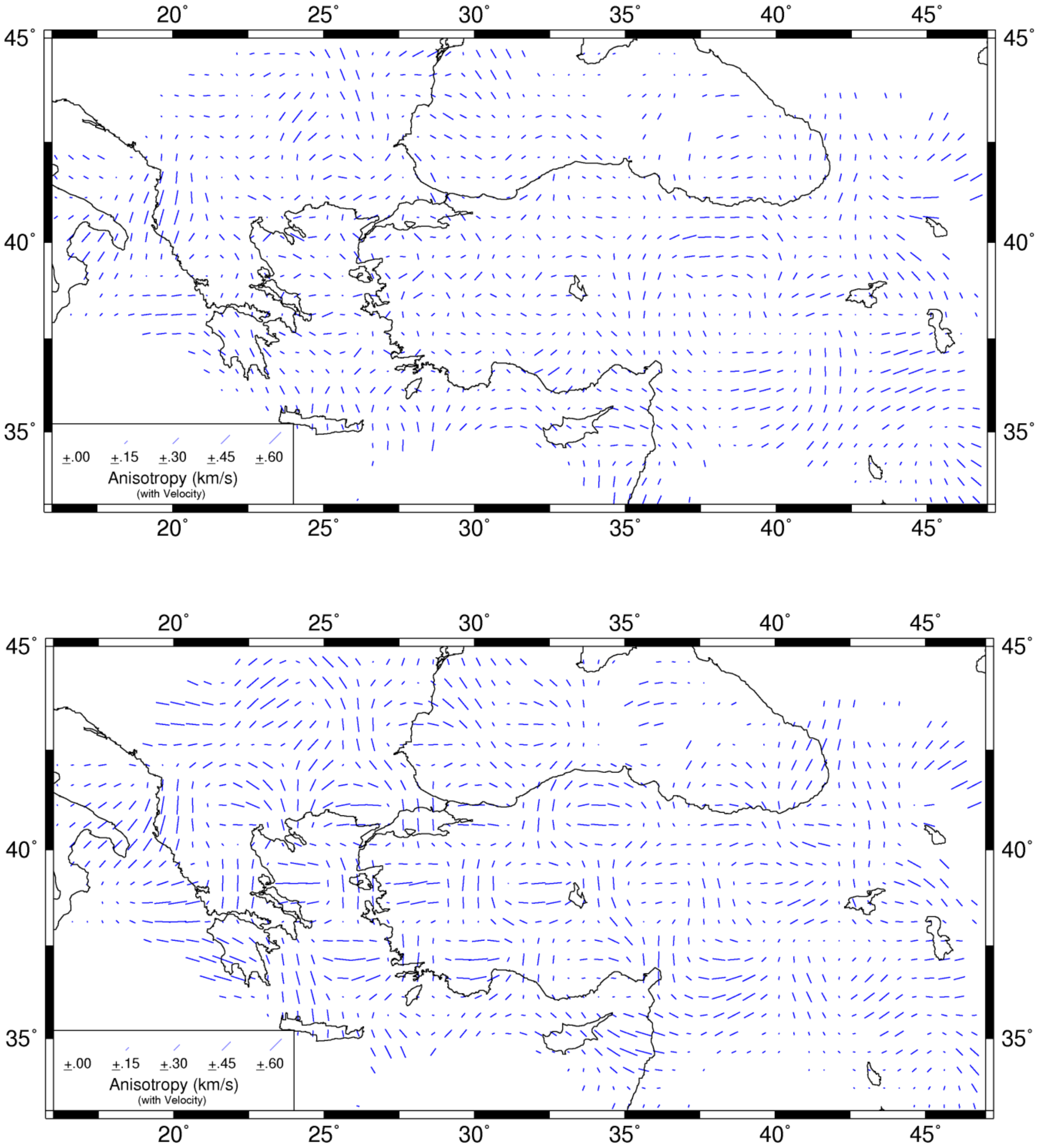

Figure 2.11. P_n anisotropy checkerboard test (with velocity): Synthetic data are generated with 5 per cent anisotropy. Anomalies change between ±0.50 km s^{-1} with a constant damping parameter of 400. Starting from top to bottom, pattern sizes are 1°, 2°, 3° and 4°

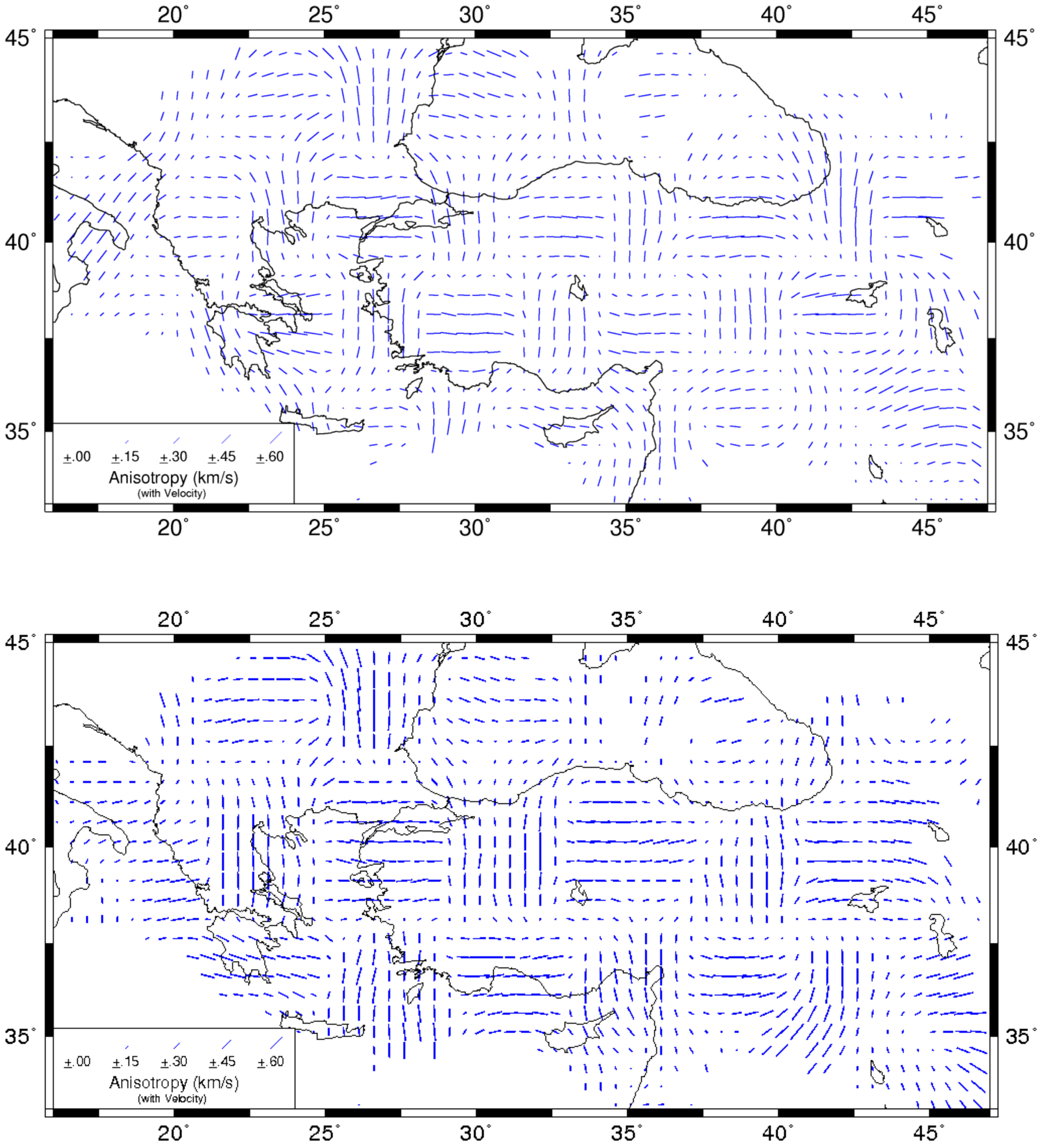

Figure 2.11. Cont.

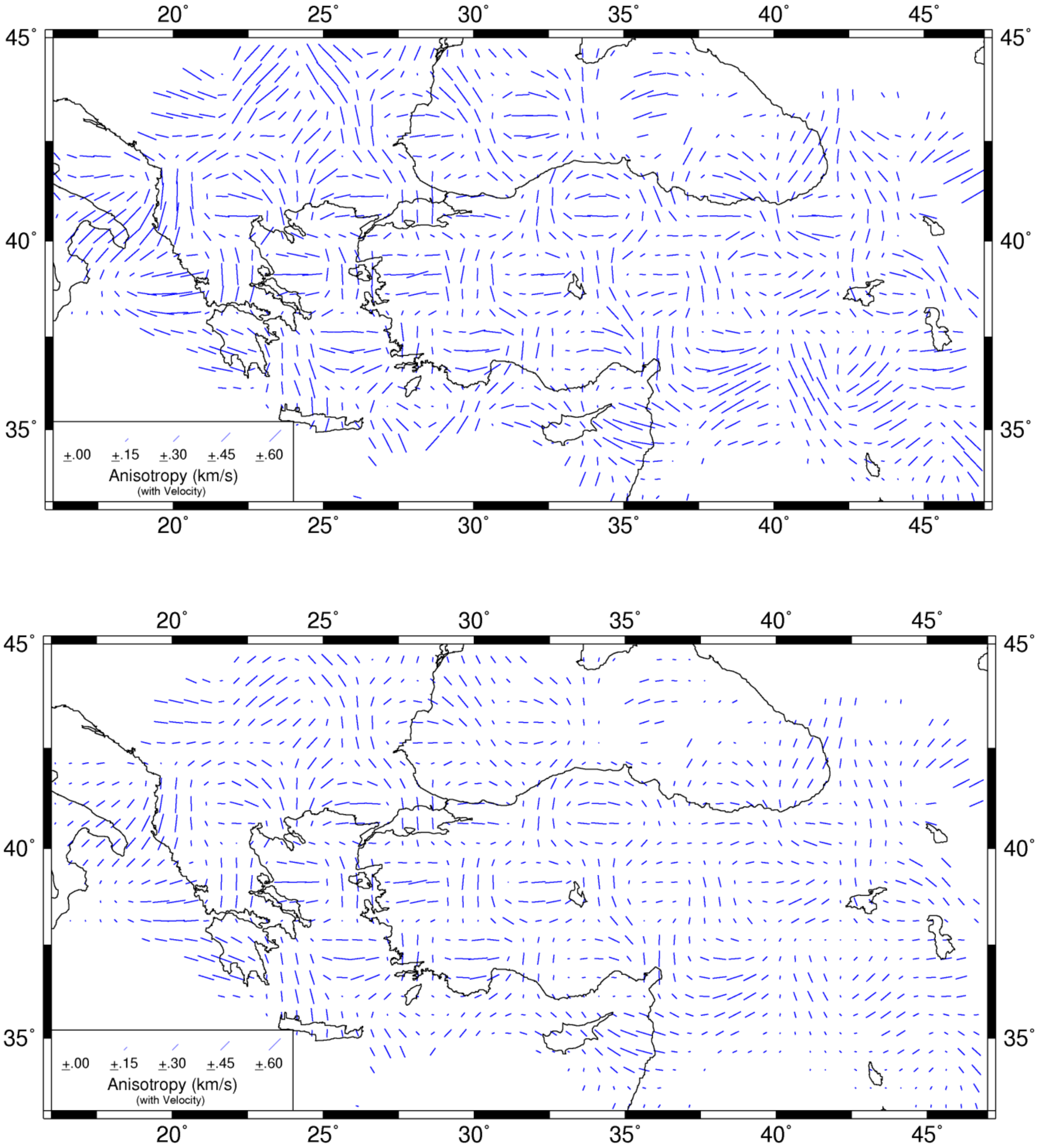

Figure 2.12. P_n anisotropy checkerboard test (with velocity): Synthetic data are generated with 5 per cent anisotropy. Anomalies change between ±0.50 km s^{-1} with a pattern size of 2°. Starting from top to bottom, damping parameters are 200, 400, 600, 800

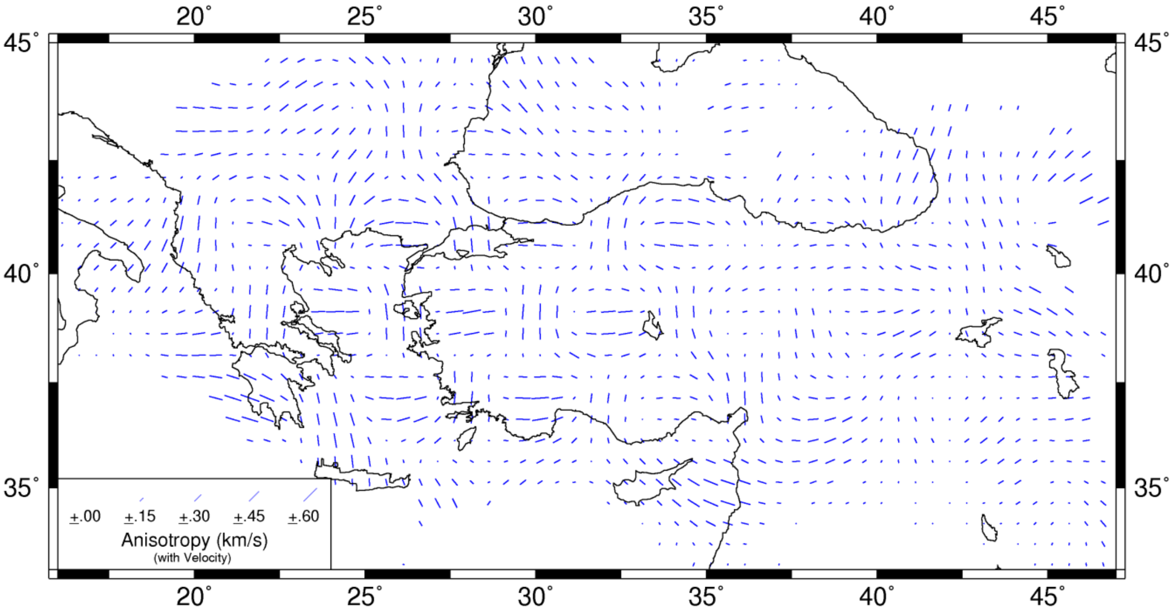

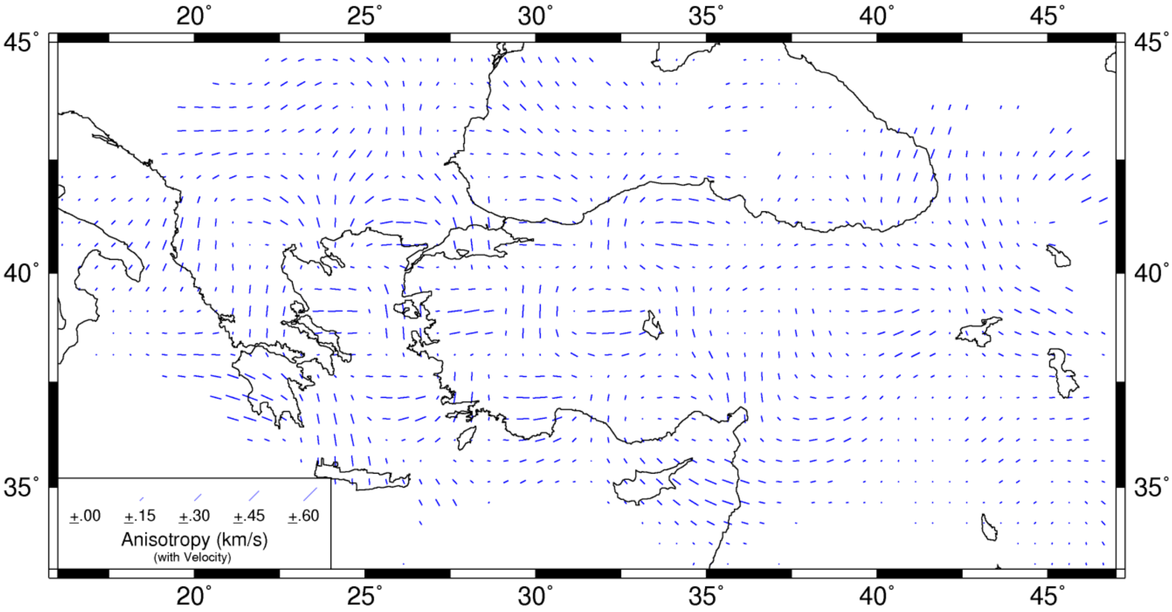

Figure 2.12. Cont.

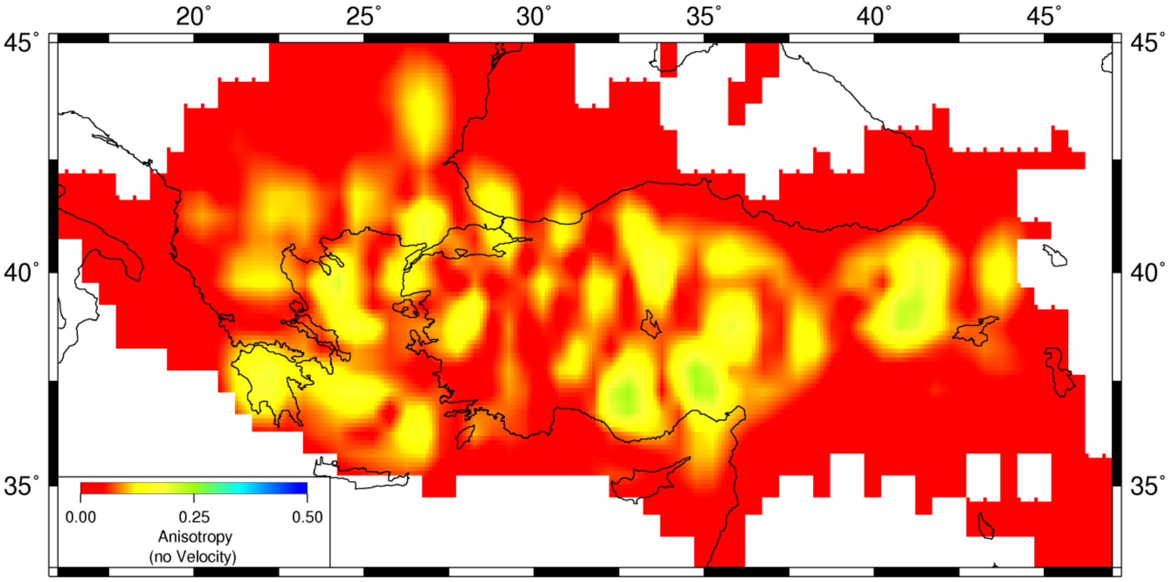

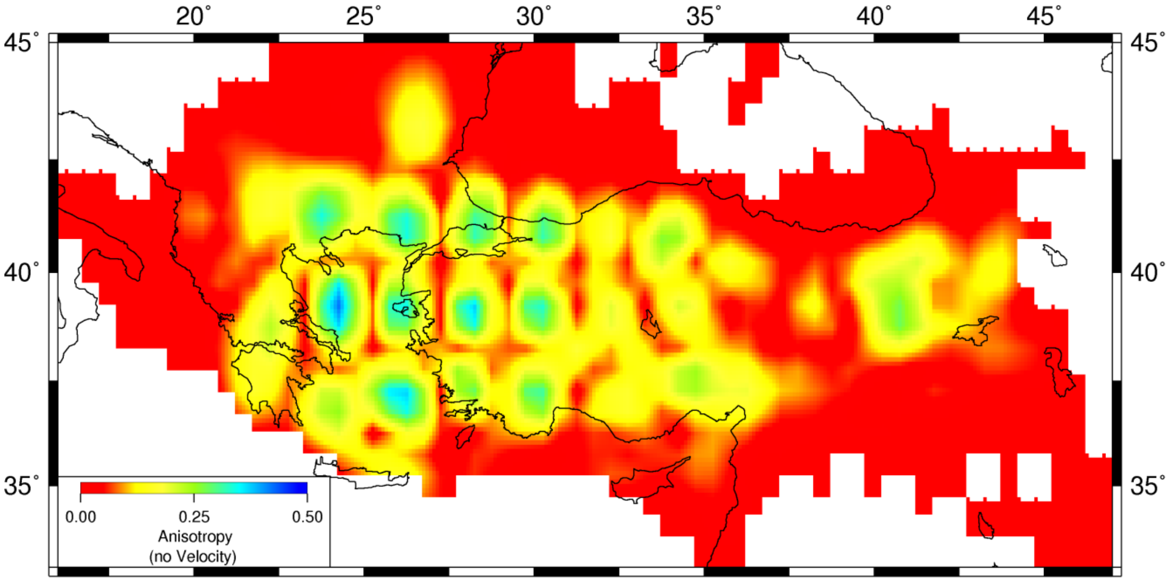

Figure 2.13. P_n anisotropy magnitude (without velocity) checkerboard tests. Starting from top to bottom, pattern sizes are 1°, 2°, 3°, 4°. The damping parameter is assumed as 400

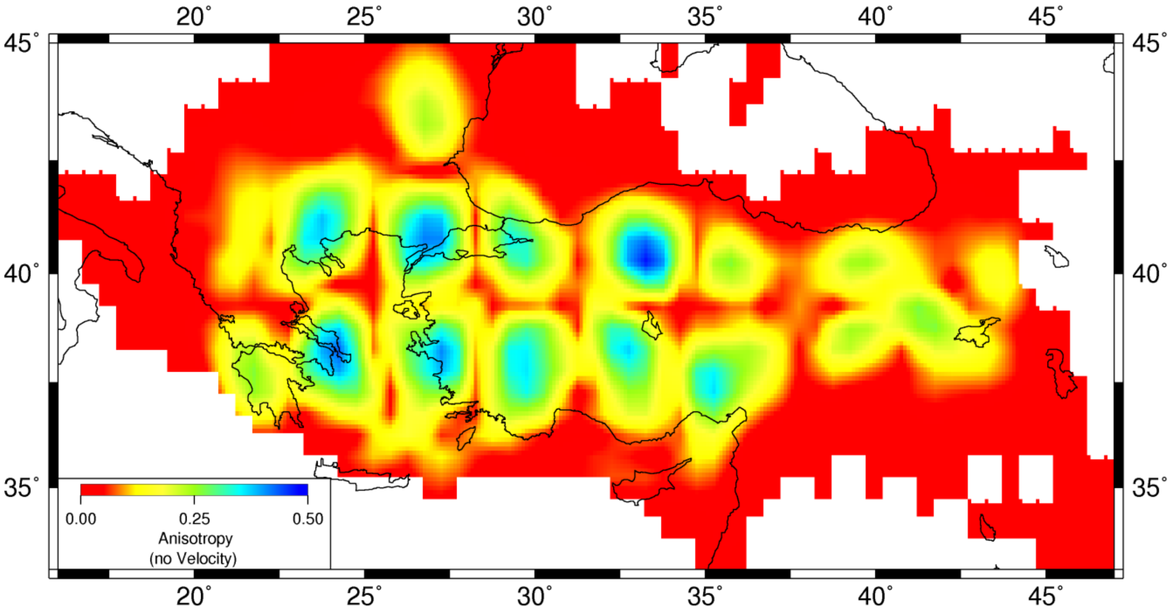

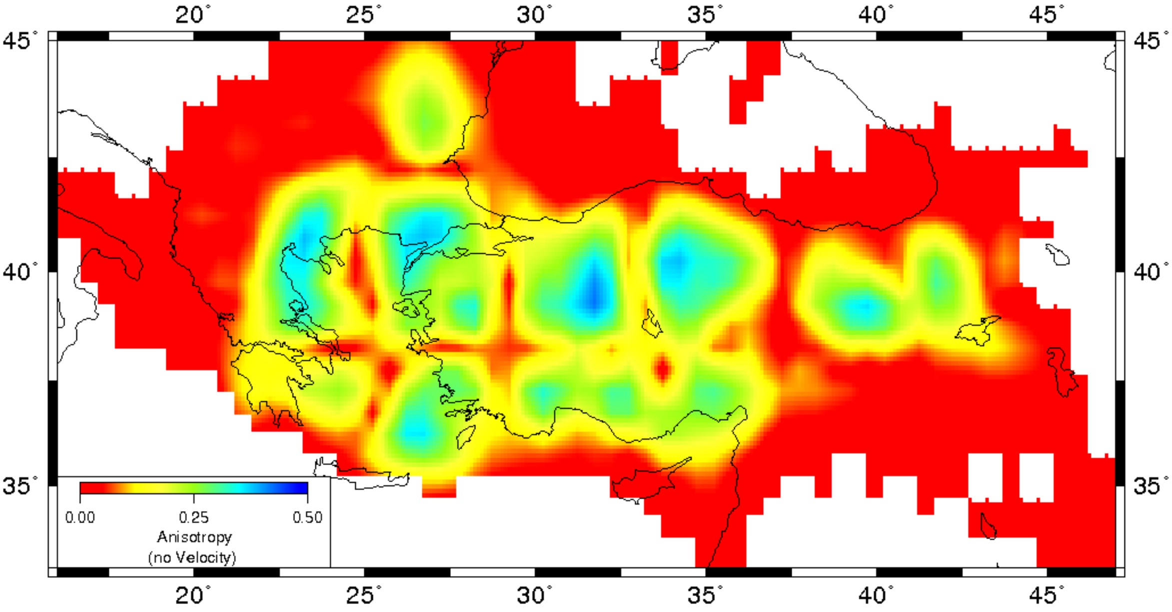

Figure 2.13. Cont.

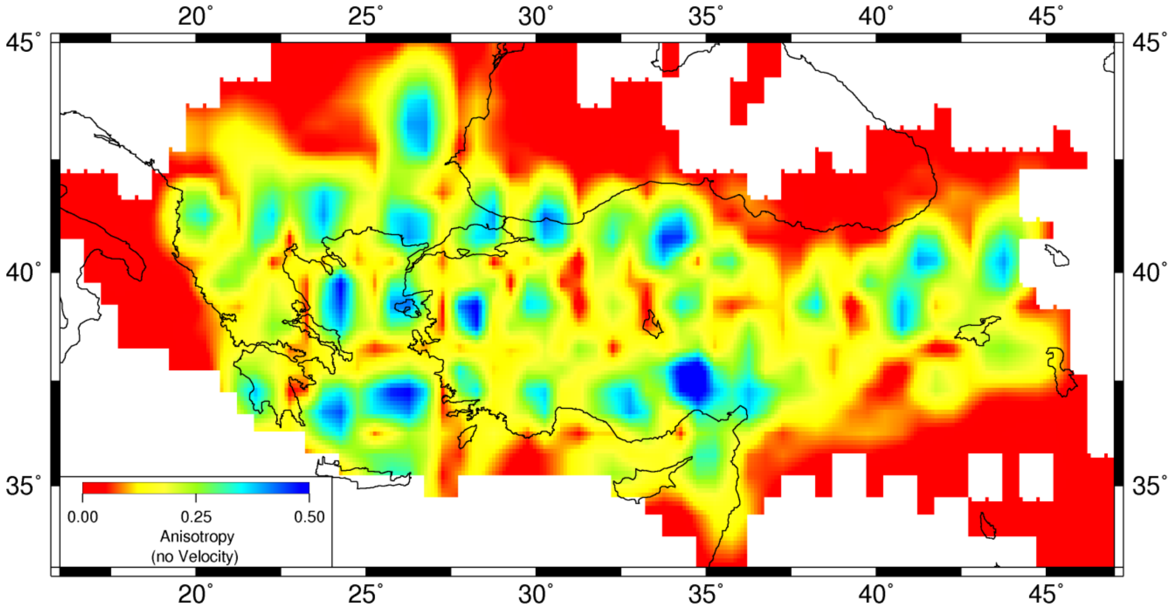

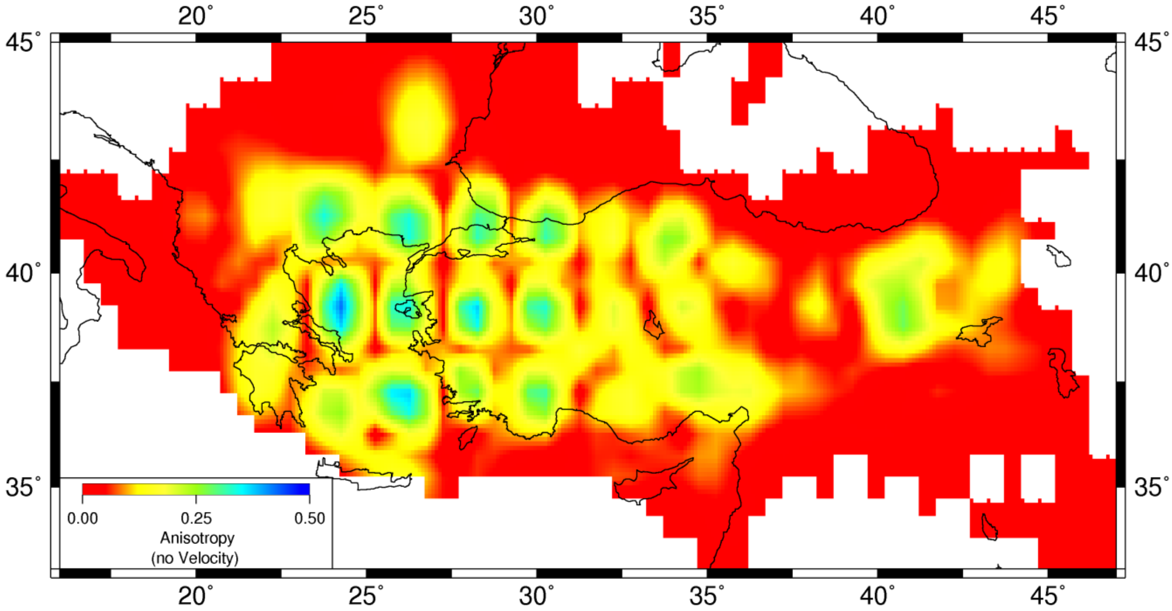

Figure 2.14. P_n anisotropy magnitude (without velocity) checkerboard tests. Starting from top to bottom, damping parameters are change as 200, 400, 600 and 800. The pattern size is assumed as 2°

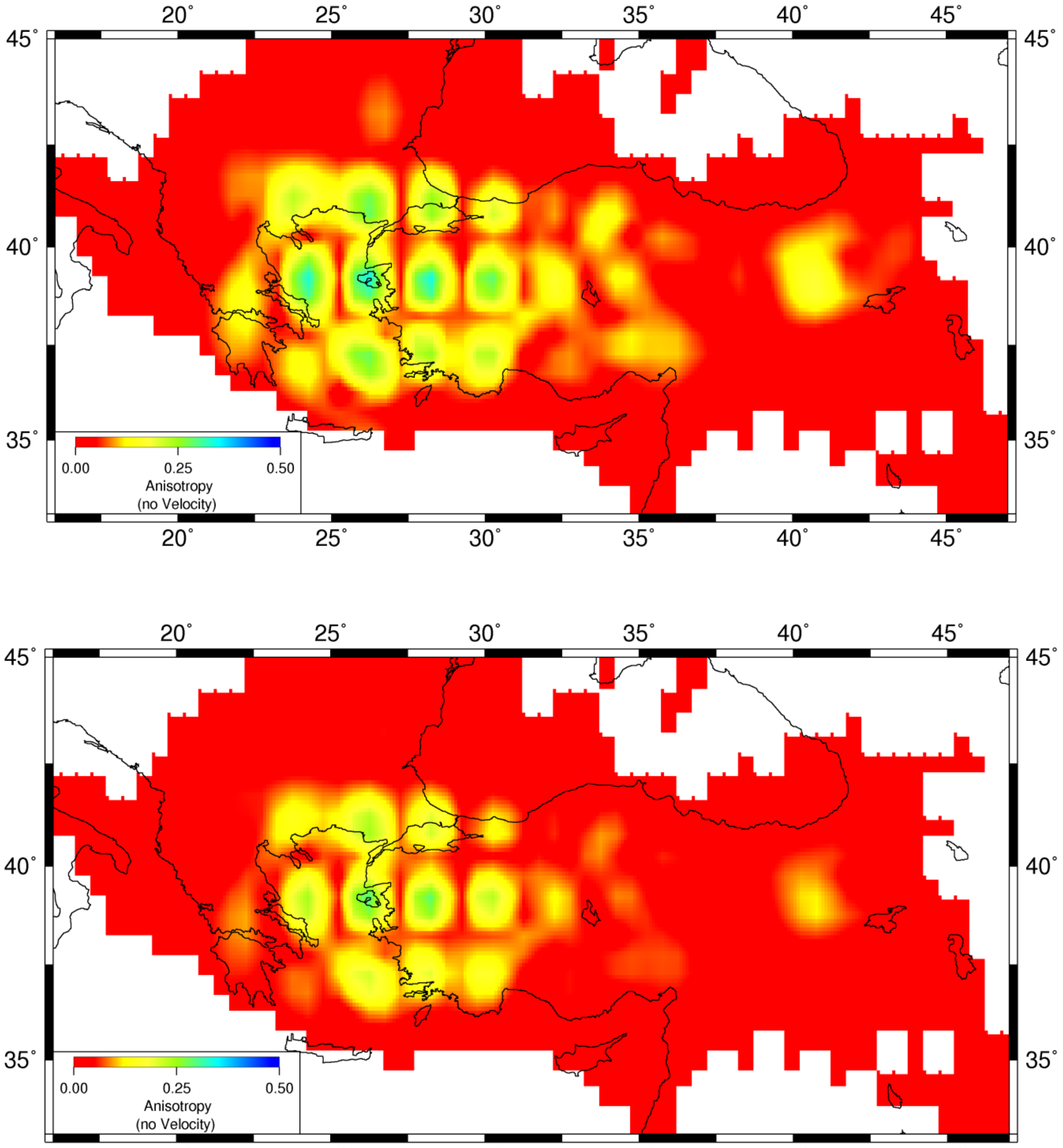

Figure 2.14. Cont.

In the areas with low ray coverage such as Black Sea and the Mediterranean Sea the patterns smaller than 2° cannot be well resolved. The smearing of the patterns also indicates insufficient ray coverage in the Arabian Plateau. The complete recovery is resulted as highest level resolution obtained in the Aegean Region and Western Turkey. The resolution depends on the ray coverage and azimuthal coverage. The anisotropic anomalies cannot be determined accurately if the azimuthal coverage is poor. A good anisotropy resolution occurs within the central to Eastern Turkey, Northern Mediterranean Sea and Western Turkey. The optimum results from the tests are obtained by using 400 for both damping constants and anisotropy. Pattern size is used as 2° for inversion.

It is important to quantify the errors to resolve the observed P_n velocity variations. Bootstrap analyses are used to estimate errors (Hearn and Ni, 1994). This method is a re-sampling technique to determine standard deviation of P_n velocities and station standard error parameters. Bootstrapping is a way to measure whether the distribution has been influenced by stochastic effects. It re-samples the data and reruns the inversion to create a sample data set from the original data. Standard errors of P_n velocity and stations are estimated from 100 runs with replacement.

The results of bootstrap errors for velocity (Figure 2.15) and for the stations (Figure 2.16) are depicted. The velocity errors are high in the Eastern Anatolia (> 0.08 km s^{-1}), eastern Black Sea (> 0.08 km s^{-1}), Arabian platform (> 0.1 km s^{-1}) and Caucasus (> 0.12 km s^{-1}). Low values are observed Western Anatolia and the Marmara region (< 0.01 km^{-1}), Aegean Sea (< 0.02 km s^{-1}), Western Black Sea (< 0.04 km s^{-1}) and central Anatolia (< 0.05 km s^{-1}). Station standard error is between 0 and 1.15 s. In eastern Anatolia systematic large errors are observed due to low coverage. The systematic picking errors and low number of recordings caused large errors (> 2 s) at isolated stations. These stations are eliminated during the final stage of the inversion.

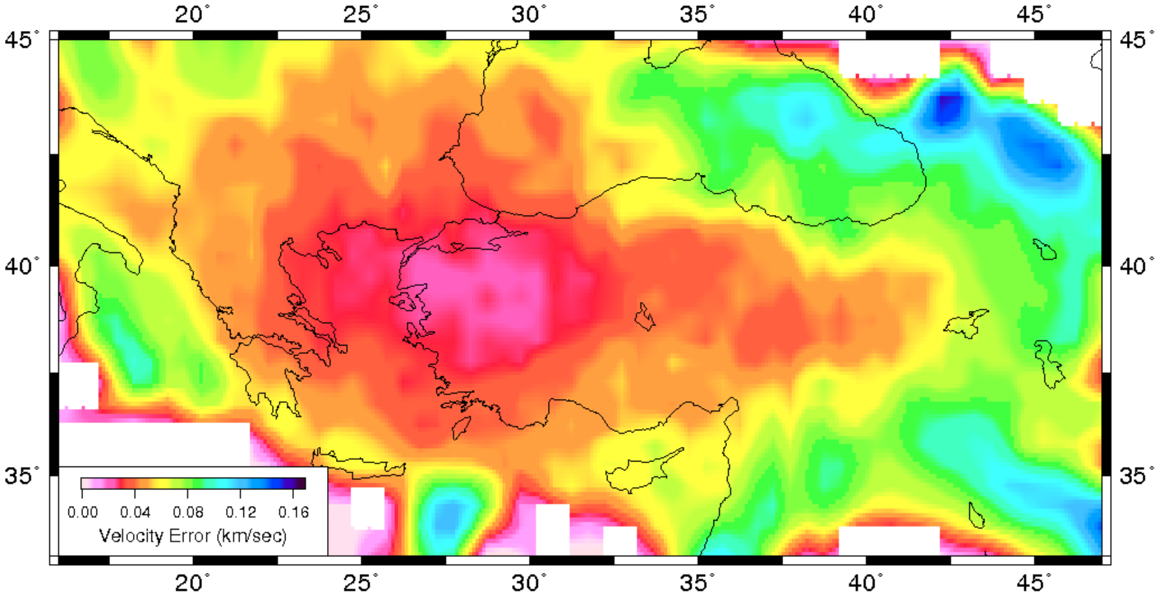

Figure 2.15. Standard deviations of P_n velocity distribution computed from bootstrap analysis. The deviations are estimated from 100 runs with replacement

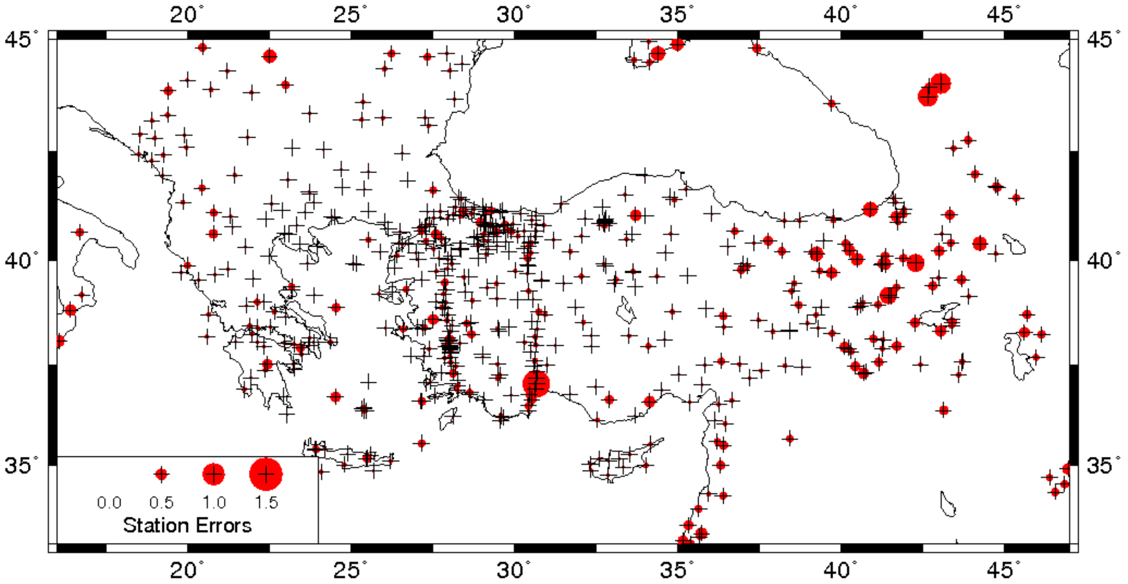

Figure 2.16. Standard deviations of station delays computed from bootstrap analysis. The deviations are estimated from 100 runs with replacement

2.5. Inversion Results

Tomographic images for velocity variations only and velocity-anisotropy are computed together. The inversion with velocity variations are presented in Figure 2.17. P_n velocity and anisotropy distributions from the combined inversion results are depicted in Figure 2.18. The differences are observed in the low velocity region of Eastern Anatolia, along the NAF and the Hellenic Arc between Figure 2.17 and Figure 2.18. Travel time residuals before and after the combined inversion with the histograms of the travel time errors are presented in Figure 2.19. The extension and magnitudes of the anomalies changes with additional anisotropy. Including anisotropy does not change the location of anomalies. The trade-off between velocity and anisotropy may exist in the areas of large velocity contrasts (Figure 2.20 and Figure 2.21). Figure 2.22 shows stations delays. Station delays for both inversions are nearly identical. Crustal thicknesses observed from station delays are presented in Figure 2.23.

Below, the general features of the P_n inversion and discuss the areas of particular interests were described.

2.5.1. P_n Velocity Variations

Large lateral variations in upper mantle velocities are reported in various tectonic settings (Wagner *et al.*, 2008, Eberhart-Phillips *et al.*, 2006; Rossi and Abers, 2006; Zheng and Lay, 2006). These variations mainly result from changes in upper mantle temperature, composition, presence of water and other volatiles (Karato and Jung, 1988; Sato *et al.*, 1989; Karato, 1995; Watanabe, 1993; Babuska and Cara, 1991). The laboratory studies on dry peridodite samples, the main constituent of the upper mantle, at high pressure and temperature indicate that seismic velocities show a rapid decrease with increasing temperature (Sato *et al.*, 1989). Small amount of water can contribute to partial melt by reducing the solidus temperature in the mantle (Karato, 1995; Karato and Jung, 1988).

Overall, the most striking feature of the P_n velocity maps in this study is the observation of very fast and very slow anomalies across the region which clearly shows the presence of a heterogeneous lithospheric structure (Figure 2.17). The P_n velocity is varying from greater than 7.5 km s^{-1} to less than 8.4 km s^{-1} in the study area. High P_n velocities (8.1-8.5 km s^{-1}) are found beneath the oceanic crusts, *i.e.*, Mediterranean Sea, Hellenic Arc, Adriatic Sea as well as Black Sea and Zagros suture zone. Velocities are generally higher beneath Western Anatolia and Aegean than in Eastern Anatolia.

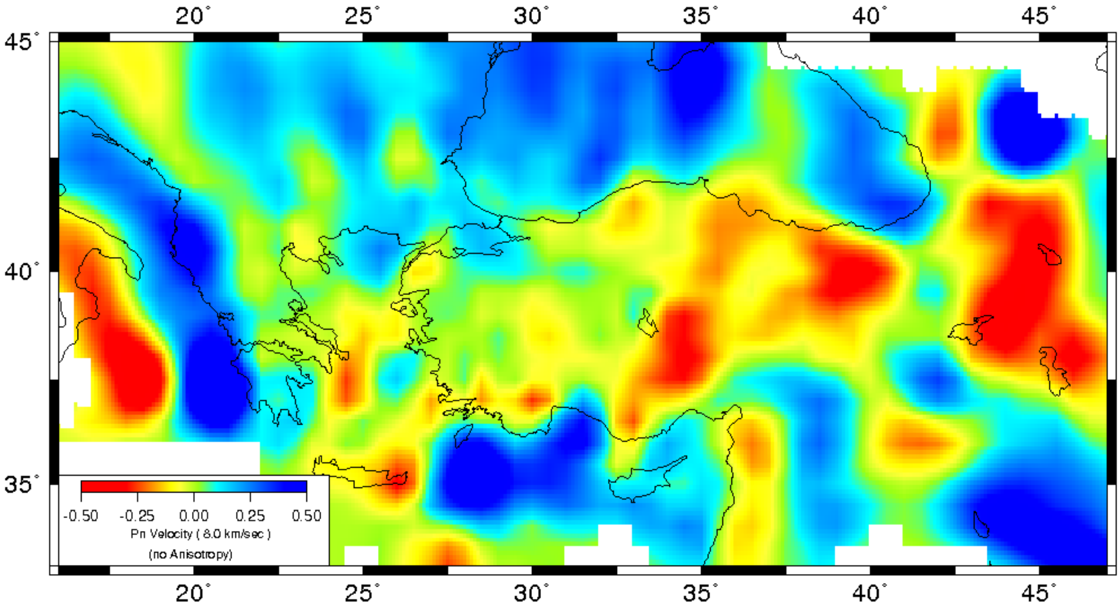

Figure 2.17. P_n velocity distribution with isotropic model only. Only cells with more than 10 arrivals are plotted

Prominent low velocity anomalies are mainly observed in the east (> 33°E) of Central Anatolia with the lowest P_n velocities are observed beneath Eastern Anatolia plateau (< 7.6 km s^{-1}) (Figure 2.18). Many of the low P_n velocity anomalies are beneath volcanic regions. Widespread volcanic activity from upper Miocene to Quaternary is associated with the complete elimination of the Neoteyhyan ocean floor as a result of collision of Arabia and Eurasia during Early Miocene (Yılmaz *et al.*, 1998). The volcanism in the region shows various compositional characters, calc-alkaline in the north and alkaline in the south. Keskin (2003) argued that the subduction component of the volcanics decreases from north to south. This indicates that the volcanism started earlier in the north (~11 Ma) and migrated to the south (~2.0 Ma) as a result of the slab detachment beneath the region (Şengör *et al.*, 2003; Keskin, 2003). The mantle lithosphere was replaced with the low velocity material of asthenosphere beneath the plateau after the detachment of the northward subducting Arabian lithosphere (Şengör *et al.*, 2003; Keskin 2003). They suggested that the lithospheric mantle is either thinned or totally removed in the region with the complete destruction of subducting slab. Low velocities in P_n tomography correlate with the volcanic activity in EAP. However, the anomalies do not appear to cover uniformly the entire region but show in two distinct patches with varying magnitudes and sizes. Similar anomalies both in magnitude and size are also observed by Al-lazki *et al.* (2004). However, in contrary to the previous studies two distinct low velocity zones are separated by relatively higher velocities (7.9-8.0 km s^{-1}). This can be either related to systematic picking errors associated with the attenuation of P_n phases or mantle lid is not completely absent in the region. Another explanation could be the presence of velocity gradient in the mantle.

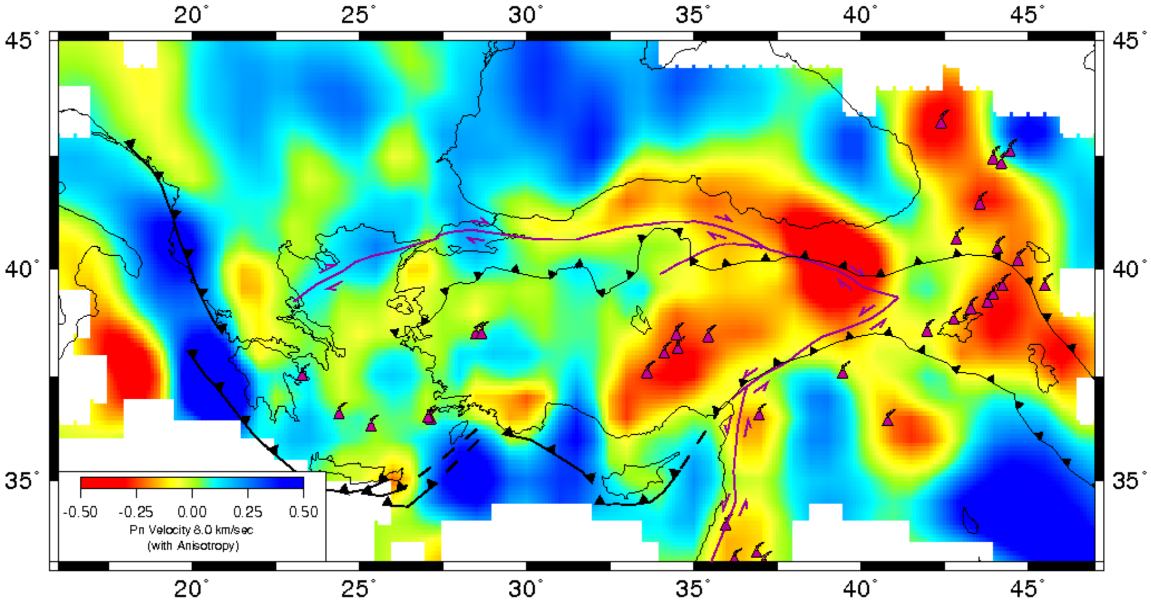

Figure 2.18. P_n velocity distribution with anisotropy. Only cells with more than 10 arrivals are plotted

A prominent low velocity anomaly also appears in Central Anatolia Volcanic Zone (CAVZ) (Figure 2.18). The low velocities (< 7.7 km s^{-1}) coincide with the Neogene-Quaternary volcanism of the area. The tomographic images of Biryol *et al.* (2010) also show slow velocity perturbations as deep as 200 km beneath the CAVZ. However, the low velocities have limited spatial extent in contrast to low velocities of P_n tomography. P_n

velocity anomaly covers a larger area and extends toward the low velocities of Eastern Anatolia.

The volcanism in the CAVZ is mainly characterized by calc-alkaline and also mild alkaline compositions (Kuşçu and Geneli, 2008). The calc-alkaline volcanism is typically observed on convergent plate margins, but is not limited only to this tectonic setting (Kuşçu and Geneli, 2008). The presence of both calc-alkaline and alkaline magmatism is explained either by opening of an asthenospheric window within the subducting oceanic plate, or through channels along major lithospheric faults (Pasquare *et al.*, 1988; Kuşçu and Geneli, 2008). Based on the analysis of the volcanic rocks in the Hasandağı of CAVZ, Deniel *et al.* (1998) also pointed the decreasing influence of the subducted or crustal component through time and the increasing contribution of melt enriched lithosphere. The calc-alkaline character of volcanism in absence of more recent subduction would indicate the influence of the early subduction of the African plate under the Eurasian plate from Eocene to Miocene (Deniel *et al.*, 1998). They suggested that the evolution towards alkaline compositions through time is related to the development of extensional tectonics in Central Anatolia in the Late Miocene.

P_n velocities are higher on the south of the Bitlis suture zone, boundary between high velocity of the Arabian platform and low velocity zone of Eastern Anatolia. Very high P_n velocities are observed beneath the Zagros suture zone (> 8.3 km s^{-1}). The ray coverage in this region is poor. However, both magnitude and size of the anomaly are so large that the patterns with a size of 3° can be determined and the results are consistent with previous studies (Al-Lazki *et al.*, 2004; Kaviani *et al.*, 2007).

Lower velocities (< 7.9 km s^{-1}) are also observed in a narrow range elongating in the N-S direction of the DSF system which forms the plate boundary between Africa and Arabia. The lower velocities there coincide with the Neogene-Quaternary volcanic outcrops observed at the surface. The low velocity region is surrounded by higher velocities of Arabian platform and Mediterranean basin (Figure 2.18).

Beneath the Eastern Mediterranean basin, P_n velocities are generally higher (> 8.2 km s^{-1}) but do not show the same strength along the Cyprus and Hellenic belt. The velocities are higher on the west of Cyprus than the east with a sharp transition at Paphos transform fault (Figure 2.18). The high velocity zone on the west of Cyprus extends from the Paphos discontinuity to Isparta Angle in the north-south direction with decreasing intensity. Further west, a more pronounced high velocity zone (> 8.4 km s^{-1}) on the south of the Rhodes Island is observed. The two high velocity zones seem to be continuous but the tomographic image has poor resolution on the south. On the north of these high velocity zones, lower velocities (< 7.8 km s^{-1}) are observed between the Rhodes Island and the Antalya Bay.

Based on the teleseismic tomography, it is proposed that once continuous subducting slab extending from Hellenic Arc to Bitlis suture have now lost its integrity and is discontinuous (Faccenna *et al.*, 2006; Biryol *et al.*, 2010). The teleseismic tomographic images show the termination of the slab on the east of Cyprus. On the west of Cyprus, a minor tear was located at the Paphos transform fault and a major tear was located at the Strabo transform zone (Faccenna *et al.*, 2006; Biryol *et al.*, 2010). The low velocity zones could be associated with the flow of low velocity asthenospheric material through the slab tears.

From the 35°E to the Aegean Sea, P_n velocities appear to be relatively uniform. The velocities are varying between 7.9 and 8.1 km s^{-1} with slight decrease on the south and increase on the north. The higher velocities (8.1 km s^{-1}) coincide with the Menderes massif in Western Anatolia and Metamorfic Core Complexes in the Aegean. Western Anatolia is characterized by a broad scale lithospheric extension. Extension started as early as late Oligocene and widespread by the late Miocene (Angelier, 1978; McKenzie, 1978; LePichon and Angelier, 1981; Şengör *et al.*, 1984; Taymaz *et al.*, 1991). The GPS surveys show that N-S oriented crustal extension increases in amplitude from north to south (Kahle *et al.*, 1998; McClusky *et al.*, 2000). Significant crustal stretching and thinning is observed both in Western Anatolia and the Aegean Sea. An initial crustal thickness of 45 km is reduced to an average of 33 km since late Miocene. Metamorphic core complexes observed in the Aegean Sea is a result of such large stretching in the crust. It was pointed out that upper mantle rocks at high temperatures (> 800° C) become entirely ductile and the viscosity contrast between lower crust and mantle drops significantly (Ribe, 1989). As a result the Moho topography remains flat and the mantle velocities are more uniform.

Beneath central Greece and Dinarid-Hellenic Mountain chain, the velocities are low (< 7.8 km s^{-1}) and there is significant trade-off between velocity and anisotropy. In the Adriatic Sea, high P_n velocities (> 8.2 km s^{-1}) are observed. Similar anomalies are also observed in previous works (Hearn, 1999; Al-Lazki *et al*., 2004).

A velocity contrast between Pontides and Anatolia-Taurides is observed along the NAF with lower velocities located on the north (Figure 2.18). The contrast is continuous from the eastern part of NAF to the west (> 32°E) with decreasing magnitude. This is an indication that the NAF is following the zone of Neotethyan suture and penetrating into the uppermost mantle (Bozkurt, 2001; Şengör *et al*., 2005; Biryol *et al*., 2010). To the west of 32°E, the NAF is crossing a higher velocity zone (> 8.1 km s^{-1}) and a velocity contrast across the fault does not appear.

In Figure 2.19 travel time residuals before (red dots) and after (green dots) inversions were depicted. The critical distance for P_n arrivals are at ~180 km. Decrease in the residuals after inversion is obvious. The residuals are changing between ±10 seconds before inversion and ±4 seconds after inversion.

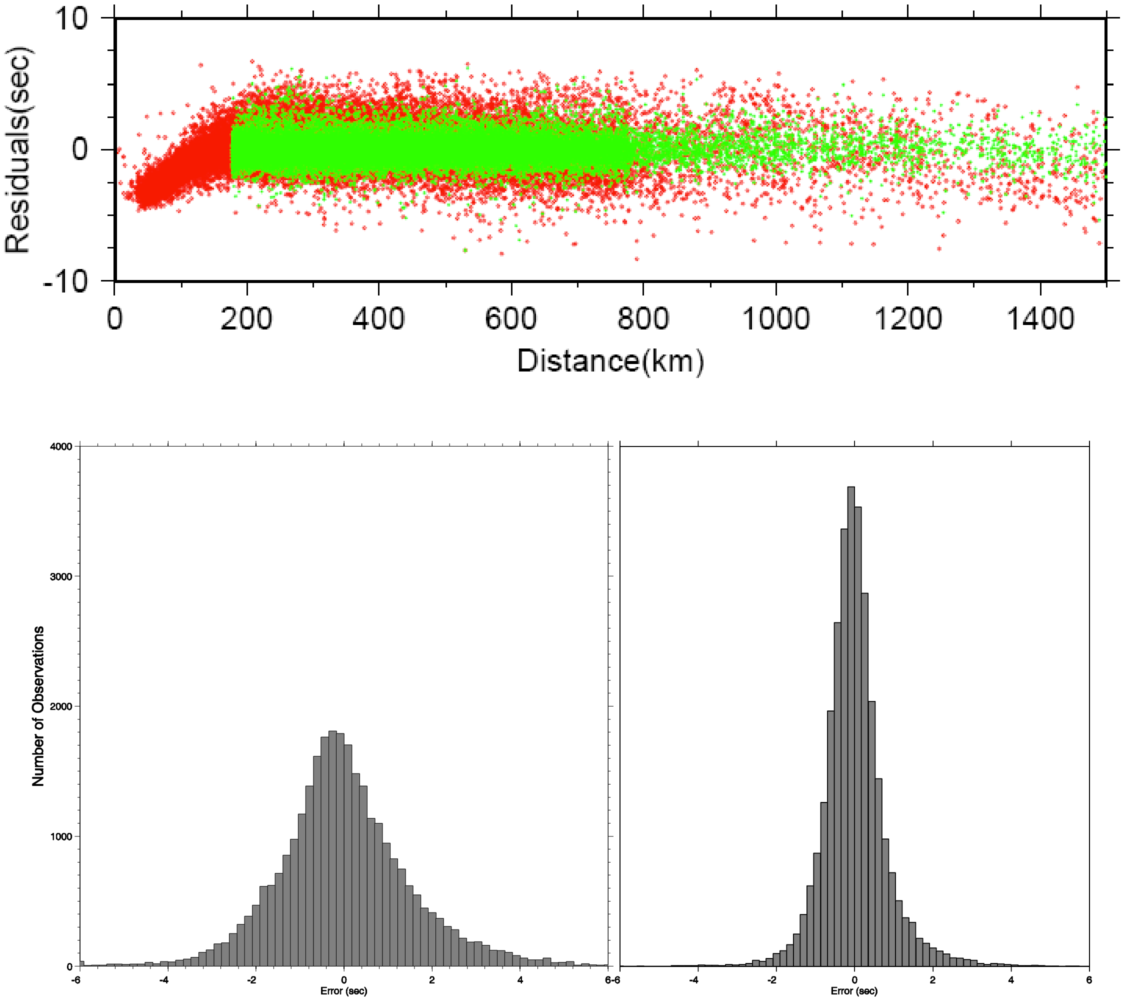

Figure 2.19. Observed travel time residuals (red dots) before and after P_n tomography (green dots). A reducing velocity of 8.0 km s^{-1} is used to plot travel times

2.5.2. P_n Anisotropy

Work on the mantle anisotropy from various tectonic environments present examples of coherent deformation of crust and mantle (Silver, 1996; Savage, 1999; Polet and Kanamori, 2002; Kreemer *et al.*, 2004). However, as in the case of the eastern Mediterranean it is not always possible to find such clear correlations. The source of anisotropy in the upper mantle is considered to be the lattice-preferred orientation (LPO) of olivine minerals as a result tectonic deformation (Nicolas and Christensen, 1987; Christensen, 2004). Deformation tends to align with the fast axis of olivine mineral in the major strain direction (Ribe, 1992). Therefore, the coherent deformation of the crust and upper mantle would reflect the latest significant deformation on the mantle. In general, the deformation is parallel to the direction of maximum shearing under a simple shear regime. In subduction zones, the fast axis is parallel to the trench and in back arc regions the fast directions are either parallel or perpendicular to trench. Arc-parallel anisotropy may be due to water in the mantle wedge changing the deformation planes in the olivine (Karato and Sato, 1998). The fast axis is parallel to the direction of extension under extensional regime (Silver, 1996; Buttles and Olson, 1998; Savage, 1999; Jolivet *et al.*, 2009).

Overall, the anisotropy anomalies observed in this study show a higher level of lateral variations than P_n velocity anomalies (Figure 2.21). A maximum value of 0.8 km s^{-1}, which corresponds to about 10 per cent of anisotropy, is observed. We obtained large anisotropic anomalies on the southern coast of Anatolia, Western Anatolia and Central Greece. Large perturbations in anisotropy are observed in the areas of volcanic activity with no clear orientation.

The P_n anisotropy in Eastern Anatolia is complex (Figure 2.20). Both directions and magnitudes of the fast axis are varying drastically in the region with low P_n velocities (Figure 2.21). The anisotropy shows no apparent correlation with GPS velocities and SKS splitting directions (Sandvol *et al.*, 2003; Biryol *et al.*, 2010). Partial melt might prevent the formation of preferred orientation by promoting a transition from dislocation creep to diffusion creep (Savage, 1999). If the thermal evolution of Eastern Anatolia as a result of subduction detachment is accepted the absence of mantle lid could explain the observed anisotropic pattern in the upper mantle.

The anisotropy directions are strongly varying along the southern coast of Anatolia indicating significant influence of the subducting plates. An interesting pattern of the anisotropy takes place in the region of Hellenic-Cyprian arcs and DSF. A strong change on the anisotropy orientations is observed between the DSF and the Paphos transform fault. This anomaly is located in a region with the minor slab tear observed in deep tomographic images (Biryol *et al.*, 2010). The flow of asthenospheric mantle through the slab tear could be responsible for such anisotropic fabric.

In Western Anatolia, the fast axis is almost in the N-S direction and the amplitude is increasing towards the south (Figure 2.20). However, deviations are apparent from N-S direction in the south, which may be related to the subduction geometry and tear in the slab. There is more consistency between the anisotropy directions and the maximum extension directions determined from GPS observations (Aktuğ *et al.*, 2009). The magnitude of the anisotropy is quite uniform in the Aegean Sea from the north to south and starts diminishing in the area of arc volcanism. P_n anisotropy, SKS splitting directions and GPS vectors are coherent in the Aegean Sea, but significantly different beneath continental Greece (Figure 2.20). The fast axis is oriented at NE-SW in the Aegean Sea and N-S in Central Greece. Shear wave splitting vectors indicate NE-SW orientations in the Aegean Sea and NW-SE direction in Central Greece (Hatzfeld *et al.*, 2001). Kreemer *et al.* (2004) indicated that the present-day extension orientations are systematically in Northern Aegean, and more N–S oriented than SKS splitting orientations and concluded that the current shear-dominated surface deformation pattern is not (yet) reflected by significant anisotropy in the lithosphere. Along the Dinarides-Hellenic belts, the fast axis is oriented in NW-SE direction parallel to the arc. The observed anisotropy is the result of the subduction although it is not active since the Miocene (Hearn, 1999).

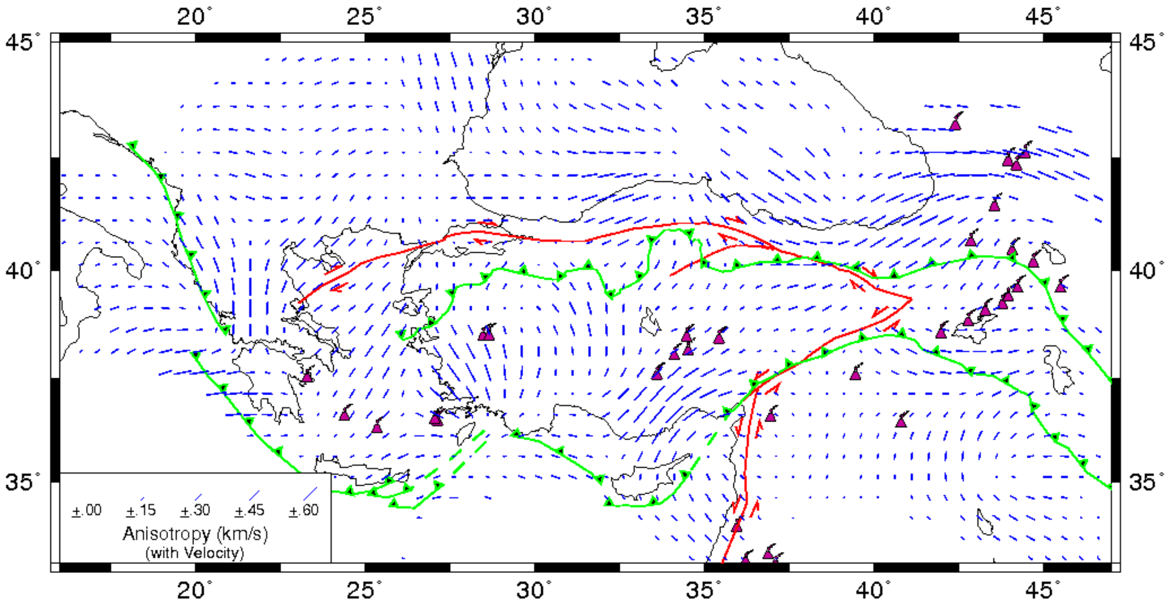

Figure 2.20. P_n anisotropy in the study area. The blue lines indicate fast direction of P_n velocity. The length of the line is proportional to the strength of anisotropy. The major faults and plate boundaries and volcanoes are also shown (pink triangles)

Central Anatolia shows very small anisotropy between 33°E and 37°E where low P_n velocities are observed (Figure 2.21). West of 33°E the fast axis is oriented almost in the N-S direction. Towards north along the İzmir-Eskişehir-Ankara suture, significant deviations from N-S direction are observed. No clear correlation was observed between the fast axis of P_n anisotropy and the trace of the NAF. The orientation of the fast axis is changing within the central NAFZ from NW in the east to NE in the west.

In the Marmara Region, the anisotropy is small and oriented in E-W direction (Figure 2.21). However, the age of the NAF in the region may not be sufficient to create detectable anisotropic mantle fabric. In order to reorient LPO in the shear-plane orientation at least 4 Ma are needed and this is consistent with the other observations that the NAF propagated into the Aegean during the Pleistocene (Kreemer *et al*., 2004; Şengör *et al*., 2005). Between Greece and Marmara Region the fast axis of anisotropy aligns better with the geometry of the NAF, but this may be more related the NE-SW regional extension.

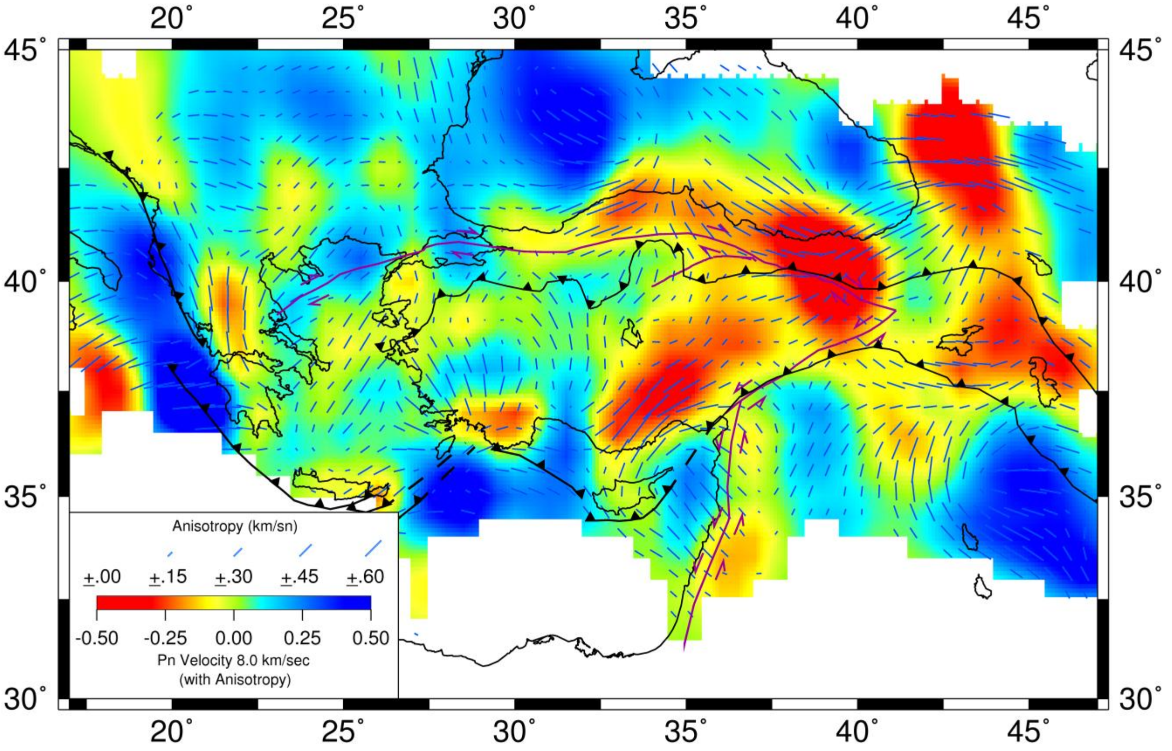

Figure 2.21. P_n velocity, anisotropy with the major faults and plate boundaries. Pink triangles represent volcanic mountains

2.6. Station delays

Figure 2.22 shows the station delays obtained from the tomographic inversion. The station delays provide information only on the relative crustal thickness variations. Early arrivals indicate thinner-faster crust and late arrivals for thicker-slower crust. The station residuals in Central Anatolia show very low values (< 0.1 s) indicating relatively flat Moho topography. Early arrivals are observed at the stations in Marmara, Western Anatolia and Aegean Sea. Large positive delays are situated along the southern coast of Anatolia and Dinarides-Hellenides. In Eastern Anatolia positive station delays are observed while very small or negative stations delays are observed on the south of Bitlis suture zone.

We computed crustal thickness variations using the station delays. We selected the stations with station errors less than 0.5 seconds, which correspond to ±6 km crustal thickness errors. The selected station delays show non-uniform distribution throughout the region. We used a krigging algorithm to interpolate the station delays for a more uniform distribution. We then converted the station delays to crustal thicknesses. The regional variations of crustal velocities are not well known. We therefore used a constant velocity of 6.3 km s^{-1}. For 1.0 second delay time, the change in the crustal thickness is approximately 11 km and ±10 per cent perturbation of the crustal velocity would result in ±1.5 km change in the thickness assuming an upper mantle velocity of 8 km s^{-1}. It is important to remember that the crustal thickness determined from the delay time of a station sample an area of ~70 km in diameter. Additional smoothing is imposed by the krigging limits the horizontal resolution.

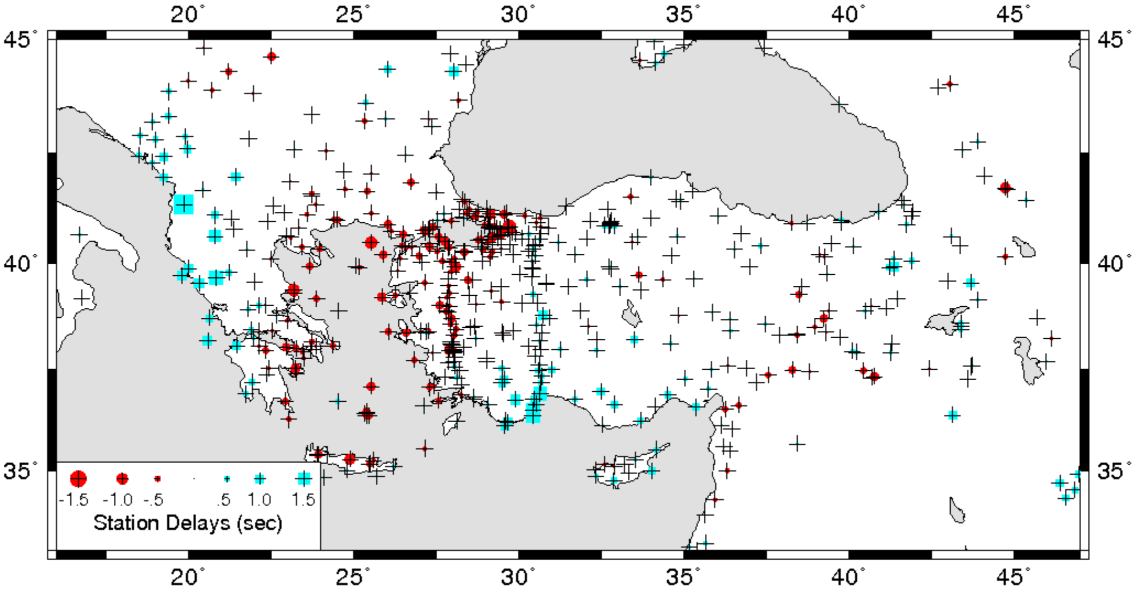

Figure 2.22. Station delays. Negative delays (red circles) are indicative of a thinner crust (thinner than the average 35 km of the reference model); positive delays (blue squares) are indicative of a thicker than average crust

Figure 2.23 shows the crustal thickness variations. Large thicknesses are observed along the southern coast of Turkey (40-48 km) and on the Dinarides-Hellenides Arc (40-48 km). In the Eastern Anatolia, thicknesses are varying from 38 to 40 km. The crust is thinner beneath the Arabian plateau varying between 32 and 36 km. In the Western Anatolia and the Aegean Sea, the thicknesses are varying between 28 and 32 km.

In Eastern Anatolia, Zor *et al*. (2003) computed crustal thickness between 40 and 48 km. The average crustal thickness is varying from 38 km beneath the Arabian platform to 50 km on the Pontides with a regional average of 45 km (Gök *et al*., 2007). The values obtained in this study are quite lower (40-42 km). The large station errors in the area are the indication of insufficient number of P_n arrivals and the average crustal velocity may not be representative of the region.

In the Marmara Region, the average crustal thickness is ~32 km. Laigle *et al*. (2008) obtained the crustal thickness beneath the Sea of Marmara as 26 km and thicker in the east and west of the sea. The receiver function analyses indicate average crustal thickness of ~30 km on the north of Marmara Sea and increasing to ~34 km on the south (Zor *et al*., 2006).

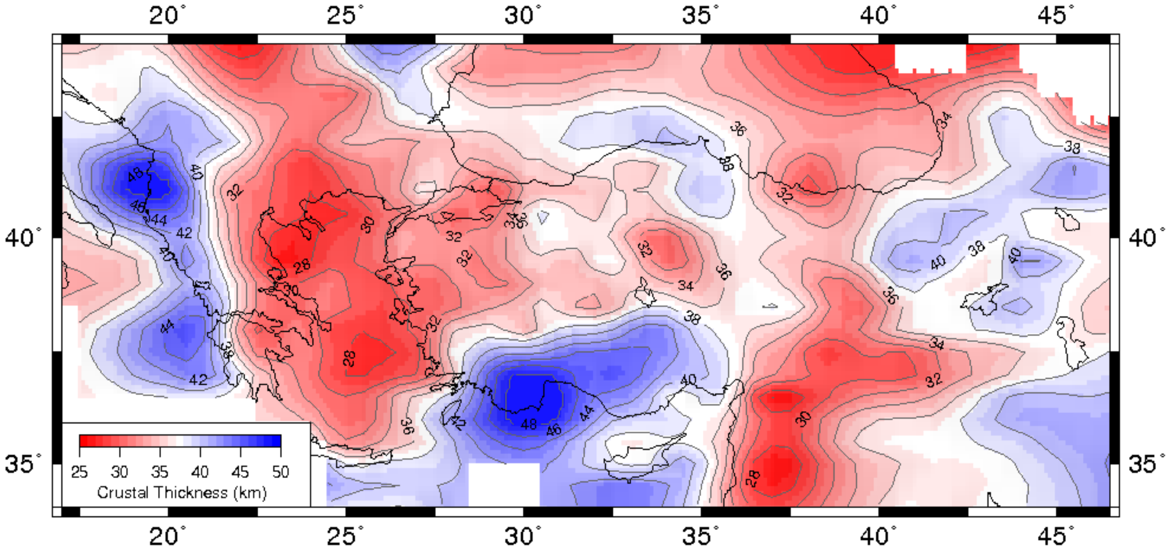

Figure 2.23. Crustal thickness map computed from the stations delays. A constant velocity of 6.3 km s^{-1} and 35 km of crustal thickness are used

The Moho depths in the Aegean are varying between 28 and 32 km. Based on the receiver function analysis, Sodoudi *et al*. (2006) computed crustal thicknesses of 20-22 km on the southern part of the Aegean and found relatively thicker crust (25-28 km) on the Northern Aegean Sea. Similar values were obtained by DiLuccio and Pasyanos (2007) indicating an increase of crustal thickness of 20-25 km in the southern, Central-Western Aegean, whereas reaching 32 km in the Northern Aegean.

The crustal thickness obtained from receiver function analysis at Isparta Angle is found ~42 km, significantly thicker than 35 km in Central Anatolia (Zhu *et al.*, 2006). The results in this study indicate a significant increase in the crustal thickness from the Isparta Angle (~39 km) towards the southern coast of Anatolia (~48 km). Such a large increase can be attributed to the subduction of African lithosphere.

2.7. Conclusions

In this study a new tomographic image of P_n velocities beneath Turkey and surroundings were presented. Both the quality and quantity of the observations provided finer details of the upper mantle velocity perturbations and anisotropy. The most general feature of the tomographic images is the Anatolian block characterized by low-moderate P_n velocities surrounded by higher velocities of oceanic crust and often associated with volcanic arcs. The low velocity anomalies observed in the eastern Anatolia is associated with the volcanism following the break-off of the subducting oceanic lithosphere. Along the NAF a large velocity contrast but no clear anisotropic orientation related to shear deformation is observed. In Western Anatolia and the Aegean Sea, P_n velocities show relatively small perturbations from the average value of 8.0 km s^{-1}. The anisotropy is mostly in the N-S direction and consistent with the regional extension. Both P_n velocity and anisotropy along the coast of Southern Anatolia and easternmost Mediterranean shows strong perturbations. These perturbations are related to the present geometry of the subducting slabs and the flow of asthenospheric mantle due to the slab tears. The large crustal thicknesses are estimated along the southern coast of Anatolia and Dinarides-Hellenides. A gradual increase in the crustal thicknesses is observed from the Aegean Sea (28-30 km) to central Anatolia (35-37 km).

The results presented in this study put more constraints on the active tectonics in the region. The coherency of the P_n anisotropy, SKS splitting directions and GPS velocities show that the Aegean Sea is the only region in the study area that whole lithosphere is deforming coherently. This may indicate that one of the driving forces for the active tectonics beneath the Aegean is mantle flow. In the other parts of the region, such coherency is not apparent. The mechanisms such as density driven convections (*e.g.*, Faccenna and Becker, 2010), smaller scale mantle flow related to slab tears as well as the extrusion of the Anatolian plate should be considered for a more comprehensive model. More detailed observations on SKS splitting directions with better density models derived from teleseismic and surface wave tomography will allow us to evaluate the alternatives. The results of the P_n tomography will play important role to validate the hypotheses as it provides the critical information on the deformation between surface observations and mantle flow.

3. UPPER MANTLE ANISOTROPY FROM SHEAR WAVE SPLITTING

3.1. Introduction

The relative motion of the tectonic plates is well constrained by the modern geodetic observations (e.g., Kreemer *et al*, 2003). However the motion of Earth's surface or lithosphere relative to the deep mantle has been in debate since the advent of the plate tectonics (Conrad and Behn, 2010). The Absolute Plate Motion (APM) is a term to define the motion of the lithosphere relative to the lower mantle. Despite the importance of the APM on the motion of the lithosphere it is still poorly known. In computing APM there are some key assumptions: 1) the lithosphere is stable relative to the lower mantle; 2) hot plumes have the origin of lower mantle, therefore do not move significantly in time and space (Kreemer, 2009). In the absence of lateral viscosity variations the convection in the mantle which drives the plate motions induce no net moment on the lithospheric plates, and no net rotation of the lithosphere (Solomon and Sleep, 1970; Conrad and Behn, 2010). Therefore no-net rotation frame (NNR) can be considered as a reference frame to characterize the global motion of the plates. However the viscosity in the mantle is not homogenous and as a result, induce net lithosphere rotation (Becker, 2006; Conrad and Behn, 2010; Kreemer, 2009). The hot spot volcanism has also been used as a deep mantle reference frame with the assumptions that they are the surface expressions of the stationary plumes rising from the deep mantle. However the later studies indicated few cm per year of the relative motions of the active plumes (Morgan, 1972; Duncan, 1981; Molnar and Stock, 1987).

More recent studies suggested that the seismic anisotropy in the asthenosphere could provide better constraints on the motion of the lithosphere relative to deep mantle (Becker, 2008). The anisotropic propagation of seismic shear waves in the mantle involves two orthogonally polarized components that split and travel with different velocities (Silver, 1996; Savage, 1999). Splitting measurements of teleseismic shear SKS waves give the azimuth of the fast wave polarization and the delay time between fast and slow waves, and the direction of fast polarization is considered as and indications for mantle deformation (Zhang and Karato, 1995; Karato *et al.*, 2008). The most significant part of the anisotropy for SKS waves is due to the upper mantle (mostly the asthenosphere) and only ~10 per cent to the crust (Silver, 1996; Savage, 1999).

The anisotropy in the asthenosphere is controlled by the differential motion between lithosphere and mantle beneath asthenosphere (Savage, 1999) and is the result of the deformation by the dislocation creep in the asthenosphere between 100 and 300 km depths which align olivine crystals with lattice preferred orientation (Karato and Wu, 1993). It is assumed that SKS anisotropy originates in the asthenosphere and aligns with the APM. However this assumption is partly true. There have been better correlations underneath oceanic lithosphere but it is more complicated on the continental lithosphere (Conrad *et al.*, 2007). In many continental areas shear wave splitting directions deviate significantly from the APM directions (Kreemer, 2009). Therefore it is important to characterize the components of the induced anisotropy in the asthenosphere: 1) induced by mantle flow, mainly by density heterogeneities; 2) relative plate motions in the NNR frame; 3) by the net rotation of the lithosphere (Conrad and Behn, 2010).

Shear Wave Splitting is a technique to detect anisotropy in the upper mantle. Shear waves refract from Core-Mantle Boundary (CMB) (such as; SKS, SKKS, PKS *etc.*,) and reaches to the station as almost vertically and polarize linearly in the ray path plane if the medium is isotropic. These phases are well observable between the epicentral distances of 90° and 130°. In this work, SKS phase, which travel through the mantle as an S wave, through the outer core as a P wave and through the lower mantle as an S wave (Figure 3.1), is used because of its high signal-noise ratio and easily recognized. The initial polarization of the SKS phase is well known due to control by P-to-S conversion at the CMB. If the medium is anisotropic, shear wave splits into two orthogonal directions traveling with different velocities. The splitting time between the fast and slow waves (δt) and the fast polarization direction (φ), provide good lateral resolution of upper mantle anisotropy. The polarization angle, φ, determines the orientation of the anisotropic symmetry system and delay time, δt, is proportional to the thickness of the anisotropic layer and strength of anisotropy.

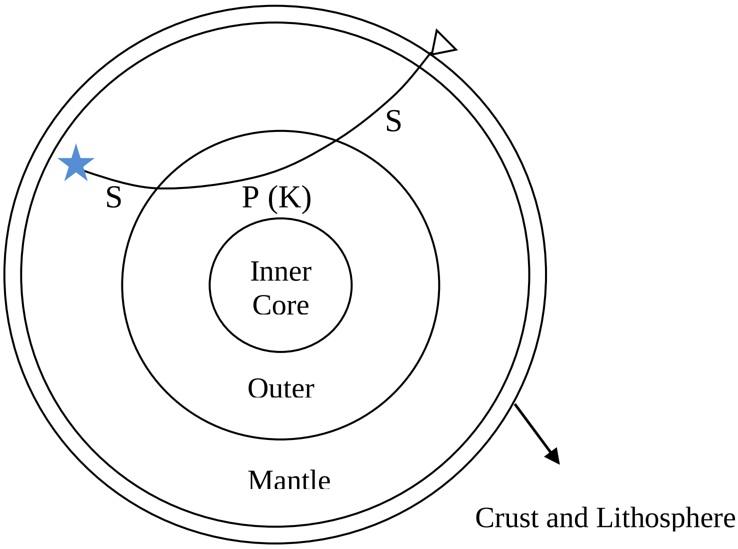

Figure 3.1 Schematic diagram of SKS shear wave propagation path

3.1.1. Previous Studies in the Eastern Mediterranean

The Eastern Mediterranean has been the focus of international efforts during the last two decades. Both the geological research and the acquisition of GPS data make the region an important area in the current debate on the mechanics of the continental lithosphere. Figure 3.2 shows the GPS data from the observations of 20 year within the eastern Mediterranean (Cocard *et al*. 1999; McClusky *et al*. 2000; Clarke *et al*. 2002; Burchfiel *et al*. 2006; Kotzev *et al*. 2006; Reilinger *et al*. 2006; Aktug *et al*. 2009; Hollenstein *et al*. 2008; Özeren and Holt, 2010). The GPS data set shows an increase of the velocities with respect to Eurasia toward the west compatible with the observed active extension. Arabian plate moves NNE with constant velocity of 25 mm per year since 40 Ma. The relative motion between Arabian plate and Anatolia is consistent with EAF as 9±1 mm per year slip rate (McClusky *et al*., 2000). The age of NAF is about 11-12 Ma and drives Arabian plate to the west with 23-26 mm per year slip rate (McClusky *et al*., 2000; Reilinger *et al*., 2006; Le Pichon and Kreemer 2010). Central Anatolia rotates counterclockwise with 20-25 mm per year. GPS velocities are greater in Aegean than Anatolian and slip rates increasing from east to west and reaching 32 mm per year in the Mediterranean (Reilinger *et al*., 2006).

Different interpretations of the observed GPS data are proposed. The models agree on the rigid motion of the main part of Anatolia about an Eulerian pole north of the Egyptian coast and the different hypotheses seem to fit the GPS velocity field in the Aegean Sea. Several rigid blocks are proposed (Nyst and Thatcher, 2004) as opposed to a continuous velocity field in driven by gravitational forces between the elevated plateau of Eastern Turkey and the oceanic crust in the west (Floyd *et al.*, 2000; Özeren and Holt, 2010) or a model using fracture mechanics and a propagating strike-slip fault (Flerit *et al.*, 2004).

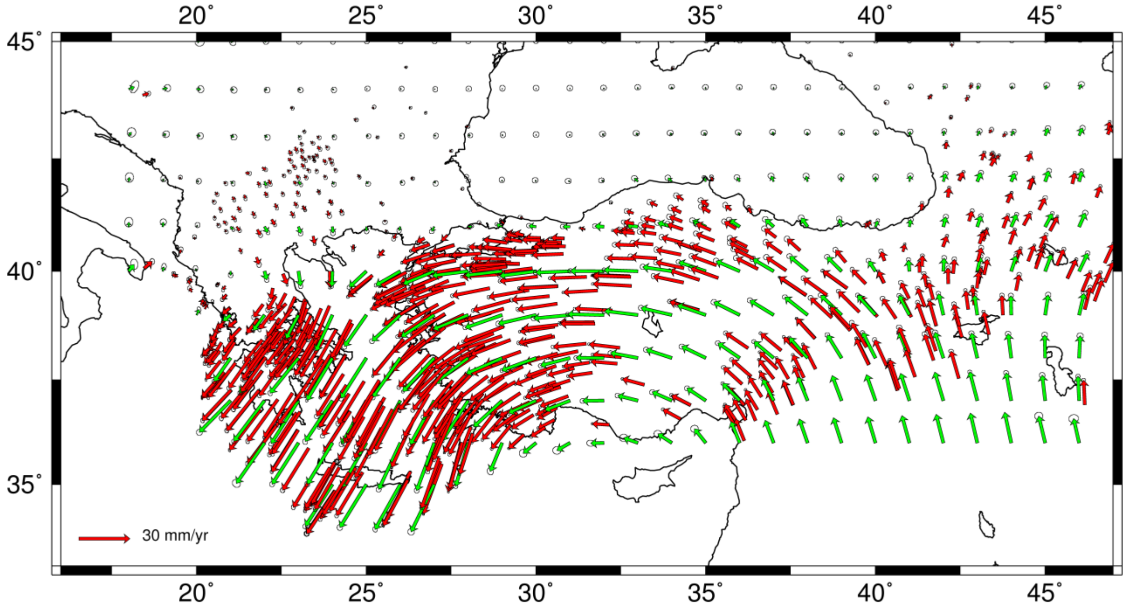

Figure 3.2. GPS velocities (red arrows) and interpolated GPS velocities (green arrows) in Turkey and adjacent regions are shown relative to the Eurasia fixed reference frame (Özeren and Bolt, 2010)

However, determining the driving force for the crustal deformation in continental environments is not a simple problem. Whether it is driven from the crust through horizontal forces or from below by the asthenospheric flow depends upon the tectonics and the thermal conditions of the lithosphere. Most of the proposed models in the Aegean do not consider the possibility of a contribution of the underlying asthenospheric flow to crustal deformation (Conrad and Behn, 2010).

Kreemer (2009) used shear wave splitting measurements at both oceanic and continental paths to constrain net lithosphere rotation about a pole at 57.6°S and 63.2ºE. He ignored the contribution of the mantle flow on the anisotropic fabric in the asthenosphere and assumed that LPO in asthenosphere always takes place parallel to absolute plate motion. He obtained a digital model (GSRM-APM-1) as the combination of horizontal velocities on Earth surface and horizontal strain rates for deforming plate boundaries (Figure 3.3). Velocities in Figure 3.3 correspond to the plate boundary motions and plate rotations. The model performs better in the global scale but is not sufficient to explain shear wave splitting measurements computed locally.

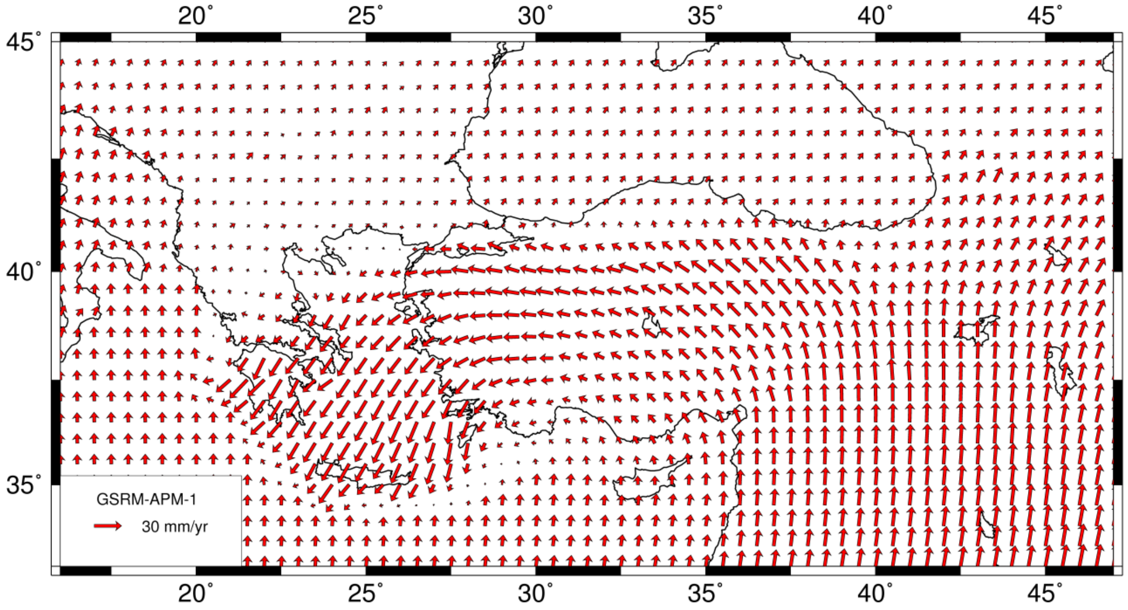

Figure 3.3. Velocity field for the study area in GSRM-APM-1 reference frame model (Kreemer, 2009)

Based on the density model produced from the seismic tomographic models Faccenna and Becker (2010) has modeled flow directions in the mantle of the Mediterranean region. They were able to reproduce the westward motion of Anatolia. However the model fails to account for the southward motion of the Aegean slab and the N-S extension in the back arc region.

Shear wave splitting measurements to analyze upper mantle was started with the work of Bowman and Ando (1987). Shear phases that propagate through the mantle (SKS, S, SKKS, *etc.*) were used at different splitting measurement methods (Vinnik *et al*., 1989; Silver and Chan, 1991). Several works based on SKS observations are performed in the Eastern Mediterranean Region. Hatzfeld *et al*. (2001) measured shear wave splitting in the Aegean from 25 stations which were located in the continental Greece and Aegean islands by using teleseismic and regional earthquakes that occurred during six month period. Earthquakes occurred at epicentral distances between 85° and 110° with magnitudes greater than 5.5. They observed 150 splitting parameter pairs which were not homogeneous over the Aegean Region. The largest delay times (> 1 s) and N20ºE fast polarization direction were observed beneath the north Aegean Sea. Small delay times or Null measurements were obtained in the Sea of Crete and in the continental Greece. The fast polarization directions (NNE-SSW in the east and NNW-SSE in the west) were observed parallel to the Hellenic Arc. They claimed that fast polarization directions are consistent with the present-day strain rates based on GPS measurements and seismicity. They observed that the crust and upper mantle deform consistently in the Aegean.

Sandvol *et al*. (2003) studied upper mantle anisotropy using shear wave splitting in the Eastern Turkey. Using the waveform data from 29 seismic stations of the ETSE network, located in the Arabian, Eurasian and Anatolian Domain, they obtained splitting parameters from SKS, PKS and SKKS phases and observed 1s average delay time and consistent NE-SW fast direction at the stations in Eastern Anatolia and northerly fast direction in the Western Arabian Plates which are claimed to be consistent with Absolute Plate Motion (Sandvol *et al*., 2003; McClusky *et al*., 2000). Due to the inconsistency between shear wave splitting and surface deformation they suggested that the measured anisotropy is asthenospheric or weakly lithospheric.

Mantle anisotropy and upper mantle strain rate in the NAFZ was studied using 140 teleseismic earthquakes with magnitudes greater than 5.0 and occurred at distances 85°-120° recorded at 39 seismic stations that located across the NAFZ (Biryol *et al*., 2010). They computed splitting parameters by using Rotation Correlation (Bowman and Ando, 1987) and Minimum Energy (Silver and Chan, 1991) techniques with SKS and SKKS phases and observed uniform strain rate and approximately 43° NE-SW fast direction polarization in average with increasing delay times from east (0.5 s) to west (1.6 s) beneath NAFZ. They suggested that the uniform anisotropy observed beneath major tectonic boundaries is asthenospheric rather than lithospheric. The SW directed asthenospheric flow from east to west is a result of slab roll-back in the Aegean and Cyprian (Biryol *et al*., 2010). NAF and San Andreas Fault (SAF) were compared in terms of anisotropy, lithospheric deformation and age differences and observed smaller delay times (0.5 s - 1.25 s) for SAF.

More recently, shear wave anisotropy beneath the southern Aegean and back-arc and near trench areas of Hellenic Arc was studied by Evangelidis *et al*. (2011) by using 54 broadband stations. Total of 14 teleseismic earthquakes recorded for approximately 2.5 years period and 66 deep earthquakes from 2003 to 2008 which occurred between 80°-120° distanced were used. In the Hellenic back-arc fast anisotropy direction was observed as perpendicular to the trench (NE-SW) with delay times increasing from south to north. No correlation was observed between anisotropy and GPS velocities.

In this study, shear wave splitting parameters are measured by using more than 850 teleseismic earthquakes with magnitudes greater than 6.0 that occurred between years 1999-2010 at epicentral distances between 84° and 130°. Total number of 4163 splitting parameter pairs are measured for 217 broadband seismic stations located in and around Turkey both from permanent and temporary networks. To compute the splitting parameters φ and δt, rotation-correlation technique (RC) (Bowman and Ando, 1987) and minimum energy technique (SC) (Silver and Chan, 1991) were employed. Both RC and SC techniques are used together to detect anisotropy in the upper mantle and quality statistics are performed for each seismic station. Null and non-Null measurements classified as good, fair or poor (Wüstefeld and Bokelman, 2007). Shear wave splitting measurements are generally found to be consistent with the previous studies in Eastern Anatolia and NAFZ with NE-SW fast polarization direction. NNE-SSW splitting direction with 1.5 seconds delay time in average is observed for the Marmara Region. Delay time decreases from Eastern to Western Turkey. Around 31°N, there is a sharp orientation change observed in the splitting fast direction. Splitting directions and GPS velocities are consistent beneath the Aegean Region.

3.2. Methodology

In isotropic medium, two types of body waves propagate with different velocities, namely P waves and S waves (Bullen and Bolt, 1985). In anisotropic medium however, wave propagation is more complex and support three body waves with perpendicular polarizations, a quasi-P wave (polarized almost in the propagation direction) and two quasi-S waves (SV and SH) (Figure 3.4). The velocity of the quasi-P wave is greater than two quasi-S waves. Quasi-S waves travel with fast and slow directions and different velocities in anisotropic medium and results in delay time (Crampin, 1977).

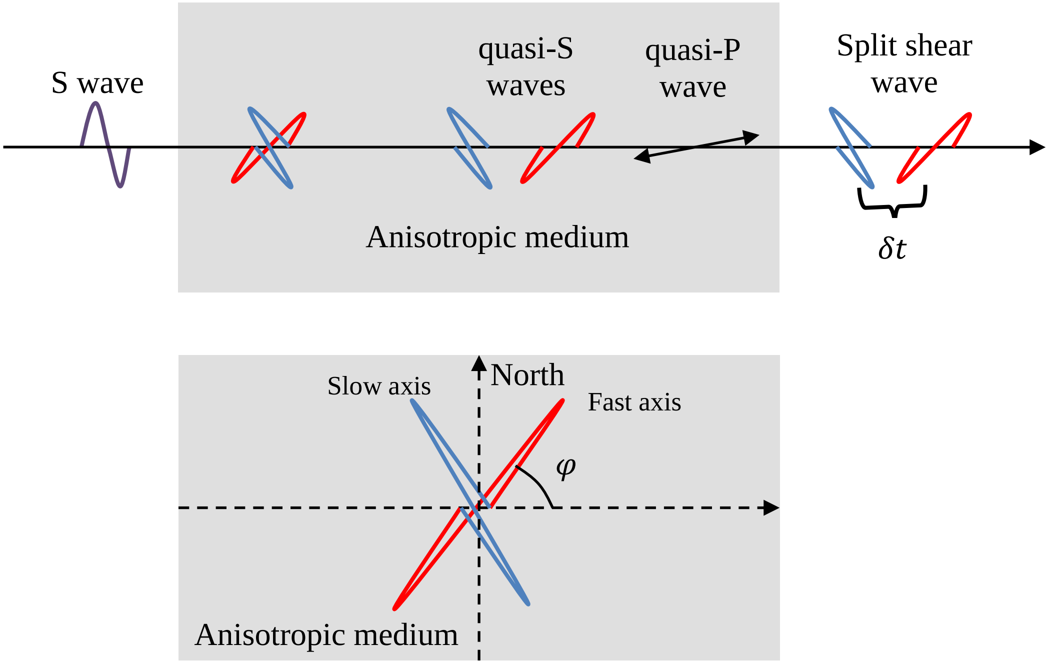

Figure 3.4. Schematic view of the shear wave splitting through anisotropic medium. Image on the top shows an incoming S wave entering anisotropic media and splits. Image below shows the fast polarization direction

In isotropic medium SKS phase polarizes vertically and arrives to the receiver as SV (Babuska and Cara, 1991). If the medium is anisotropic, it polarizes in two different direction perpendicular to each other and reaches to the station as in near-vertical propagation. The two split SKS wave polarizations; fast (s_1) and slow (s_2) and shear wave signal on radial component s(t) can be written as (Vinnik *et al.*, 1989) (Figure 3.5);

$$s_1(t) = s(t)\cos\varphi \tag{3.1}$$

$$s_2(t) = s(t-\delta t)\sin\varphi \tag{3.2}$$

φ is the azimuthal angle between fast S wave polarization and radial direction. δt is delay time between fast and slow polarized split waves. The fast and slow polarized SKS waves on radial ($R(t)$) and transverse ($T(t)$) components are (Babuska and Cara, 1991);

$$R(t) = s(t)cos^2\varphi + s(t-\delta t)sin^2\varphi \tag{3.3}$$

$$T(t) = [s(t) - s(t-\delta t)/2]\, sin2\,\varphi \tag{3.4}$$

The time derivative of the radial component will be approximately equal to the transverse component for weak anisotropy (δt~0) or strong anisotropy with fast or slow polarized backazimuth (Silver and Chan, 1988; Vinnik *et al.*,1989; Babuska and Cara, 1991).

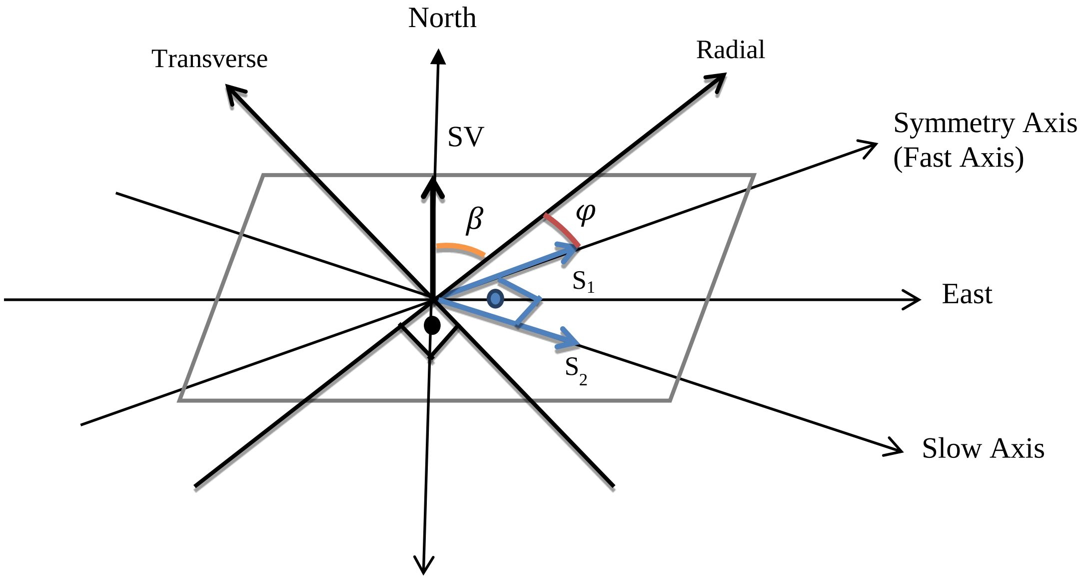

Figure 3.5. Schematic view of the shear wave splitting through anisotropic medium

There are two inversion techniques to measure shear wave splitting; multi event method and single event method. Multi event method determines splitting parameters and combines several of them for a single station to map the energy on the transverse component (Kosarev *et al.*, 1984; Vinnik *et al.*, 1989, Wolfe and Silver, 1998). Single event method determines splitting parameters and does grid search to determine fast polarization direction φ and delay time δt that best removes the splitting effect (Fukao, 1984; Ansel and Nataf, 1989; Silver and Chan, 1991; Menke and Levin, 2003). Two techniques of single-event method used in this study are described below briefly.

3.2.1. The Rotation Correlation Method

This method is also called cross-correlation method (Bowman and Ando, 1987) (in the following is called as RC). The technique assumes that the waveform of the fast component is alike to the slow component and searches for the polarization direction and delay time by maximizing the cross-correlation between Radial and Transverse components. The first shear arrival is seen on the fast direction, second shear arrival is seen on the slow direction, time between these two arrivals is δt.

3.2.2. Minimum Energy Method

Minimum energy method is a widely used method (in the following is called as SC). This method has a basis of minimizing energy on the transverse component (Silver and Chan, 1991). The main idea of this method is to remove anisotropy effect from the data by minimizing the energy on the transverse component. Core refracted and core reflected phases (SKS, SKKS, PKS *etc.*) can be used.

The formulation of projection horizontal and vertical seismograms to radial and transverse directions in two dimensional medium and three dimensional medium is given as below respectively;

$$\begin{bmatrix} F \\ S \end{bmatrix} = \begin{bmatrix} cos\varphi & -sin\varphi \\ sin\varphi & cos\varphi \end{bmatrix} . \begin{bmatrix} R \\ T \end{bmatrix} \tag{3.5}$$

$$\begin{bmatrix} L \\ Q \\ T \end{bmatrix} = \begin{bmatrix} cos\delta & -sin\delta sin\beta & -sin\delta cos\beta \\ sin\delta & cos\delta sin\beta & cos\delta cos\beta \\ 0 & -cos\beta & sin\beta \end{bmatrix} . \begin{bmatrix} Z \\ E \\ N \end{bmatrix} \tag{3.6}$$

δ refers to the incidence angle measured from vertical (assumed to be radial in this case), β refers to the backazimuth. In three dimensional medium, vertical (Z), north (N) and east (E) components of the seismogram need to rotated in to the ray system as longitudinal (L), radial (Q) and transverse (T) components in order to determine time separation (Equation 3.6) (Wüstefeld *et al.*, 2008). L is vertical component parallel to the ray, Q is radial component pointing direction from source to receiver and T is transverse component perpendicular to the ray. N and E are the North-South and East-West component seismograms respectively, Z is vertical component seismogram. If anisotropy is small or strong but the back azimuth is along the fast or slow polarization direction $T(t)$ will be zero.

Shear wave splitting measurement is mainly based on the polarization analysis (Plesinger *et al.*, 1986) due to the fact that in the single event method (both in RC and SC methods) initial polarization of the waveform is assumed to be radial. If the medium is isotropic or the initial polarization corresponds to the fast or slow direction or no splitting is observed this measurement called “Null”. RC and SC techniques behave differently in fast polarization direction and delay time near Null directions. By using this difference, Null measurements were identified and quality of the result was determined (Wüstefeld and Bokelmann, 2007). For a Null measurement,

$$\Delta\varphi = \varphi_{SC} - \varphi_{RC} \approx n * 45^{\circ} \tag{3.7}$$

$\Delta\varphi$ is the angular difference between RC and SC techniques. “n” is a positive or negative integer. RC technique is off and δt_{RC} goes to zero for near Null measurements.

By comparing the result of RC and SC techniques, it is easier to recognize measurements with very low delay time and measurements with zero (Wüstefeld and Bokelmann, 2007). When the splitting is Null at a station, the SC method gives very small values of δt for all non-Null measurements. Null or non-Null measurements can be recognized with quality criteria’s below:

$$\Delta\varphi = |\varphi_{SC} - \varphi_{RC}| \text{ and } \rho = \delta t_{RC}/\delta t_{SC} \tag{3.8}$$

For “Null” measurements;

if	$37° < \Delta\varphi < 53°$	and	$0 < \rho < 0.2$	“good”
if	$32° < \Delta\varphi < 58°$	and	$0 < \rho < 0.3$	“fair”

For “non-Null” measurements;

if	$\Delta\varphi < 8°$	and	$0.8 < \rho < 1.1$	“good”
if	$\Delta\varphi < 15°$	and	$0.7 < \rho < 1.2$	“fair”

Remaining measurements are considered as “poor” quality. The quality assessment for each splitting parameter pair is obtained by using these criteria’s for RC and SC methods are shown in Figure 3.6. Difference between fast axis estimates ($|\Delta\varphi|$) with respect to delay time ratio (ρ) of splitting measurements compared for RC and SC methods is depicted (Figure 3.6). Red areas represent good, blue represents fair and green represents poor Null and non-Null measurements. Time ratio between 0 and 0.2s refers good Nulls with fast axis difference between 37° and 53° while near-Null measurements classified as time ratio between 0 and 0.3 seconds and fast axis difference between 32° and 58° (Figure 3.6). This is a good way to determine the quality of the results and to identify real null splitting.

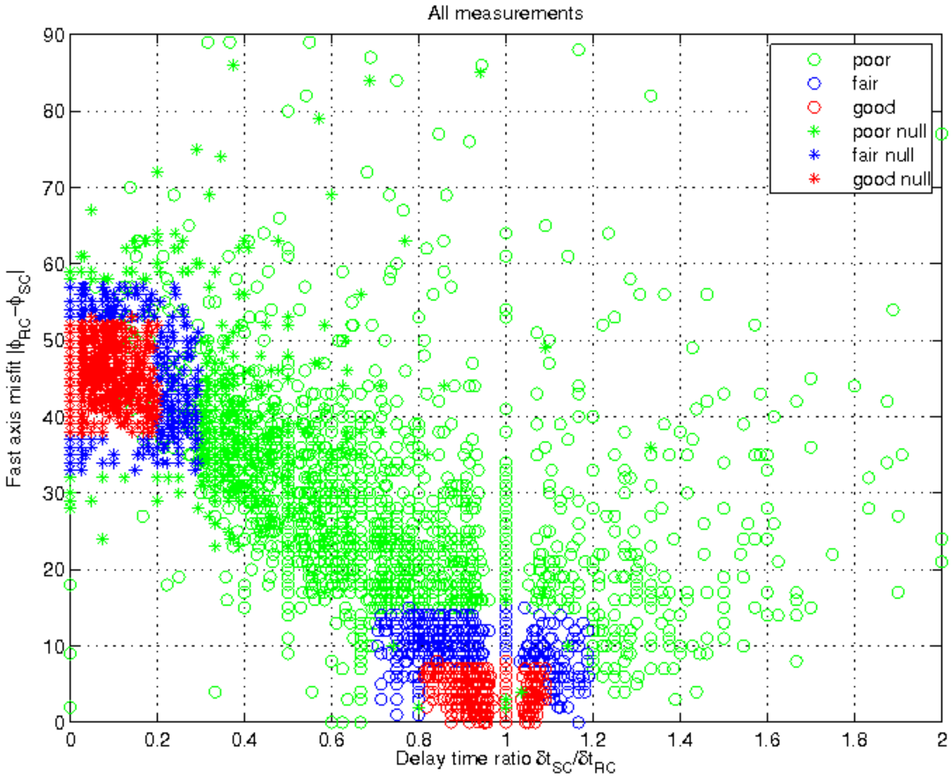

Figure 3.6. Delay times and fast axis misfits between RC and SC methods are calculated from 4163 observations. Good (red), fair (blue) and poor (green) measurements are shown with different colors

In order to identify SKS phases and to measure splitting parameters SplitLab with a graphical user interface MATLAB code was used (Wüstefeld *et al.*, 2007). SplitLab modules associate event and waveform database, performs measurements and view the results for qualification by user, respectively. Data managing is the first step of the SplitLab which includes catalog preparation, waveform and event association, input station information (such as latitude, longitude, elevation, network code *etc.*). Database view in ENZ or LQT coordinate systems, filter selection, SKS phase selection are done before running splitting measurements by using RC and SC methods. Qualification and decision of the results if they are Null or non-Null are done in the later stage (Figure 3.7). Result screen for both Null and non-Null single measurements is shown in Figure 3.8 and 3.9 which depict general information for the selected event (origin time, latitude, longitude, magnitude, depth, backazimuth *etc.*), selected SKS phase window, RC and SC corrected fast-slow and radial-transverse component plots, particle motion before and after correction and qualification for the result. The particle motion appears to be elliptical before correction and linear after correction.

The splitting parameters φ (polarization orientation of the first-arrival phase) and δt (time delay between fast and slow polarizations) are measured using the rotation–correlation method (*e.g.* Bowman and Ando, 1987) and minimum energy method (Silver and Chan, 1991) after filtering the seismograms in the SplitLab environment (Wüstefeld *et al.*, 2007), generally between 0.02 Hz and 0.2 Hz. The error for each measurement is defined by the 95 per cent confidence contour of the maximum correlation. The measurements are considered as acceptable when (1) the horizontal particle motion is elliptical when anisotropy is present, (2) the two horizontal fast and slow component waveforms are coherent, (3) the particle motion becomes linear following correction for anisotropy, and (4) time lags are larger than 0.5 seconds. Final result is presented only for stations with at least three non-Null fair and good measurements with different initial polarizations.

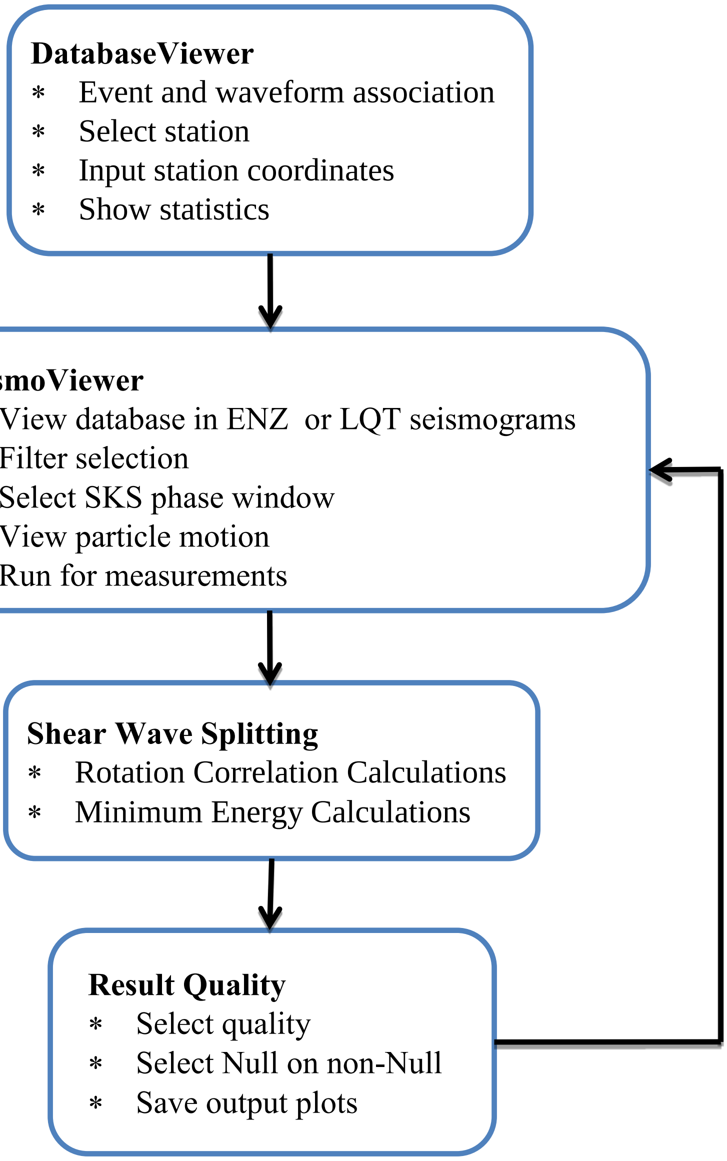

Figure 3.7. Flowchart of the SplitLab processing steps

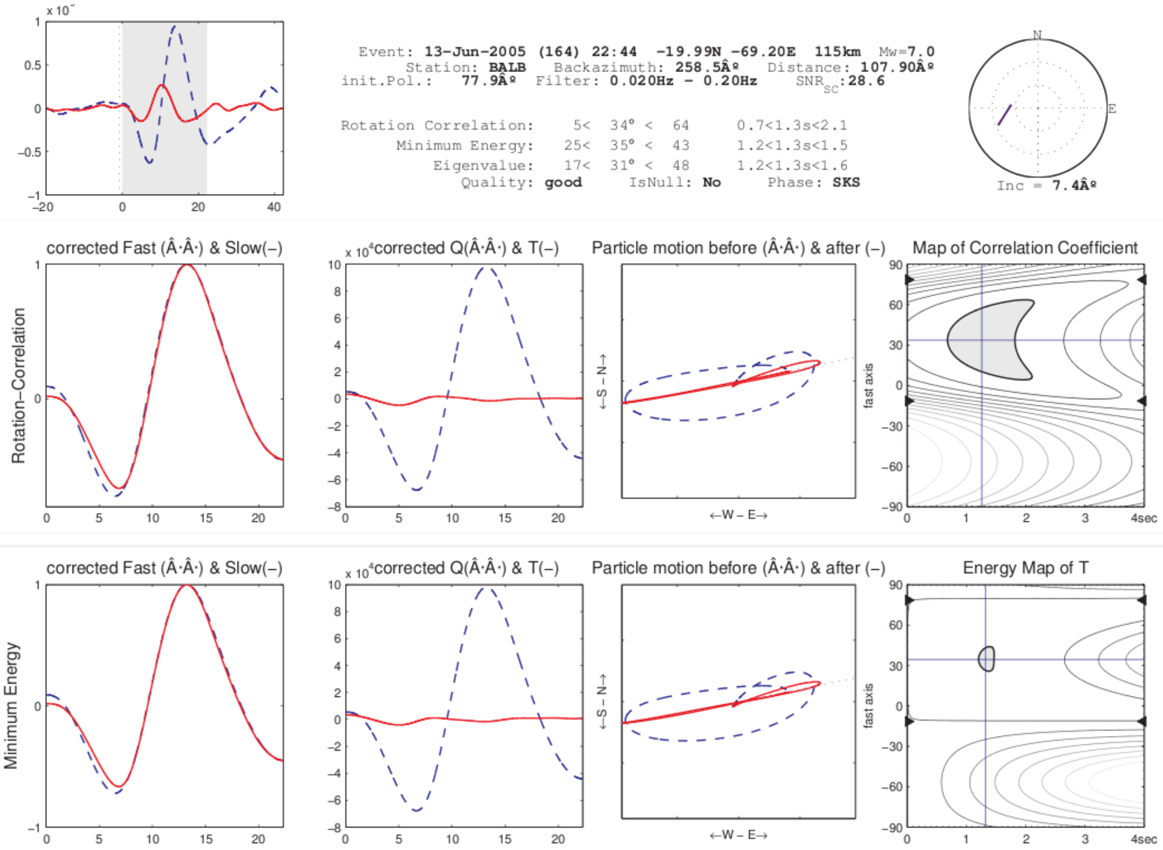

```
   Event: 13-Jun-2005 (164) 22:44  -19.99N -69.20E  115km  Mw=7.0
       Station: BALB   Backazimuth: 258.5Âº   Distance: 107.90Âº
 init.Pol.:   77.9Âº  Filter: 0.020Hz - 0.20Hz    SNR_SC:28.6

 Rotation Correlation:    5<  34° <  64      0.7<1.3s<2.1
      Minimum Energy:   25<  35° <  43      1.2<1.3s<1.5
         Eigenvalue:   17<  31° <  48      1.2<1.3s<1.6
           Quality: good      IsNull: No      Phase: SKS
```

Figure 3.8. SplitLab code output image for a single non-Null measurement for BALB (Balıkesir) station. Splitting parameters are measured using both RC and SC techniques. Upper panel presents radial (blue dashed line) and transverse (red line) components of SKS phase in selected window (shaded area) on the left, information about the teleseismic earthquake used for measurements in the middle and incidence angle on the right. Center panel displays in turn from left to right normalized, radial and transverse components after the correction from RC, particle motion before and after correction and map of correlation coefficient. The gray shaded area shows the location of the estimated splitting parameters. Lower panel displays in turn from left to right normalized components after rotation in SC anisotropy system, corrected radial and transverse components, particle motion before and after correction and map of minimum energy on transverse component for SC technique

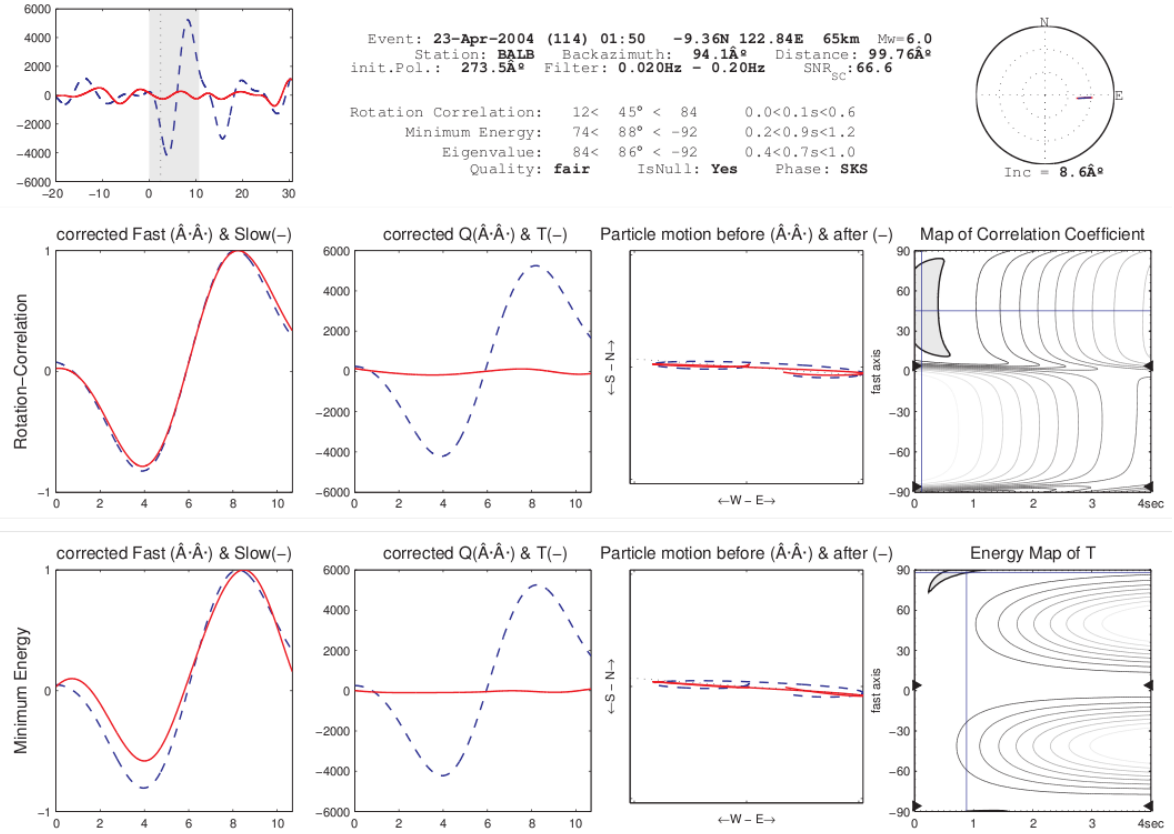

```
   Event: 23-Apr-2004 (114) 01:50   -9.36N 122.84E  65km  Mw=6.0
      Station: BALB   Backazimuth:  94.1Âº  Distance: 99.76Âº
init.Pol.:  273.5Âº  Filter: 0.020Hz - 0.20Hz    SNR_SC:66.6

Rotation Correlation:   12<  45° <  84      0.0<0.1s<0.6
      Minimum Energy:   74<  88° < -92      0.2<0.9s<1.2
         Eigenvalue:   84<  86° < -92      0.4<0.7s<1.0
           Quality: fair      IsNull: Yes     Phase: SKS
```

Figure 3.9. SplitLab code output image for a single Null measurement for BALB (Balıkesir) station. Splitting parameters are measured using both RC and SC techniques. Upper panel presents radial (blue dashed line) and transverse (red line) components of SKS phase in selected window (shaded area) on the left, information about the teleseismic earthquake used for measurements in the middle and incidence angle on the right. Center panel displays in turn from left to right normalized, radial and transverse components after the correction from RC, particle motion before and after correction and map of correlation coefficient. The gray shaded area shows the location of the estimated splitting parameters. Lower panel displays in turn from left to right normalized components after rotation in SC anisotropy system, corrected radial and transverse components, particle motion before and after correction and map of minimum energy on transverse component for SC technique

3.3. Data Processing

SKS phases are analyzed by using teleseismic earthquakes recorded at epicentral distances between 84° and 130° on permanent broadband seismographs which are maintained by the KOERI and ORFEUS and temporary network of SIMBAAD (Appendix A). The station distribution is not irregular over the area. The distribution is sparse in Central and Eastern Anatolia and relatively denser in Northwestern Turkey and Aegean (Figure 3.10). Recordings from 217 seismic stations during the time period from November 1999 to December 2010 are used for SKS splitting analysis. Splitting parameter pairs are computed at 217 seismic stations, 35 of these stations are marked either Null or did not provide enough splitting measurements.

The recordings of 2324 teleseismic earthquakes between 1999 and 2010 with magnitudes greater than 6.0 are collected using the NEIC catalogue and more than 700 of them are identified as candidates for SKS analysis (Figure 3.11). The events with good signal-to-noise ratio are selected for the analysis and 4163 good, fair or poor non-Null splitting measurements for 182 seismic stations are presented (Figure 3.12).

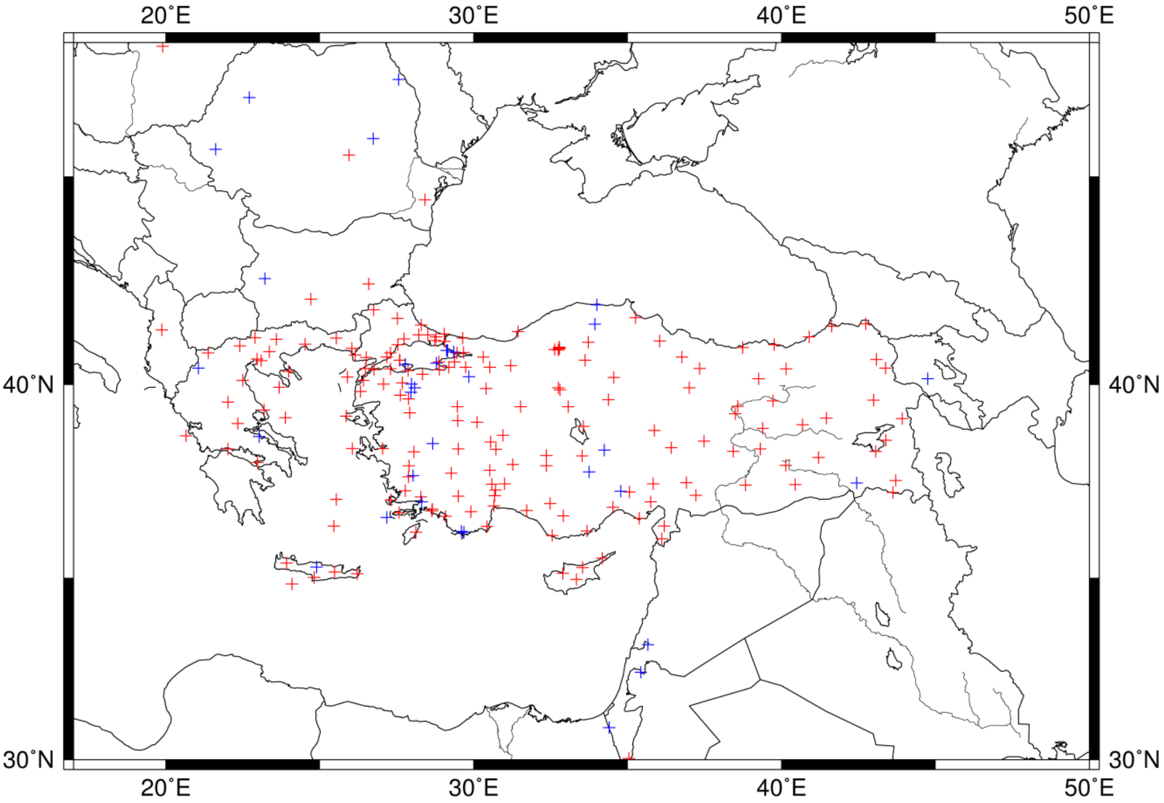

Figure 3.10. Broadband seismic stations used to measure SKS splitting. Stations with non-Null measurements (+) and stations with Null or not enough measurements (+) are shown with different colors

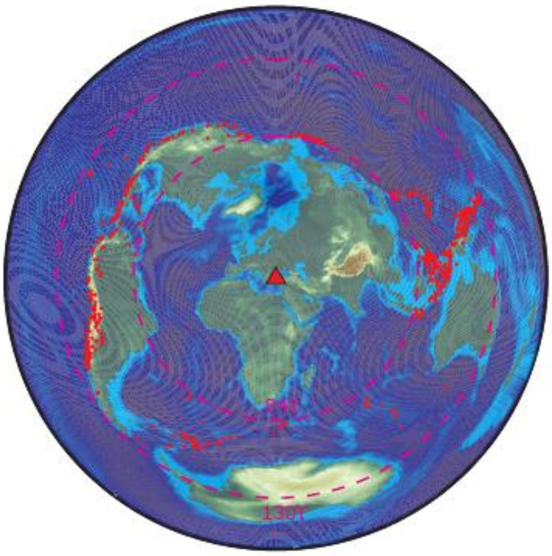

Figure 3.11. Equidistant projection of the locations of teleseismic events used in this study (red dots). The two circles (dashed lines) represent epicentral distances of 84° and 130°

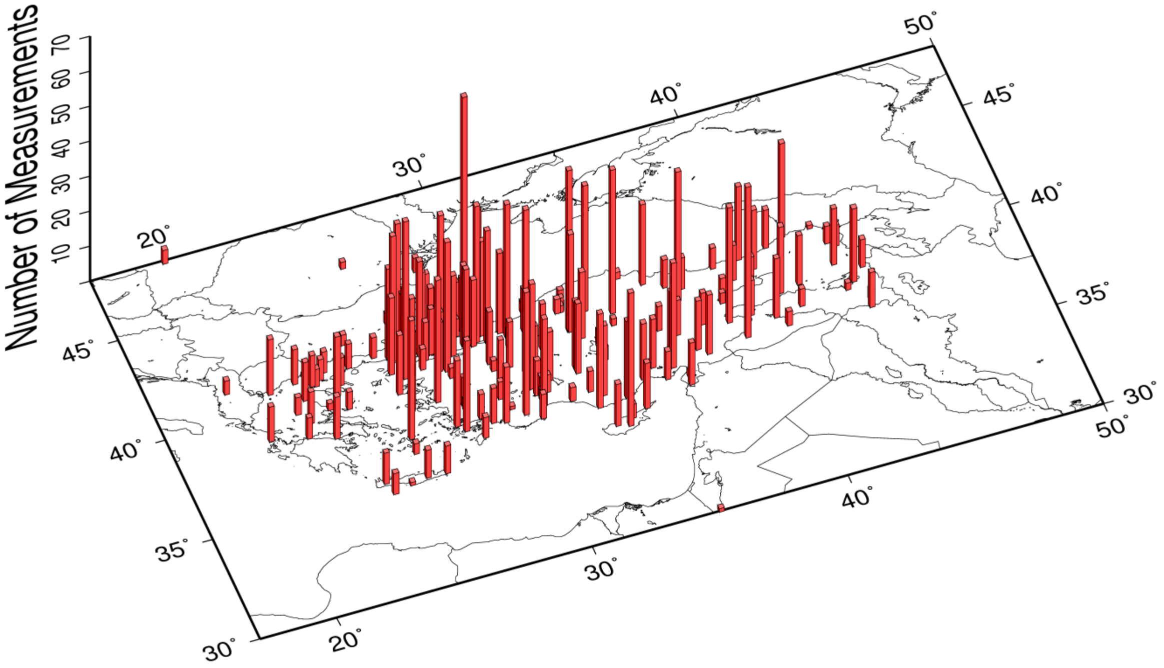

Figure 3.12. The number of non-Null splitting measurements at each broadband station

3.4. The Analysis of SKS Measurements at Various Stations

BALB (Balıkesir), BAYT (Bayburt), CSS (Cyprus), ISK (İstanbul), ISP (Isparta), MALT (Malatya) and VANB (Van) stations are selected to discuss SKS measurements in detail. BALB broadband station is located in southern Marmara Region (39.64°N, 27.88°E). Total numbers of 347 teleseismic earthquakes from different back azimuths are analyzed between 15 January 2004 and 26 November 2010 (Figure 3.13). A total of 43 SKS splitting parameter pairs are measured. Of those measurements six of them are classified as good, 8 as fair, 23 as poor and 6 as Nulls (Figure 3.14). The average fast polarization direction is computed as 22° and average delay time as 1.4 seconds. ISK is located in the Marmara Region (41.06°N, 29.06°E) and 366 waveforms are processed between 15 January 2004 and 26 November 2010 (Figure 3.15). These measurements are qualified as 24 good, 15 fair, 29 poor and 15 Nulls (Figure 3.16) with average fast polarization direction as 40° and delay time as 1.3 seconds. Şapaş and Boztepe-Güney (2005) measured fast polarization direction as 43.7°±5° and delay time 1.96 s for ISP station. Average splitting angle in the Marmara Region is about 45° NE-SW direction and delay times are higher in the Northern Marmara (1.5s) with respect to Southern Marmara Region (1.0 s) (Figure 3.27).

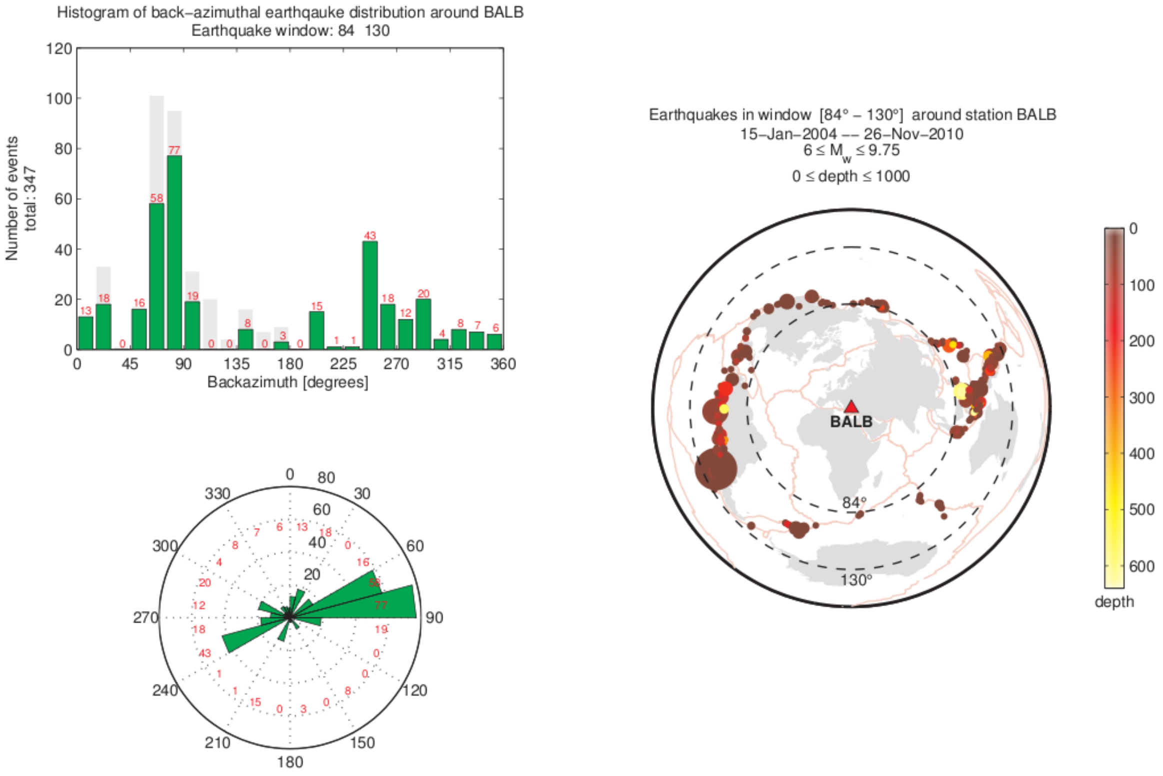

Figure 3.13. Earthquake distribution statistics for BALB broadband station. Histogram view (top left) and globe view (down left) show distribution of the earthquakes with back azimuth. On the right hand side earthquakes are plotted in different colors according to their magnitude

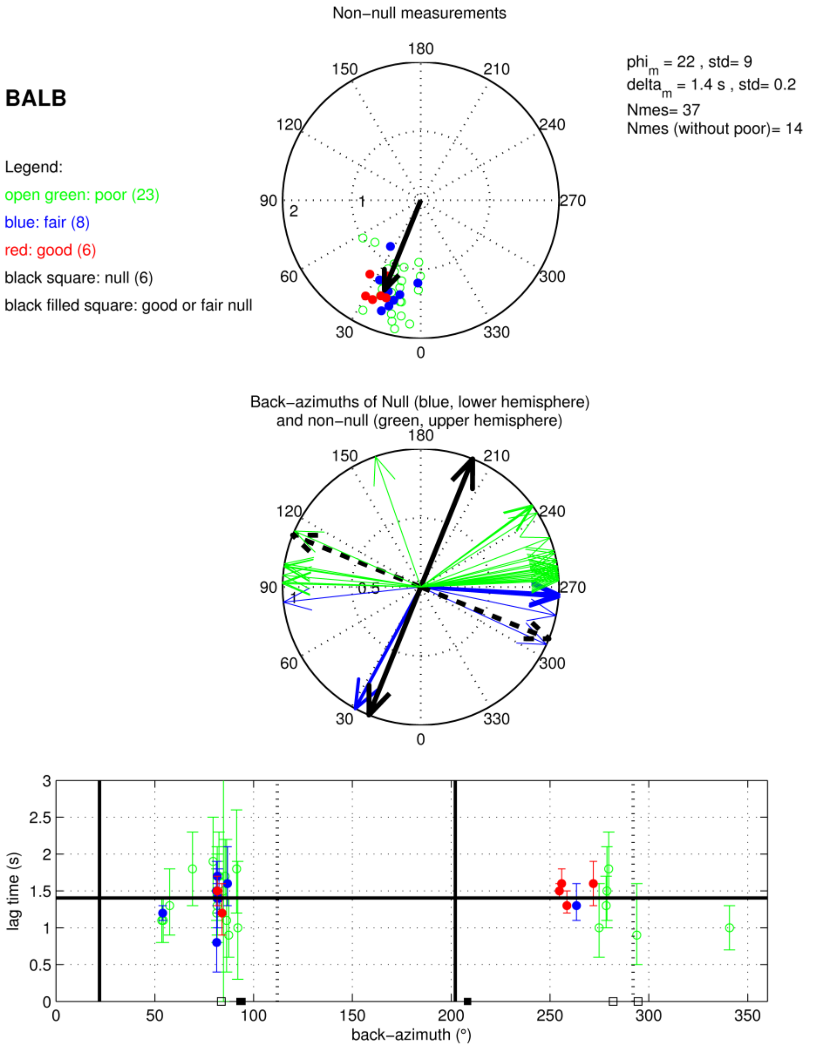

Figure 3.14. Polar diagram of BALB seismic station for good, fair and poor non-Null measurements. In the upper panel φ and δt are presented with standard deviations and black row represents the fast polarization direction. In the central panel polar plot of back azimuths are shown. The thick blue arrows in the lower hemisphere show the back azimuth of events with good or fair Null measurements. The thin blue arrows correspond to events with poor Null measurements. The lower panel displays delay times as a function of back azimuth. The black filled squares show Null measurements rated as good or fair. Poor Nulls are plotted as open black squares

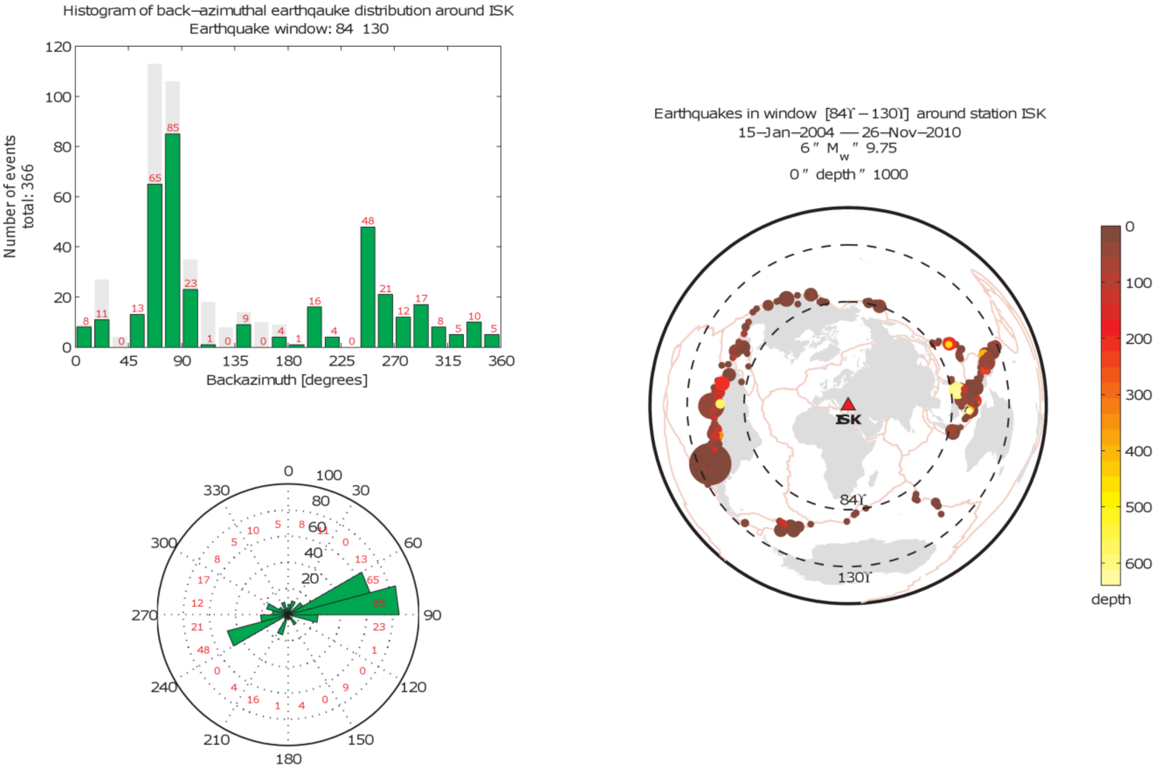

Figure 3.15. Earthquake distribution statistics for ISK broadband station. Histogram view (top left) and globe view (down left) show distribution of the earthquakes with back azimuth. On the right hand side earthquakes are plotted in different colors according to their magnitude

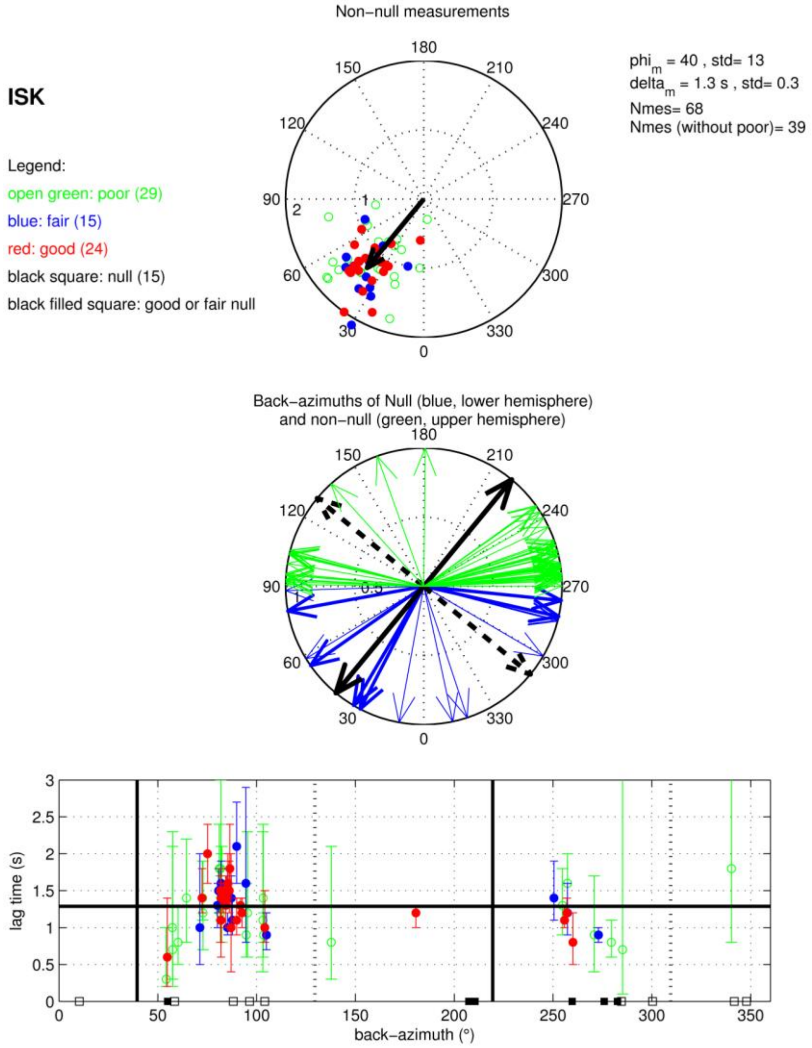

Figure 3.16. Polar diagram of ISK seismic station for good, fair and poor non-Null measurements. In the upper panel φ and δt are presented with standard deviations and black row represents the fast polarization direction. In the central panel polar plot of back azimuth are depicted. The thick blue arrows in the lower hemisphere show the back azimuth of events with good or fair Null measurements. The thin blue arrows correspond to events with poor Null measurements. The lower panel displays delay time as a function of back azimuth. The black filled squares show Null measurements rated as good or fair.

Poor Nulls are plotted as open black squares

ISP station is located in southwestern Anatolia (37.82°N, 30.52°E). This place called Isparta angle, a triangular-shaped region which is the boundary between Aegean and central Anatolia. Total numbers of 235 teleseismic earthquakes recorded between 2 March 2004 and 20 December 2010 are used to compute splitting parameter (Figure 3.17) and 59 waveforms are processed as 4 good, 2 fair and 24 poor. Total numbers of 29 Nulls are measured and average φ and δt are computed as -10° and 1.3 seconds respectively (Figure 3.18). ISP station is located in such a wedge where fast polarization directions change from NE-SW to NW-SE and crustal thickness is relatively thick. Fast polarization direction and delay time at ISP station were computed as 10.85° and 1.46 seconds by Schmid *et al.* (2004) and $56° \leq \varphi \leq 205°$ and $0.37 \leq \delta t \leq 4$ seconds by Şapaş and Boztepe-Güney (2009).

CSS is located in Cyprus (33.33°N, 34.96°E). By using 341 teleseismic earthquakes occurred between 21 February 2004 and 23 December 2010 splitting parameters are measured (Figure 3.19). 48 SKS phases are marked as 4 good, 10 fair, 24 poor and 10 good Nulls (Figure 3.20). Average fast polarization direction is computed as 40° and delay time as 1.1 seconds.

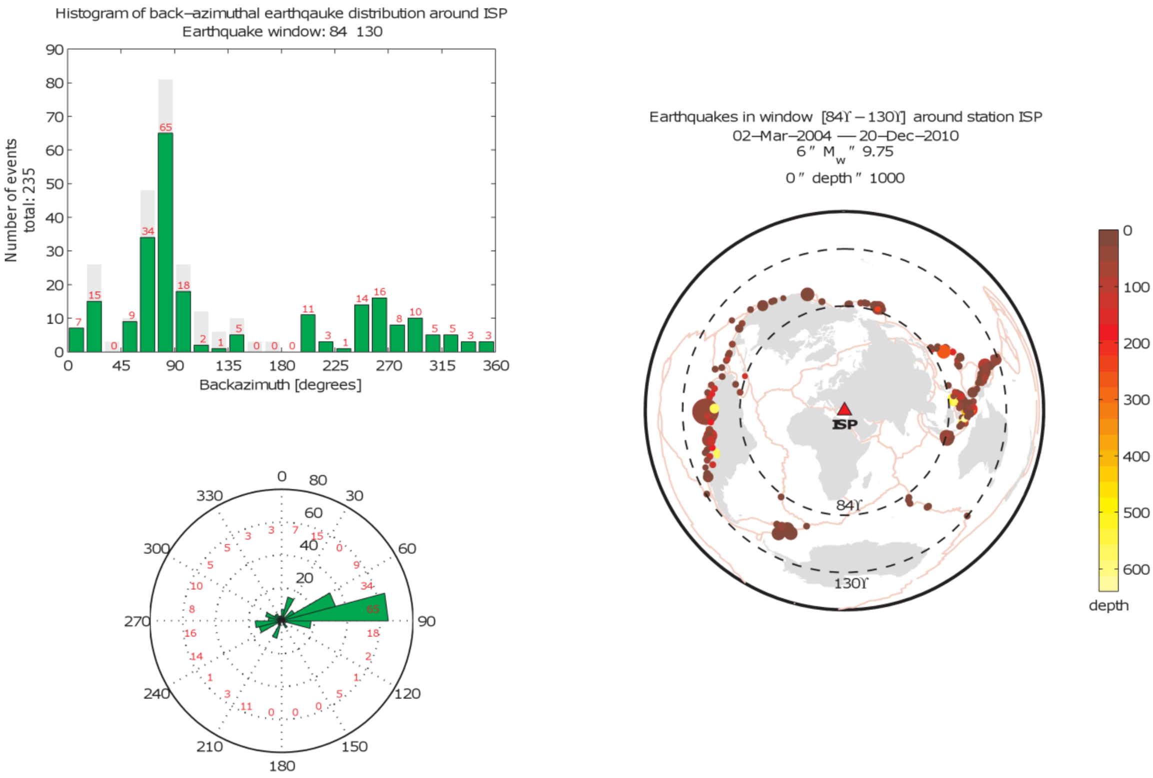

Figure 3.17. Earthquake distribution statistics for ISP broadband station. Histogram view (top left) and globe view (down left) show distribution of the earthquakes with back azimuth. On the right hand side earthquakes are plotted in different colors according to their magnitude

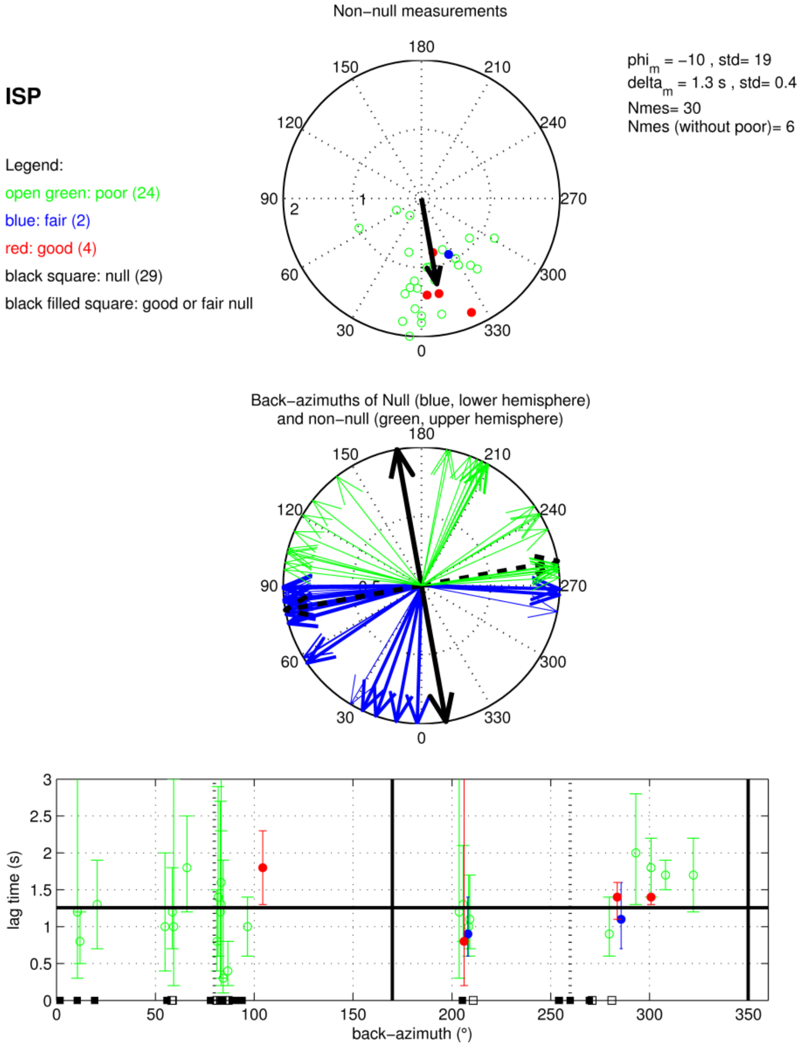

Figure 3.18. Polar diagram of ISP seismic station for good, fair and poor non-Null measurements is plotted. In the upper panel φ and δt are presented with standard deviations and black row represents the fast polarization direction. In the central panel polar plot of back azimuth are depicted. The thick blue arrows in the lower hemisphere show the back azimuth of events with good or fair Null measurements. The thin blue arrows correspond to events with poor Null measurements. The lower panel displays delay time as a function of back azimuth. The black filled squares show Null measurements rated as good or fair. Poor Nulls are plotted as open black squares

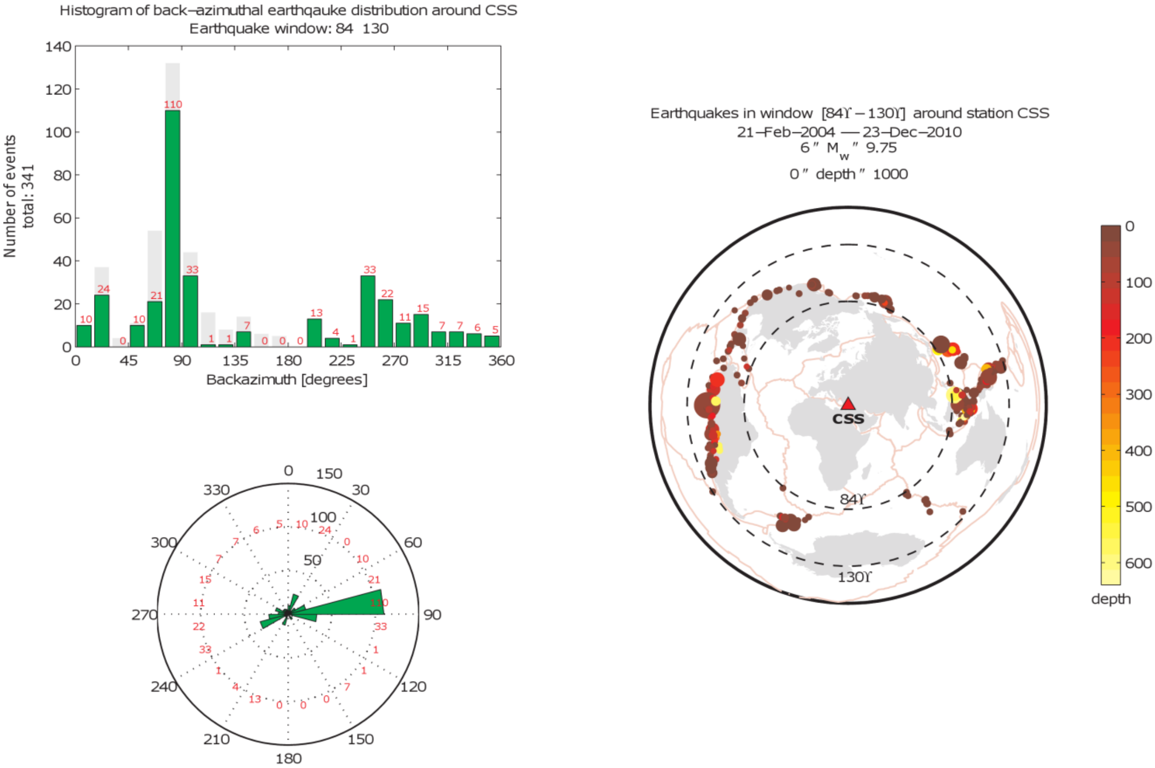

Figure 3.19. Earthquake distribution statistics for CSS broadband station. Histogram view (top left) and globe view (down left) show distribution of the earthquakes with back azimuth. On the right hand side earthquakes are plotted in different colors according to their magnitude

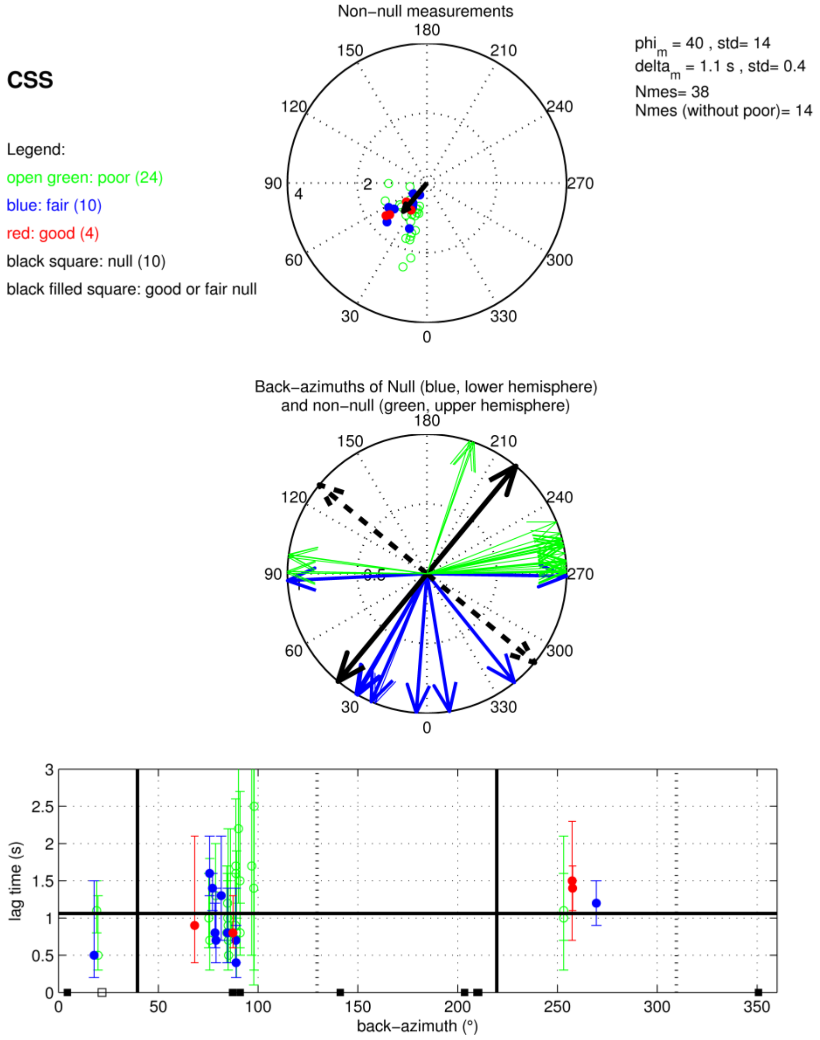

Figure 3.20. Polar diagram of CSS seismic station is performed for good, fair and poor non-Null measurements. In the upper panel φ and δt are presented with standard deviations and black row represents the fast polarization direction. In the central panel polar plot of back azimuth are depicted. The thick blue arrows in the lower hemisphere show the back azimuth of events with good or fair Null measurements. The thin blue arrows correspond to events with poor Null measurements. The lower panel displays delay time as a function of back azimuth. The black filled squares show Null measurements rated as good or fair. Poor Nulls are plotted as open black squares

MALT station is located in the eastern Anatolia near EAF (38.42°N, 38.31°E). By using 238 teleseismic earthquakes located between 2 March 2004 and 21 December 2010 (Figure 3.21). Forty-three waveforms are analyzed and as 4 qualified as good, 6 fair, 23 poor and 10 Nulls (Figure 3.22). Average splitting parameters for MALT station are computed as 22° for fast polarization direction and 1s delay time. The values are consistent with Sandvol *et al*. (2004) (φ =. 17°±10°, δt = 1.1 ± 0.3 s). VANB station is located close to the eastern coast of Anatolia (43.38°N, 38.59°E). Splitting parameters of VANB station ($\varphi = 58°$ and $\delta t = 0.9$ s) are computed by using 287 teleseismic events occurred between 15 January 2004 and 26 November 2010 (Figure 3.23). 26 SKS measurements provided 5 good, 1 fair, 15 poor and 5 Nulls (Figure 3.24). BAYT station is located in northern Anatolia (40.14°N, 40.39°E). Computed fast polarization direction ($\varphi = 54°$) and lag time ($\delta t = 1.5$ s) is consistent with the ETSE results (Sandvol *et al*., 2004). By using 153 teleseismic earthquakes occurred between 24 September 2008 and 26 November 2010 (Figure 3.25), 18 SKS phases are analyzed and marked as 2 good, 3 fair, 12 poor and 1 Null (Figure 3.26).

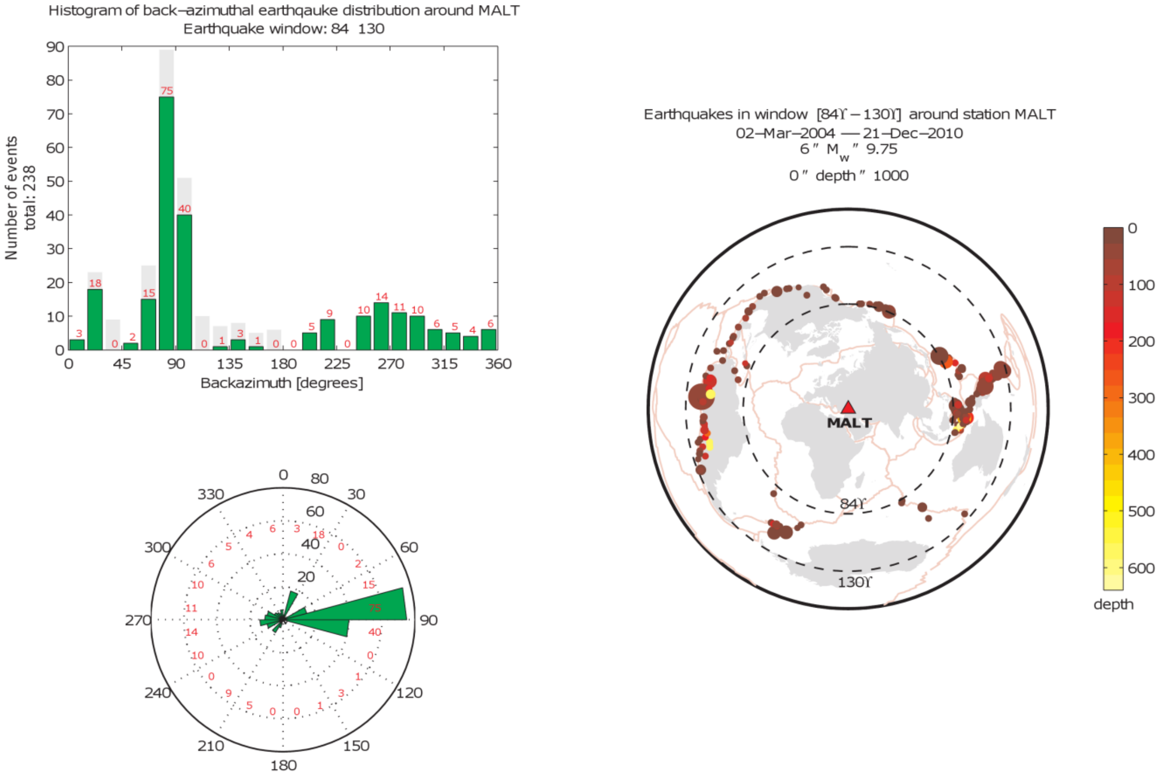

Figure 3.21. Earthquake distribution statistics for MALT broadband station. Histogram view (top left) and globe view (down left) show distribution of the earthquakes with back azimuth. On the right hand side earthquakes are plotted in different colors according to their magnitude

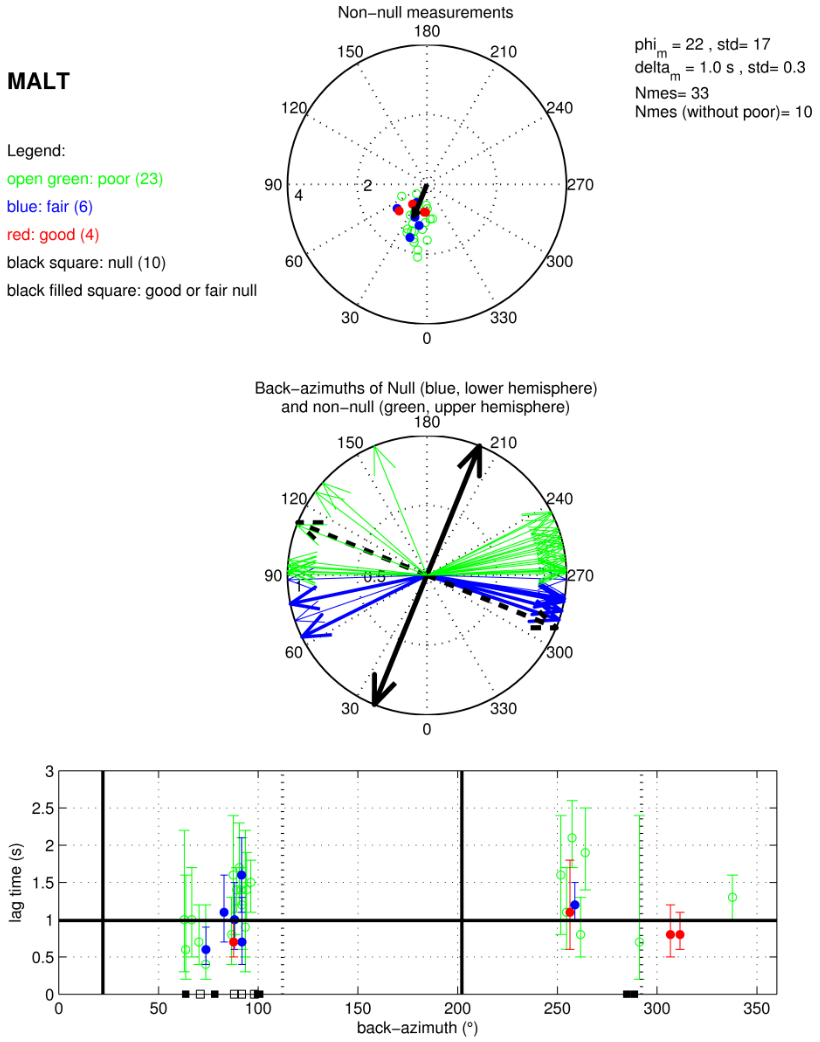

Figure 3.22. Polar diagram of MALT seismic station for good, fair and poor non-Null measurements is depicted. In the upper panel φ and δt are presented with standard deviations and black row represents the fast polarization direction. In the central panel polar plot of back azimuth are depicted. The thick blue arrows in the lower hemisphere show the back azimuth of events with good or fair Null measurements. The thin blue arrows correspond to events with poor Null measurements. The lower panel displays delay time as a function of back azimuth. The black filled squares show Null measurements rated as good or fair. Poor Nulls are plotted as open black squares

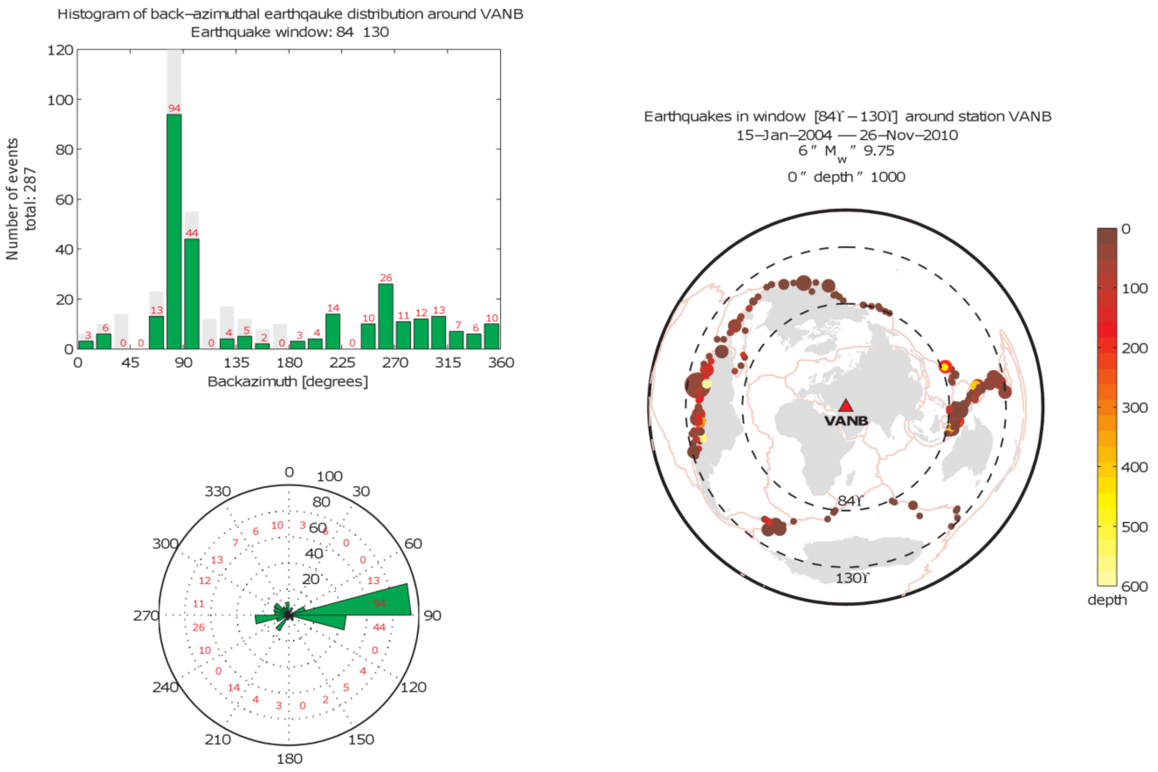

Figure 3.23. Earthquake distribution statistics for VANB broadband station. Histogram view (top left) and globe view (down left) show distribution of the earthquakes with back azimuth. On the right hand side earthquakes are plotted in different colors according to their magnitude

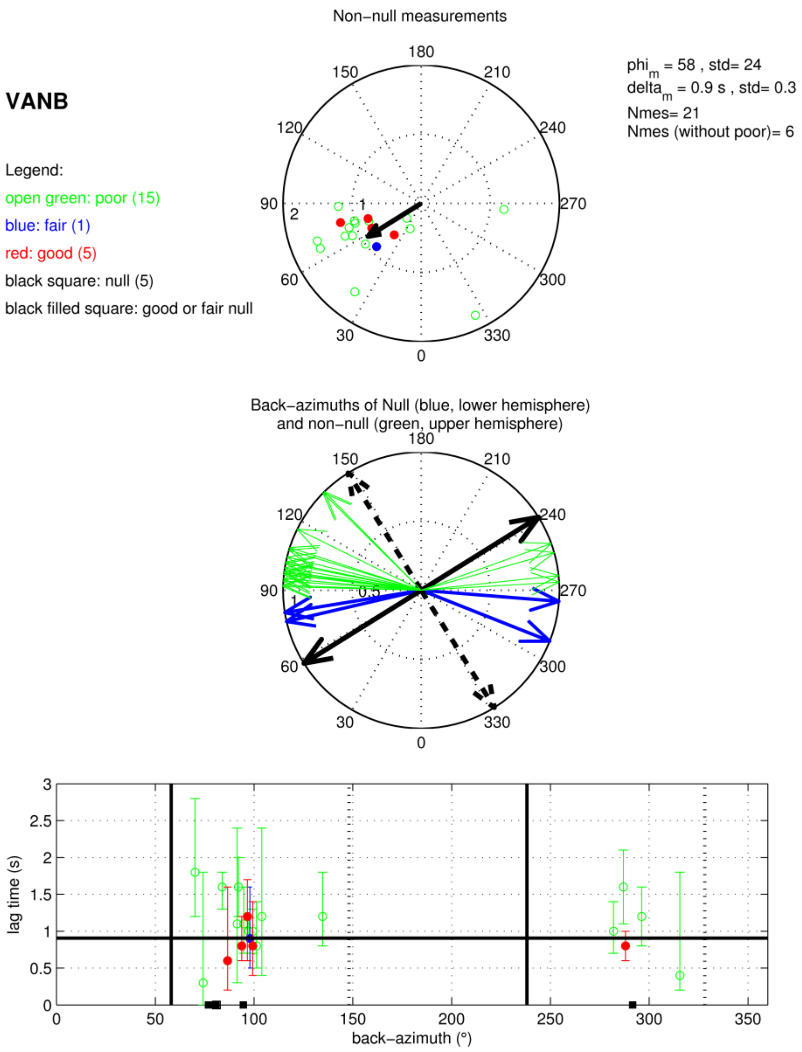

Figure 3.24. Polar diagram of VANB seismic station is depicted for good, fair and poor non-Null measurements. In the upper panel φ and δt are presented with standard deviations and black row represents the fast polarization direction. In the central panel polar plot of back azimuth are depicted. The thick blue arrows in the lower hemisphere show the back azimuth of events with good or fair Null measurements. The thin blue arrows correspond to events with poor Null measurements. The lower panel displays delay time as a function of back azimuth. The black filled squares show Null measurements rated as good or fair. Poor Nulls are plotted as open black squares

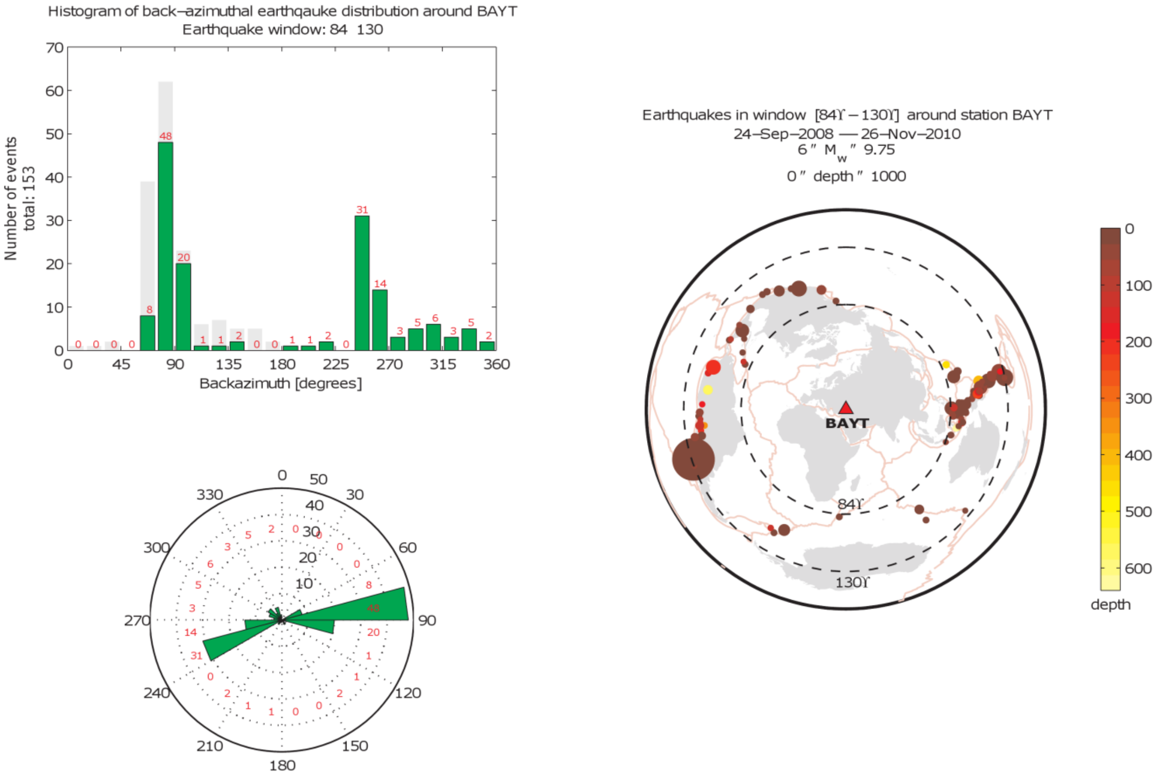

Figure 3.25. Earthquake distribution statistics for BAYT broadband station. Histogram view (top left) and globe view (down left) show distribution of the earthquakes with back azimuth. On the right hand side earthquakes are plotted in different colors according to their magnitude

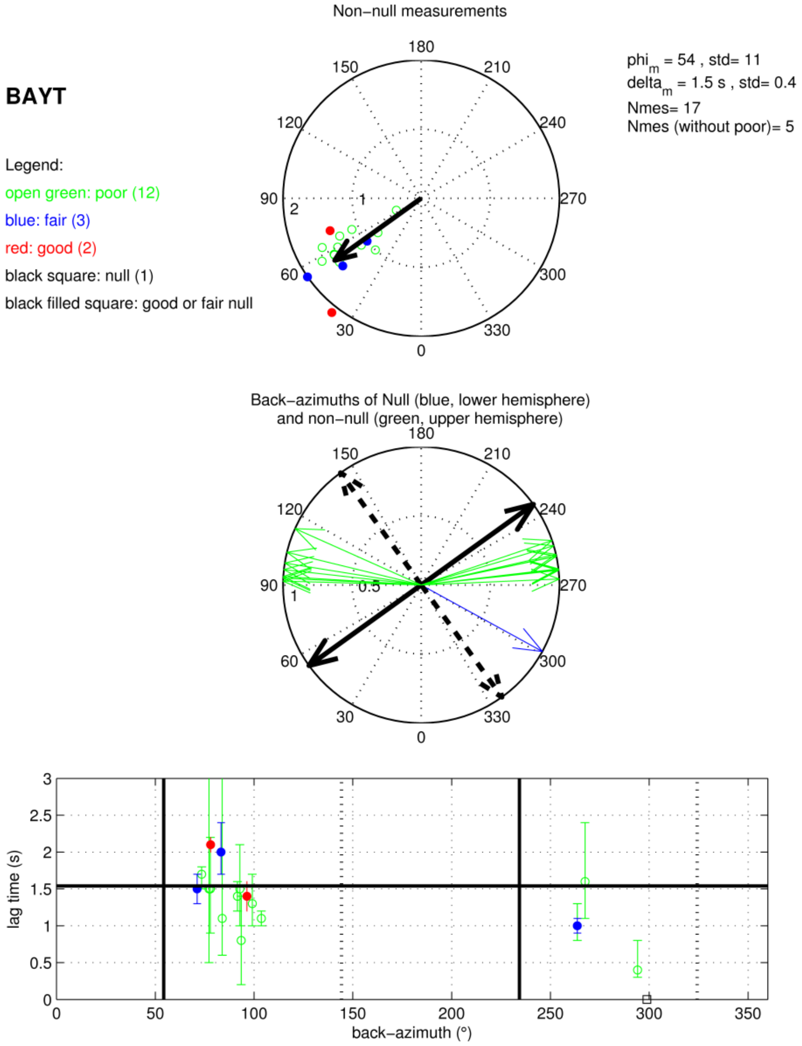

Figure 3.26. Polar diagram of BAYT seismic station is shown for good, fair and poor non-Null measurements. In the upper panel φ and δt are presented with standard deviations and black row represents the fast polarization direction. In the central panel polar plot of back azimuths are depicted. The thick blue arrows in the lower hemisphere show the back azimuth of events with good or fair Null measurements. The thin blue arrows correspond to events with poor Null measurements. The lower panel displays delay time as a function of back azimuth. The black filled squares show Null measurements rated as good or fair. Poor Nulls are plotted as open black squares

3.5. An Overview of the SKS Splitting Observations

Shear-wave splitting measurements are performed on the records of core-refracted SKS phases at the 182 permanent and temporary broadband stations located in Turkey and adjacent regions. The total dataset includes 4163 splitting measurements from 700 events at epicentral distances between 86° and 130°. Delay time (δt) and polarization orientation of the first-arrival phase (φ), splitting parameters, are measured using the rotation–correlation method (*e.g*. Bowman and Ando, 1987) and minimum energy method (Silver and Chan, 1991) in the SplitLab environment (Wüstefeld *et al*., 2007).

The station density and the number of measurements vary over the region. The permanent stations with more data yield better estimates of the splitting parameters. The mean standard errors are generally smaller than 27° for φ and 0.8 seconds for δt. Figure 3.27 shows a map of the measured anisotropy at the stations in this study (blue lines) with previous measurements (red, green, orange).

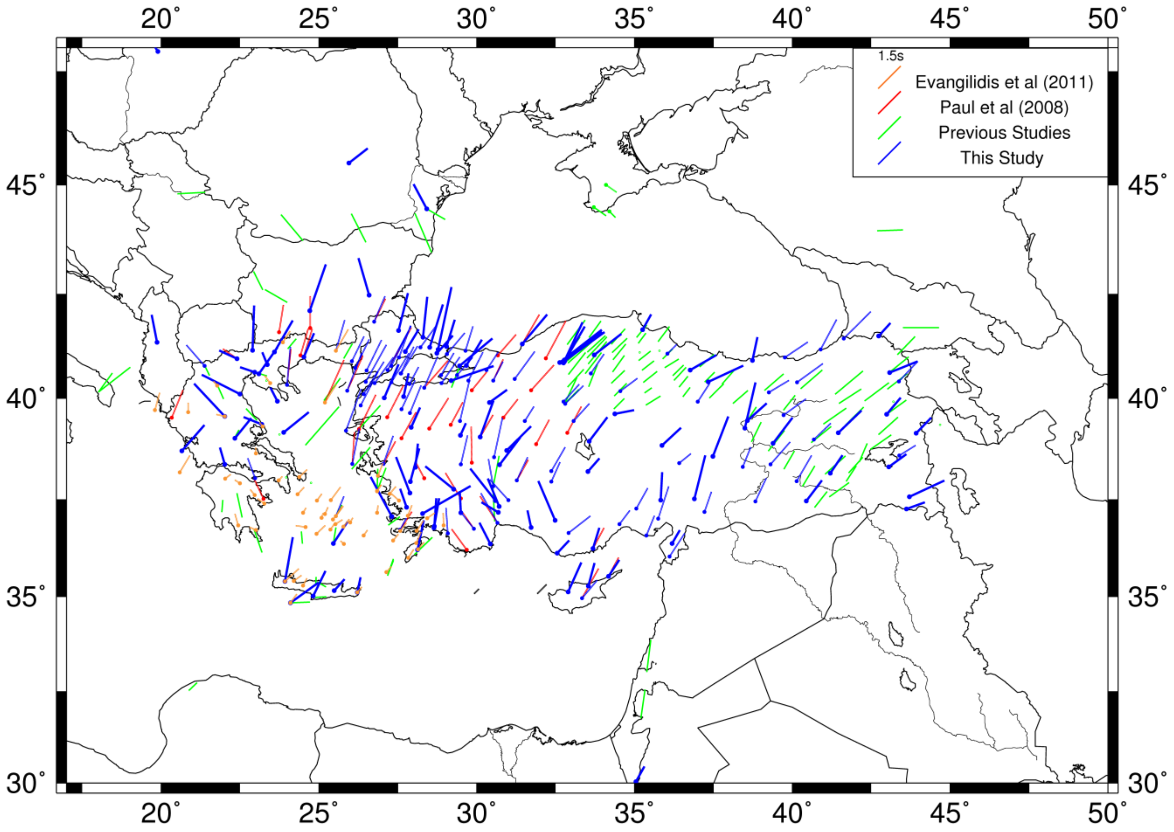

Figure 3.27. Average fast splitting directions with delay times from the SKS observations. Previous studies are also shown with different colors

Overall, the splitting parameters show regional patterns as a result of complex geodynamic process beneath the region. Fast splitting directions are almost uniform with NE-SW orientation (~43°) in the Eastern Anatolia. The delay times are also uniformly varying between 0.9 and 1.5 seconds in the region with a regional average of ~1.3 seconds. The measurements are mostly consistent with the results of Sandvol *et al*. (2003). Change from NE-SW to NNE-SSW on the splitting angles is observed in the Central North Anatolian Fault Zone (CNAFZ) with a decrease of delay times to ~0.5 seconds. The majority of the measurements in this zone (green lines) are from the CNAFZ experiment (Biryol *et al*., 2010). A gradual decrease of the delay times from the Eastern Anatolia to CNAFZ is observed. On the western part of the NAFZ (WNAFZ) the splitting angles are still in NE-SW direction with an average of 43°. There is an apparent increase on the delay times from ~0.5 seconds to ~1.3seconds toward the east of 34°E and toward the west of

37°E (Biryol *et al.*, 2010). On the continuation to the Marmara Region the delay times are largest (~1.5-2 s) with average splitting angle of NNE-SSW (~28°).

In the Central Anatolia the station coverage is not dense. There are significant variations on the splitting directions as well as delay times toward the Southern and Western Anatolia. The measurements are not uniformly distributed in region and the parameters are varying locally. As the splitting parameters are coherent in the regions closer to Marmara and NAFZ they change drastically in the Southeastern Anatolia. On the west of the Cyprus (< 31°E), a sudden change on splitting angles from NE-SW to NW-SE is apparent. This continues to the Aegean coast of the Western Anatolia. In the Western Anatolia the splitting angles are in NE-SW direction with average delay times of ~1.3 seconds and coherent with the Marmara Region (Figure 3.27). In the Aegean Sea few stations located on the islands show NE-SW direction with large delay times (~1.5 s), with the exception of the measurements on Southern Aegean Sea (*e.g.* Crete). There appear to be significant differences on the splitting parameters of the Southern Aegean Sea observed in this study and previous works (Hatzfeld, *et al.*, 2001; Evangelidis *et al*, 2011). Beneath the continental Greece the splitting parameters are strongly varying from south to north and there is no regionally consistent splitting direction while the delay times are increasing from the Southern Greece (~1.3 s) to Northern Greece (~1 s).

Figures 3.28 and 3.29 compare the variations of splitting angles and delay times from the Eastern Turkey to the Western Greece for the latitude ranges 39°-43° and 35°-39°, respectively. The azimuth of fast directions starts changing on both profiles at 31°E to the west with increasing delay times. The change is smooth up to 23°E for the latitude range of 39°-43° and sharper for longitudes greater than 23°E. Similarly the delay times increase suddenly at latitudes greater than 23°E. The variations for the latitudes between 39°-43° are more striking. Larger perturbations on the splitting parameters are observed on the west of Cyprus (< 32°E). The geographical distribution of the observed delay dimes are shown in Figure 3.30. A general increase can also be seen clearly from Eastern Anatolia to Aegean.

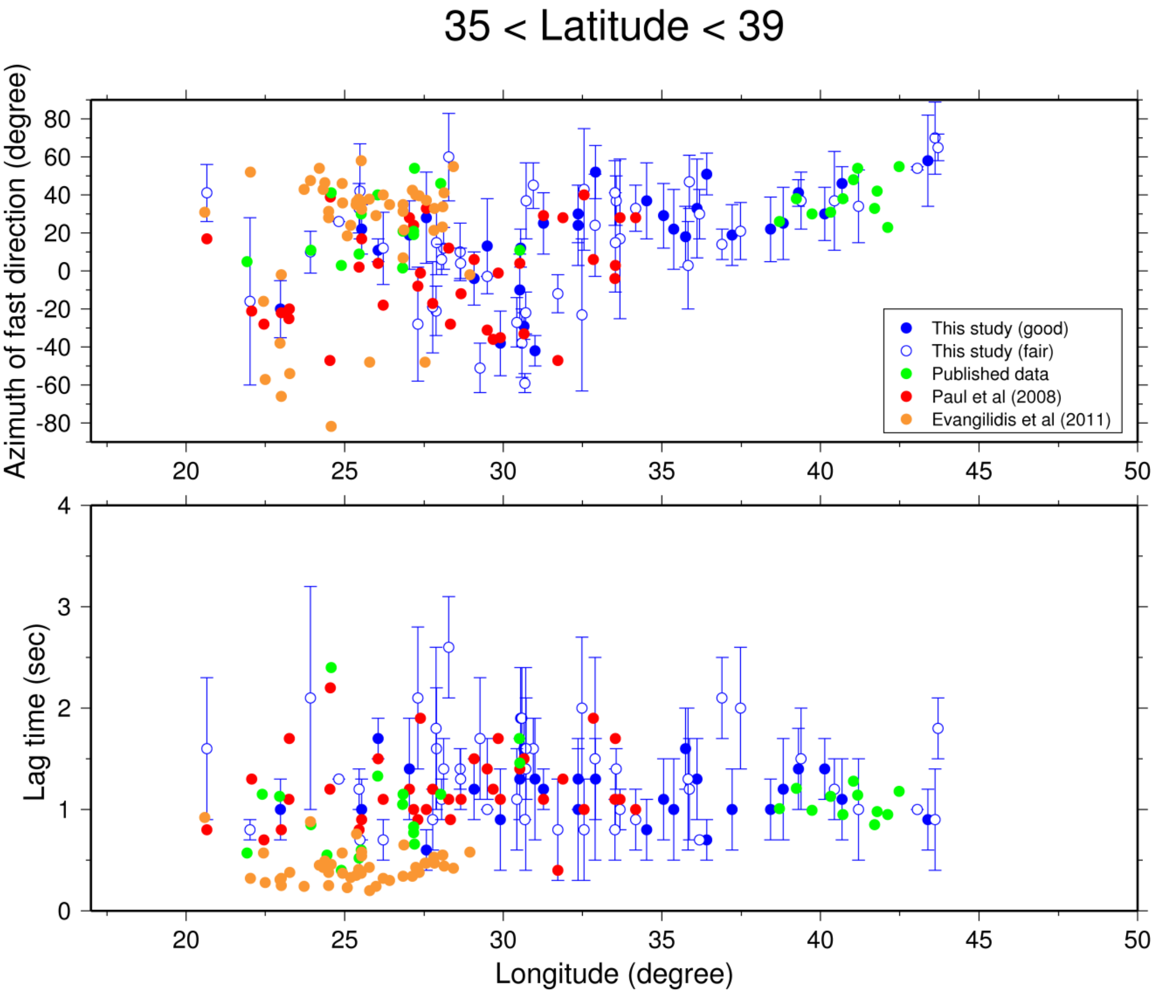

Figure 3.28. Fast polarization directions (above) and lag times (below) for longitudes from Eastern Anatolia to Greece between 35°N and 39°N (same colors as in Figure 3.27 are used for the various studies)

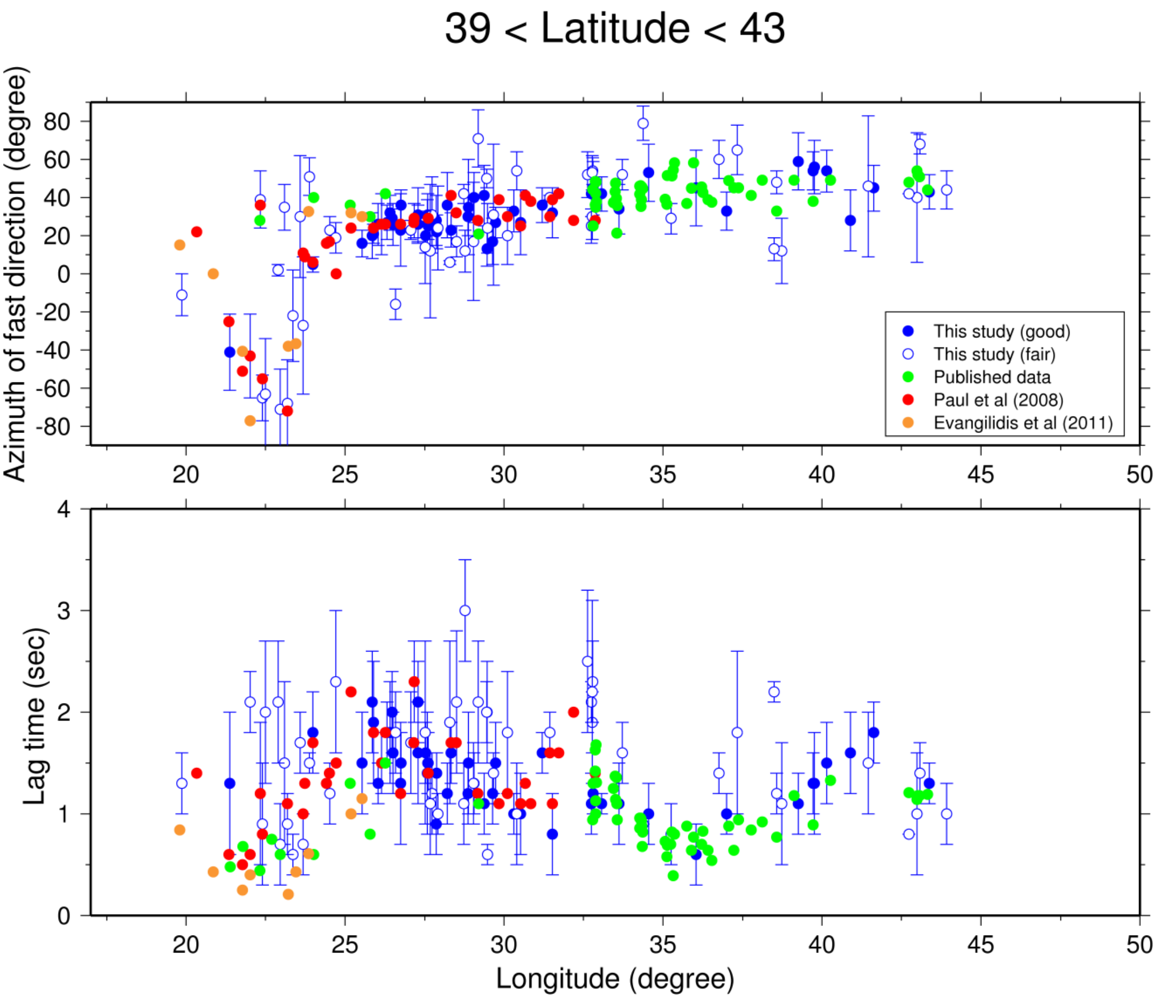

Figure 3.29. Fast polarization directions (above) and lag times (below) for longitudes from Eastern Anatolia to Greece between 39°N and 43°N (same colors as in Figure 3.27 are used for the various studies)

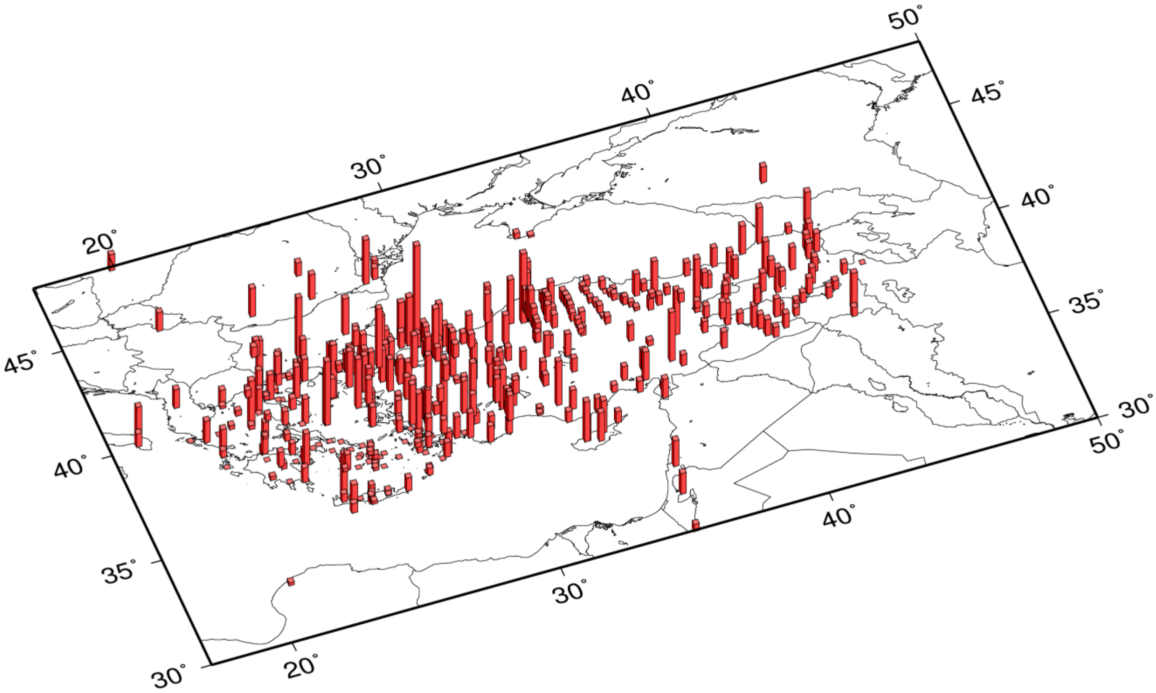

Figure 3.30. The average delay times observed at each station. The figure shows all the observations of present and previous works (For better visibility the delay times are squared)

3.6. The Origin of SKS Anisotropy

It is assumed that the maximum crustal contribution to the splitting delay times is less than 0.2 seconds (Barruol and Mainprice, 1993). Large splitting delay times (> 1 s) suggest that both lithosphere and asthenosphere are involved in the process. Assuming 4 per cent anisotropy would require ~120 km of thick anisotropic layer for 1 s delay time. On the other hand, a more complicated anisotropic layering cannot be ruled out. In the presence of 2 layers with different anisotropic properties, systematic azimuthal variations for φ and δt with a $\pi/2$ periodicity should be observed (Silver and Savage, 1994). We checked the permanent stations with sufficient azimuthal coverage that neither delay times nor orientations show systematic variations, indicating that anisotropy is concentrated in a single layer.

A qualitative interpretation of the observed anisotropy is based on comparisons of the fast orientations with surface deformation or absolute plate motions (Silver and Holt, 2002). A regional coherency of anisotropy with surface motion suggests a lithospheric origin assuming a uniform vertical strain throughout the lithosphere. On the other hand a uniform distribution of fast axis orientations at broader scale coherent with plate motion directions would support an asthenospheric origin (Kaviani *et al.*, 2009). To compare fast polarization directions with plate motions it is necessary to select an appropriate reference frame. A commonly used reference frame in the area is the relative motion of the Anatolia and surrounding plates with respect to fixed Eurasia (McClusky *et al.*, 2000). In this case, the direction of lithospheric motion does not necessarily represent an absolute plate motion that can be used for comparison with anisotropy measurements (Figure 3.2). Kreemer (2009) attempted to put constraints on the absolute plate motions in a hotspot reference frame based on observations of shear wave splitting orientations (GSRM-APM-1). The results of Kreemer (2009) show an overall mismatch between observed anisotropy directions and absolute plate velocity directions (Figure 3.3).

3.7. Discussions

In general the measurements in this study show a complicated behavior of anisotropy. The splitting parameters are regionally coherent in the Eastern Anatolia with splitting directions consistent with the APM (Sandvol *et al.*, 2003). The regional average delay times of ~1.3 seconds indicate the source of anisotropy is in the asthenosphere as the thickness of the lithosphere is ~60-80 km (Özacar *et al.*, 2010). A similar argument has been assumed for the observations on the CNAFZ by Biryol *et al.* (2010). Changes on the regional behavior of the splitting parameters are observed for longitudes less than 31°E. A relative increase on delay times from east to west in the central part of the NAFZ was interpreted by the influence of the differential motion between Hellenic and Cyprus trenches on the flow of the asthenosphere (Biryol *et al.*, 2010). The regional changes on the observed splitting parameters indicate rotation of the splitting angles and increase in the delay times to the west. The variations are more pronounced by the stations closer to the Hellenic and Cyprus Arcs (compare Figures 3.28 and 3.29) indicating the influence of the distance from the Hellenic and Cyprian trenches. However the mechanism is not just a function of geometry. Seismic tomographic images of Hellenic and Cyprus Arcs indicate discontinuities on the geometry slabs, suggesting tears at least in two locations (Faccenna *et al.*, 2006; Biryol *et al.*, 2010). The first one is associated with an alkaline volcanism along a N-S trending line parallel to the western coast of Anatolia during the Middle Miocene (Pe-Piper and Piper, 2007; Dilek and Altunkaynak, 2009). The second slab tear is located in Eastern Turkey below the Bitlis collision zone. Tomographic models show that the slab is detached there and that the continental lithosphere is thin and hot. Volcanism suggesting an asthenospheric window and slab delamination is recognized in the Late Miocene below Eastern Turkey (Şengör *et al.*, 2008). The strong variations observed on the anisotropy along the tear zones indicate the influence of mantle flow.

In Western Turkey the direction of the anisotropy is NE-SW on the north and progressively NNE-SSW on the south (Figure 3.27). Aktuğ *et al.* (2009) computed the strain rate from GPS velocities. They observed that the main direction of extension is NE-SW to NNE-SSW in the northern half of Western Turkey (38°N). This direction rotates counterclockwise as one moves southward, becoming NNW-SSE in the Southeastern Aegean. The orientation of the anisotropy is along the direction of principal extension in the Western Turkey. In the Aegean Sea, between Western Anatolia and continental Greece the anisotropy is oriented in NE-SW (~35°) direction and consistent with the GPS velocities.

4. CONCLUSIONS

This study is an attempt to contribute to the understanding of a long debated question on active tectonics in the eastern Mediterranean region: What is the source of continental deformation? It is a fact that this is not a simple question to answer. Two competing hypothesis exist on the deformation of the continental lithosphere. The first one suggests that the lithosphere consists of rigid blocks which float on the asthenosphere separated by lithospheric faults and the deformation is a result of forces at their edges (England and McKenzie, 1982; Taymaz *et al*., 1991; Le Pichon *et al*., 1995; McClusky *et al*., 2000). The second one assumes that flow in the asthenosphere control the deformation in the upper crust and a component of shear at the base of the lithosphere can be transmitted all the way to the crust (Molnar, 1988; Bokelmann, 2002). There is compelling evidence that two hypothesis are not completely independent, but coupled in a complex and nonlinear way (Jolivet *et al*., 2009; Le Pichon and Kreemer, 2010). The viscosity and thermal state of the lithosphere are the key elements of the degree of such coupling. It requires observations, analyses and models contributed from various disciplines of science. Seismology can only provide a snapshot on the evolution of this complex system with vaguely known initial and boundary conditions. The imprints on the present state can be useful to infer the past of a long and complex evolutionary process.

The Mediterranean Region has been the focus of international efforts to reconcile geological evolution with mantle structure and plate tectonics (Dewey and Şengör, 1979; Şengör and Yılmaz, 1981; McKenzie, 1972; Aktuğ *et al*., 2009; Le Pichon and Kreemer, 2010; Reilinger *et al*., 2010). High-resolution tomographic models and geological studies and GPS surveys have become available during the last two decades. The tomographic images of various resolutions and depths have provided the details of the upper mantle structure and the anisotropic properties have been revealed through the studies of body and surface waves. This study is a similar attempt to some of the previous works but take into account of the improved data quality and quantity. The results therefore present a higher resolution look to the upper mantle structure.

P_n velocities and anisotropy provide information on the chemical, thermal state of the uppermost mantle and the deformation patterns as a result of the shear forces between crust and mantle. On the other hand, the SKS splitting measurements provide the thickness of the anisotropic layer of the asthenosphere. Therefore both measurements are complementary yielding a better characterization of the upper mantle. Overall, there are significant differences on the P_n anisotropy and SKS splitting directions. The differences are partly due to the tradeoff between velocity and anisotropy perturbations from the P_n tomography. In the presence of large velocity perturbations in a region with low azimuthal coverage of the station and events may result larger errors on the estimates of the P_n anisotropy. However, the majority of the Anatolian and Aegean domain are well covered by the crossing rays and the influence of the poor coverage was evaluate in detail in Chapter 2.3.

Figure 4.1 compares the SKS splitting parameters with P_n velocities. The strong velocity perturbations observed in Eastern Anatolia has no apparent correlations with the splitting parameters. The observed low velocities indicate that the lithosphere is thin and most of the anisotropy is asthenospheric origin. Therefore the splitting directions are more related to the asthenosphere. However, this changes on the west of Cyprus (< 32°E). High P_n velocities between 30°-32° longitudes show strong correlations with the splitting parameters (Figure 4.1). The splitting directions change their orientations across the slab characterized by the high P_n velocities and these variations continue to the western coast of Anatolia. There is no obvious coherency between P_n anisotropy and splitting angles. This can be related to the influence of the subducting plate. The flow of the asthenospheric mantle through the tear zones and in the mantle wedge will have varying orientation of anisotropy at crust mantle boundary and beneath the slab.

The influence of the Hellenic slab can be observed on the splitting parameters and P_n anisotropy at different magnitudes. In Western Anatolia the P_n anisotropy is well correlated with the principal extension direction (Figure 4.2). Longer wavelength variations are observed on the splitting parameters starting at longitudes greater than 31°E even at the stations of large distances, e.g. NAFZ (Figures 3.28 and 3.29). The gradual rotation of the splitting angles and increasing delay time to the west indicate that the slab roll back is the dominant mechanism on the deformation of the lithosphere and mantle flow. The coherency of P_n anisotropy and splitting directions increases in the Aegean Sea. Similar observations were reported by Hatzfeld *et al*. (2001).

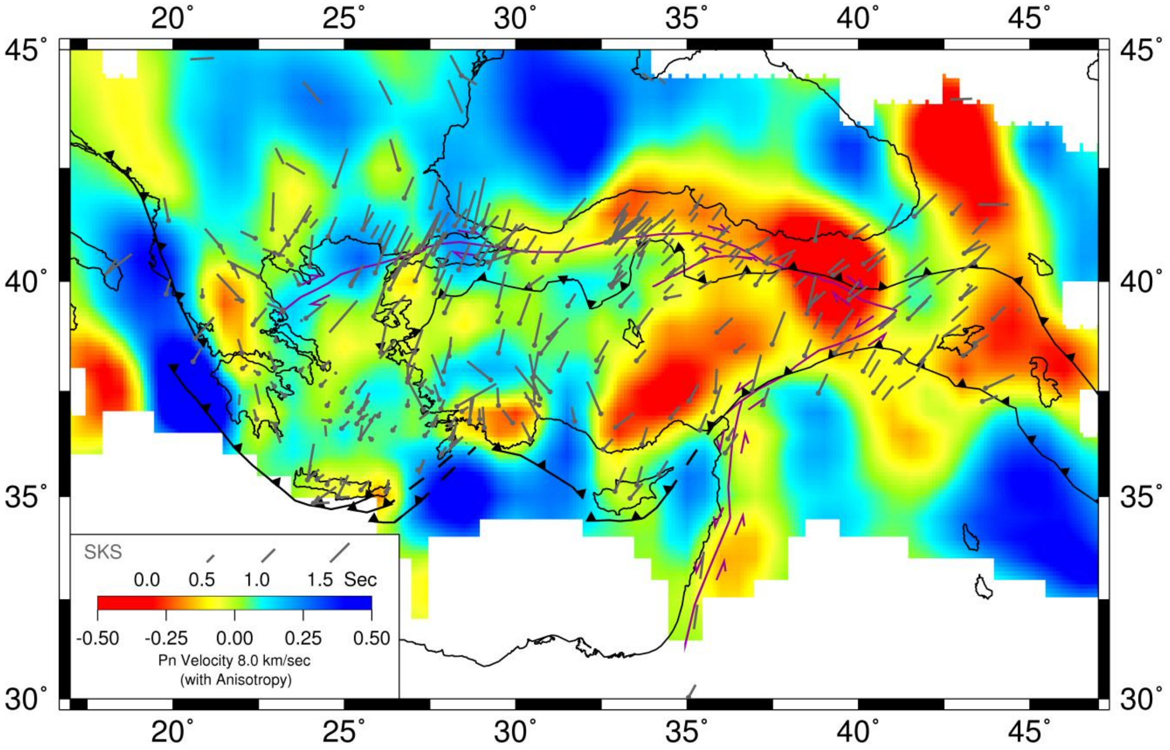

Figure 4.1. P_n velocities and SKS splitting (gray) measurements with major tectonic boundaries (thick black lines)

The observations in this study and previous works cannot be explained by a simple model for the whole region. The coherency between P_n anisotropy, SKS splitting and GPS vectors in the Aegean show that the crust and mantle deforms similarly (Figure 4.2). This requires a good coupling between the crust and mantle. The coupling may indicate that the lithospheric mantle and the lower crust are weak. However, the alternative may also be a valid hypothesis. When the crust and the mantle are subjected to the same boundary condition imposed along the retreating Hellenic trench they also deform coherently which would fit the observed P_n anisotropy, SKS splitting directions and GPS vectors.

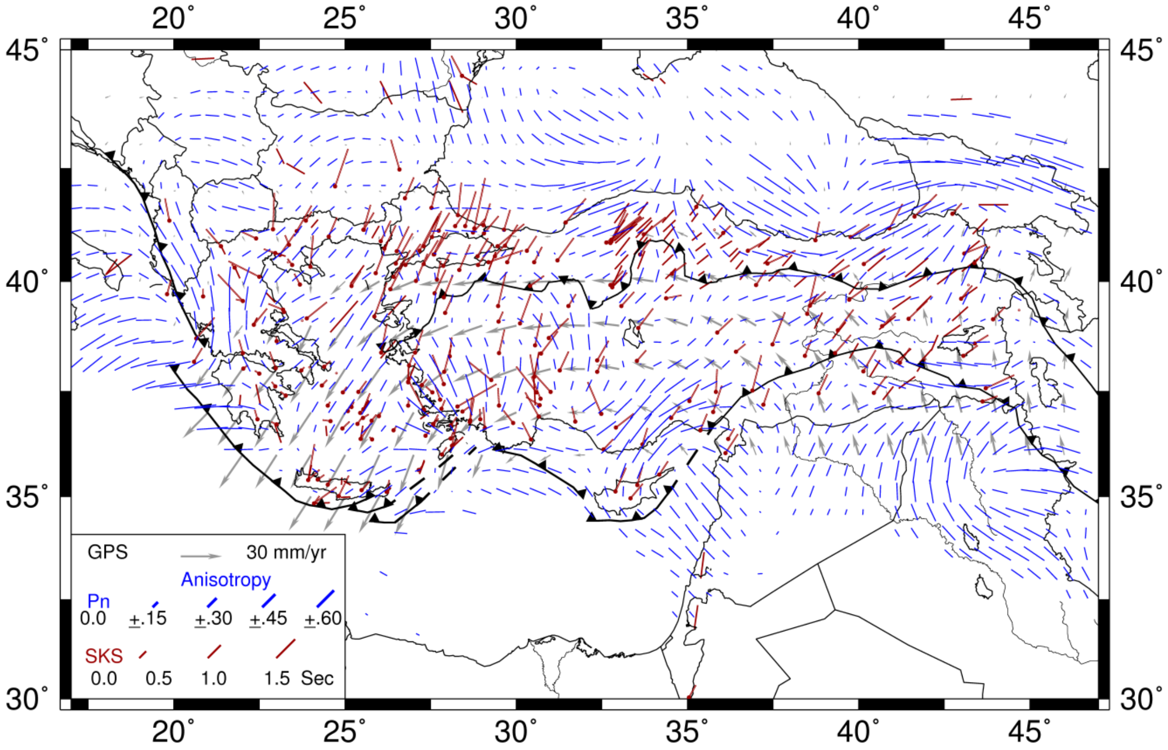

Figure 4.2. P_n anisotropy (blue), GPS velocities (gray) and SKS splitting (red) measurements. Thick black lines show the major plate boundaries

The incoherency in the Eastern and Central Anatolia between P_n anisotropy, SKS and GPS observations cannot be explained easily (Figure 4.2). A simple approach to explain observed GPS vectors in the Anatolia is to consider the westward motion of Anatolia through an extrusion model with the Arabia-Eurasia collision zone. In this case the Anatolian plate would be pushed by the Arabian plate across the Bitlis suture zone and most of the stress would be transmitted through the upper crust. The lithosphere is thin in the region and the asthenosphere is decoupled from the lithosphere. This could explain the observed differences between SKS splitting and the GPS measurements. However, we cannot completely rule out the effect of the mantle flow on the motion of the lithosphere. It is still possible to present a model to explain the westward motion of Anatolia by a westward mantle flow. If the flow is too recent, the anisotropic fabric may not be recorded. The source of the westward flow could be a gradient of dynamic topography between an upwelling of asthenosphere below the collision zone and the downgoing slab in the Aegean as proposed by Faccenna and Becker (2010). Based on the seismic tomographic models and using the distribution of temperature anomalies, Faccenna and Becker (2010) have modeled flow directions of the mantle. They were able reproduce the westward motion of Anatolia but failed to explain the southward motion of the Aegean slab and the N-S extension in the backarc region. However it is promising to observe that more comprehensive models including the effect of slab retreat with its complex geometry and better parameterized lithosphere may explain the majority of the observations.

REFERENCES

Aktuğ, B., *et al.*, 2009, "Deformation of Western Turkey from a Combination of Permanent and Campaign GPS Data: Limits to Block-like Behavior", *Journal of Geophysical Research*, Vol. 114.

Akyol, N., L. Zhu, B. J. Mitchell, H. Sözbilir and K. Kekovalı, 2006, "Crustal Structure and Local Seismicity in Western Anatolia", *Geophysical Journal International*, Vol. 166, No. 3, pp. 1259-1269.

Al-Lazki, A., E. Sandvol, D. Seber, M. Barazangi, N. Turkelli and R. Mohamad, 2004, "P_n Tomographic Imaging of Mantle Lid Velocity and Anisotropy at The Junction of The Arabian, Eurasian and African Plates", *Geophysical Journal International*, Vol. 158, pp. 1024-1040.

Angelier, J., 1978, "Tectonic Evolution of the Hellenic Arc Since The Late Miocene", *Tectonophysics*, Vol. 49, pp. 23–36.

Angelier, J., N. Lyberis, X.L. Pichon and P. Huchon, 1982, "The Tectonic Development of The Hellenic Arc and The Sea of Crete: A Synthesis", *Tectonophysics*, Vol. 86, pp. 159-196.

Ansel, V., and H. Nataf, 1989, "Anisotropy Beneath 9 Stations of the GEOSCOPE Broadband Network as Deduced From Shear-Wave Splitting", *Geophysical Research Letters*, Vol. 16(5), pp. 409–412.

Arpat, E. and F. Şaroğlu, 1972, "The East Anatolian Fault System: Troughs on its Development", *Mineral Research* and *Exploration Institute* of *Turke*y, Vol. 78, pp. 33-39.

Babuska, V. and M. Cara, 1991, *Seismic Anisotropy in the Earth*, Kluwer Academic Publisher, Netherlands.

Backus, G. E., 1965, "Possible Forms of Seismic Anisotropy of the Uppermost Mantle Under Oceans", *Journal of Geophysical Research*, Vol. 70, pp. 3429-3439.

Barka, A. A. and K. Kadinsky-Cade, 1988, “Strike-slip Fault Geometry in Turkey and its Influence on Earthquake Activity”, *Tectonics*, Vol. 7.

Becker, T. W., 2006, “On the Effect of Temperature and Strain-Rate Dependent Viscosity on Global Mantle Flow, Net Rotation, and Plate-Driving Forces”, *Geophysical Journal International,* Vol.167, pp. 943– 957.

Becker, T. W., 2008, “Azimuthal Seismic Anisotropy Constrains Net Rotation of the Lithosphere”, *Geophysical Research Letters*, Vol. 35.

Beghoul, N. and M. Barazangi, 1990, “Azimuthal Anisotropy of Velocity in the Mantle Lid Beneath the Basin and Range Province”, *Nature*, Vol. 348, No. 6301, pp. 536-538.

Behn, M. D., C. P. Conrad, and P. G. Silver, 2004, “Detection of Upper Mantle Flow Associated With the African Super Plume”, *Earth and Planetary Science Letters*, Vol. 224, pp. 259– 274.

Biryol, C. B., G. Zandt, S. L. Beck, A. A. Özacar, H.E. Adıyaman, and C. R. Gans, 2010, “Shear Wave Splitting Along A Nascent Plate Boundary: the North Anatolian Fault Zone”, *Geophysical Journal International*, Vol. 181, pp. 1201-1213.

Biryol, C. B., S. L. Beck, G. Zandt and A. A. Özacar, 2011, “Segmented African Lithosphere Beneath the Anatolian Region Inferred from Teleseismic P-Wave Tomography”, *Geophysical Journal International*, Vol. 184, pp. 1037–1057.

Bokelmann, G.H.R., 2002, “Which Forces Derive North America?”, *Geology*, Vol. 30, pp. 1027-1030.

Bowman, J. R. and M. Ando, 1987, “Shear Wave Splitting in the Upper-Mantle Wedge Above the Tonga Subduction Zone”, *Geophysical Journal of the Royal Astronomical Society*, Vol. 88, pp. 25-41.

Bozkurt, E., 2001, “Neotectonics of Turkey - A Synthesis, Geodinamica Acta: The Europian”, *Journal of Geodynamics*, Vol. 14 (1-3), pp. 3-30.

Bullen, K. E. and A.Bolt, 1985, *An Introduction to the Theory of Seismology*, Cambridge University Press.

Buttles, J., and P. Olson, 1998, “A laboratory model of subduction zone anisotropy” *Earth and Planetary Science Letters*, Vol. 164, pp. 245–262.

Calvert, A., E. Sandvol, D. Seber, M. Barazangi, F. Vidal, G. Alguacil and N. Jabour, 2000, “Propagation of Regional Seismic Phases (L_g and S_n) and P_n Velocity Structure Along the Africa Iberia Plate Boundary Zone: Tectonic Implications”, *Geophysical Journal International,* Vol. 142, pp. 384-408.

Cambaz, M. D. and H. Karabulut, 2010, “Love Wave Group Velocity Maps of Turkey and Surrounding Regions”, *Geophysical Journal International*, Vol. 181, pp. 502–520.

Carlson, R. W., D. G. Pearson and D. E. James, 2005, “Physical, Chemical, and Chronological Characteristics of Continental Mantle”, *Reviews of Geophysics*, Vol. 43.

Chakrabarti R., A. R. Basu, and A. Ghatak, 2011, “Chemical Geodynamics of Western Anatolia”, *International Geology Review*, iFirst article, pp. 1-22.

Christensen, N.I., 2004, “Serpentinites, Peridotites, and Seismology”, *International Geology Review*, Vol. 46, pp. 795 – 816.

Condie, K.C.,1989, *Plate Tectonics and Crustal Evolution*, Pedrgamon Press, New York, 476, pp.

Conrad, C. P., and M. D. Behn, 2010, “Constraints on Lithosphere Net Rotation and Asthenospheric Viscosity from Global Mantle Flow Models and Seismic Anisotropy”, *Geochemistry Geophysics Geosystems*, Vol. 11.

Conrad, C. P., M. D. Behn, and P. G. Silver, 2007, “Global Mantle Flow and the Development of Seismic Anisotropy: Differences Between the Oceanic and Continental Upper Mantle”, *Journal of Geophysical Research,* Vol. 112.

Crampin, S., 1977, “A Review of the Effects of Anisotropic Layering on the Propagation of Seismic Waves”, *Geophysical Journal of the Royal Astronomical Society*, Vol. 49, pp. 9-27.

Deniel, C., E. Aydar and A. Gourgaud, 1998, “The Hasan Dağı Strato Volcano (Central Anatolia, Turkey): Evolution from Calc-alkaline to Alkaline Magmatism in A Collision Zone”, *Journal of Volcanology and Geothermal Research*, 87, 275–302.

Dewey, J.F. and A.M.C. Şengör, 1979, “Aegean and Surrounding Regions: Complex Multiplate and Continuous Tectonics in a Convergent Zone.”, *Geological Society of America Bulletin*, Vol. 90, pp. 84-92.

Dilek, Y., and Altunkaynak, S., “Geochemical and Temporal Evolution of Cenozoic Magmatism in Western Turkey: Mantle Response to Collision, Slab Breakoff, and Lithospheric Tearing in an Orogenic Belt”, in van Hinsbergen, D.J.J., Edwards, M.A., and Govers, R., (eds.), *Collision and Collapse at the Africa-Arabia-Eurasia Subduction Zone*, v. 311, p. 213–233, Geological Society of London Special Publications, 2009.

DiLuccio, F. and M. E. Pasyanos, 2007, “Crustal and Upper Mantle Structure in the Eastern Mediterranean from the Analysis of Surface Wave Dispersion Curves”, *Geophysical Journal International*, Vol. 169, pp. 1139–1152.

Duncan R. A., 1981, “Hotspots in the Southern Oceans—An Absolute Frame of Reference For Motion of the Gondwana Continents”, *Tectonophysics*, Vol. 132, pp. 29–42.

Dziewonski, A. M., 1984, “Mapping the Lower Mantle Determination of Lateral Heterogeneity in P-velocity up to Degree and Order 6”, *Journal of Geophysical Research,* Vol. 89, pp. 5929-5952.

Eberhart-Phillips, D., D. Christensen, T.M. Brocher, R. Hansen, N.A. Ruppert, P.J. Haeussler and G. A. Abers, 2006, “Imaging the Transition From Aleutian Subduction to Yakutat Collision in Central Alaska, With Local Earthquakes and Active Source Data”, *Journal of Geophysical Research*, Vol. 111.

England, P.C. and McKenzie, D.P., 1982, "A Thin Viscous Sheet Model for Continental Deformation", *Geophysical Journal of the Royal Astronomical Society,* Vol. 70, pp. 295-321.

Evangelidis, C. P., W.T. Liang, N. S. Melis, and K. I. Konstantinou, 2011, "Shear Wave Anisotropy Beneath the Aegean Inferred from SKS Splitting Observations", *Journal of Geophysical Research*, Vol. 116.

Faccenna, C. and T. W. Becker, 2010, "Shaping Mobile Belts by Small-Scale Convection", *Nature*, Vol. 465(3), pp. 602-605.

Faccenna, C., O. Bellier, J. Martinod, C. Piromallo, and V. Regard, 2006, "Slab Detachment Beneath Eastern Anatolia: A Possible Cause for the Formation of the North Anatolian Fault", *Earth* and *Planetary Science Letters*, Vol. 242, pp. 85-97.

Flerit, F., R. Armijo, G. King, B. Meyer, 2004, "The Mechanical Interaction Between the Propagating North Anatolian Fault and the Back-Arc Extension in the Aegean", *Earth* and *Planetary Science Letters*, Vol. 224 (3-4), pp. 347-362.

Floyd, P. A., M. C. Göncüoğlu, J. A. Winchester and M. K. Yalınız, "Geochemical Character and Tectonic Environment of Neotethyan Ophiolitic Fragments and Metabasits in the Central Anatolian Crystalline Complex, Turkey", in E. Bozkurt, J. A. Winchester, J. D. A. Piper (eds.) *Tectonics and Magmatism in Turkey and the Surrounding Area,* Vol. 173, pp. 183-202, Geological Society, London, 2000.

Fukao, Y., 1984, "Evidence From Core-Reflected Shear Waves for Anisotropy in the Earth's Mantle", *Nature,* Vol. 309, pp. 695-698.

Gans, C. R., S. L. Beck, G. Zandt, C. B. Biryol and A. A. Özacar, 2009, "Detecting the Limit of Slab Break-off in Central Turkey: New High-Resolution P_n Tomography Results", *Geophysical Journal International,* Vol. 179, pp. 1566-1572.

Glover, C. and A. H. F. Robertson, 1998, "Neogen Intersection of the Aegean and Cyprus Arcs: Extensional and Strike-Slip Faulting in the Isparta Angle, SW Turkey." *Tectonophysics,* Vol. 298, pp. 103-132.

Gök, R., M. Pasyanos, E. Zor, 2007, "Lithospheric Structure of the Continent–Continent Collision Zone: Eastern Turkey", *Geophysical Journal International,* Vol. 169, pp. 1079–1088.

Göncüoğlu, M.C., N. Turhan, K. Şentürk, A. Özcan, Ş. Uysal and M. K. Yalınız, "A Geotraverse Across Northwestern Turkey: Tectonic Units of the Central Sakarya Region and Their Tectonic Evolution." in E. Bozkurt, J. A. Winchester, J. D. A. Piper, (eds.), *Tectonics and Magmatism in Turkey and the Surrounding Area,* Vol. 173, pp. 139-161, Geological Society, London, 2000.

Hatzfeld, D., E. Karagianni, I. Kassaras, A. Kiratzi, E. Louvari, H. Lyon-Caen, K. Makropoulos, P. Papadimitriou, G. Bock and K. Priestley, 2001, "Shear Wave Anisotropy in the Upper-Mantle Beneath the Aegean Related to Internal Deformation", *Journal of Geophysical Research*, Vol. 106 , pp. 30,737-30,753.

Hearn, T. M. and J. Ni, 1994, "P_n Velocities Beneath Continental Collision Zones: The Turkish-Iranian Plateau", *Geophysical Journal International,* Vol. 117, pp. 273-283.

Hearn, T. M., 1999, "Uppermost Mantle Velocities and Anisotropy Beneath Europe", *Journal of Geophysical Research*, Vol. 104, No. B7, pp.15, 123-15,139.

Hearn, T., 1984, "P_n Travel Times in Southern California", *Journal of Geophysical Research*, Vol. 89, pp.1843-1855.

Hearn, T.M., 1996, "Anisotropic P_n Tomography in the Western United States" *Journal of Geophysical Research*, Vol. 101, No. B4, pp. 8403-8414.

Helffrich, G., P. Silver and H. Given, 1994, "Shear-Wave Splitting Variation Over Short Spatial Scales on Continents", *Geophysical Journal International,* Vol. 119, pp. 561–573.

Hess, H.H., 1964, "Seismic Anisotropy of the Uppermost Mantle Under Oceans", *Nature*, Vol. 203, pp. 629-631.

Hollenstein, C., M. Mueller, A. Geiger, and H.-G. Kahle, 2008, "Crustal Motion and Deformation in Greece from A Decade of GPS Measurements", *Tectonophysics,* Vol. 449, pp. 17–40.

Jackson, J., 1994, "Active Tectonics of the Aegean Region", *Annual Review of Earth and Planetary Sciences*, Vol. 22, pp. 239-271.

Jolivet, L., C. Faccenna and C. Piromallo, 2009, "From Mantle to Crust: Stretching the Mediterranean", *Earth and Planetary Science Letters*, Vol. 285, pp. 198– 209.

Kahle, H. -G., C. Straub, R. Reilinger, S. McClusky, R. King, K. Hurst, G. Veis, K. Kastens and P. Cross, 1998, "The Strain Field in the Eastern Mediterranean Region, Estimated by Repeated GPS Measurements", *Tectonophysics*, Vol. 294, pp. 237-252.

Karabulut, H., J. Schmittbuhl, S. Özalaybey, O. Lengliné, A. Kömeç Mutlu, V. Durand, M. Bouchon, G. Daniel, and M.P. Bouin, 2011, "Evolution of the Seismicity in the Eastern Marmara Sea a Decade Before and After the 17 August 1999 Izmit Earthquake", *Tectonophysics*, Vol. 510 (1–2), pp. 17–27.

Karagianni, E. E., C. B. Papazachos, D. G. Panagiotopoulos, P. Suhadolc, A. Vuan, and G. F. Panza, 2005, "Shear Velocity Structure in the Aegean Area Obtained by Inversion of Rayleigh Waves", *Geophysical Journal International*, Vol. 160, pp. 127–143.

Karato, S. and H. Jung, 1988, "Water, Partial Melting and the Origin of the Seismic Low Velocity and High Attenuation Zone in the Upper Mantle", *Earth and Planetary Science Letters*, Vol. 157, pp. 193-207.

Karato, S., and P. Wu, 1993, "Rheology of the Upper Mantle: A Synthesis", *Science,* Vol. 260, pp. 771–778.

Karato, S.I., 1995, "Effects of Water on Seismic Wave Velocities in the Upper Mantle", *Proceeding of the Japan Academy*, Vol. 71, pp. 61-66.

Karato, S.I., H. Jung, I. Katayama and P. Skemer, 2008, “Geodynamic Significance of Seismic Anisotropy of the Upper Mantle: New Insights from Laboratory Studies”, *Annual Review of Earth and Planetary Sciences,* Vol. 36, pp. 59-95.

Kaviani, A., A. Paul, D. Hatzfeld, J. Vergne and M. Mokhtari, 2007, “A Strong Seismic Velocity Contrast in the Shallow Mantle Across the Zagros Collision Zone (Iran)”, *Geophysical Journal International*, Vol. 171, pp. 399–410.

Kaviani, A., D. Hatzfeld, A. Paul, M. T. and K. Priestley, 2009, “Shear-Wave Splitting, Lithospheric Anisotropy, and Mantle Deformation Beneath the Arabia–Eurasia Collision Zone in Iran”, *Earth and Planetary Science Letters*, Vol. 286, pp. 371-378.

Keskin, M., 2003, “Magma Generation by Slab Steepening and Break off Beneath a Subduction–Accretion Complex: An Alternative Model for Collision-Related Volcanism in Eastern Anatolia, Turkey”, *Geophysical Research Letters*, Vol. 30, pp. 8046.

Kissling, E., W. L. Ellsworth, D. Eberhart-Phillips and U. Kradolfer, 1994, “Initial Reference Models in Local Earthquake Tomography”, *Journal of Geophysical Research*, Vol. 99 (B10), pp. 19635–19646.

Koçyiğit, A., E. Ünay and G. Saraç, 2000, “Episodic Graben Formation and Extensional Neotectonic Regime in West Central Anatolia and the Isparta Angle: A Case Study in the Akşehir-Afyon Graben, Turkey”, *Geological Society of London,* Vol. 173, pp. 405-421.

Kosarev, G. L., L. I. Makeyeva and L. P. Vinnik, 1984, “Anisotropy of the Mantle Inferred from Observations of P to S Converted Waves”, *Goephysical Journal International*, Vol. 76, pp. 209-220.

Kotzev V., R. Nakov, T. Georgiev, B. C. Burchfiel and R. W. King, 2006, “Crustal Motion and Strain Accumulation in Western Bulgaria”, *Tectonophysics*, Vol. 413, pp. 127-145.

Kreemer, C., 2009, “Absolute Plate Motions Constrained by Shear Wave Splitting Orientations with Implications for Hot Spot Motions and Mantle Flow”, *Journal of Geophysical Research*, Vol. 114.

Kreemer, C., N. Chamot-Rooke and X. Le Pichon, 2004, “Constraints on the Evolution and Vertical Coherency of Deformation in the Northern Aegean from a Comparison of Geodetic, Geologic and Seismologic Data”, *Earth and Planetary Science Letters*, Vol. 225, pp. 329-346.

Kreemer, C., W.E. Holt, and A.J. Haines, 2003, “An Integrated Global Model of Present-Day Plate Motions and Plate Boundary Deformation”, *Geophysical Journal International*, Vol. 154, pp. 8-34.

Kuşçu, G. G. and F. Geneli, 2008, “Review of Post-Collisional Volcanism in the Central Anatolian Volcanic Province (Turkey), With Special Reference to the Tepeköy Volcanic Complex”, *International Journal of Earth Sciences*, Vol. 99, pp. 593–621.

Laigle, M., A. Becel, B. de Voogd, A. Him, T. Taymaz and S. Özalaybey, 2008, “A First Deep Seismic Survey in the Sea of Marmara: Deep Basins and Whole Crust Architecture and Evolution”, *Earth and Planetary Science Letters,* Vol. 270, pp. 168-179.

Le Pichon, X. and J. Angelier, 1979, “The Hellenic Arc and Trench System: A Key to the Neotectonic Evolution of Eastern Mediterranean Area”, *Tectonophysics,* Vol. 60, pp 1-42.

Le Pichon, X. and J. Angelier, 1981, “The Aegean Sea”, *Philosophical Transactions of the Royal Society of London,* A300, pp. 357–372.

Le Pichon, X., Chamot-Rooke, N., Lallemant, S.L., Noomen, R. and G. Veis, 1995, “Geodetic Determination of the Kinematics of Central Greece With Respect to Europe: implications for Eastern Mediterranean Tectonics”, *Journal of Geophysical Research*, Vol. 100, pp. 12675-12690..

Le Pichon, X., and C. Kreemer, 2010, “The Miocene to Present Kinematic Evolution of the Eastern Mediterranean and Middle East and its Implications for Dynamics”, *Annual Review of Earth and Planetary Sciences*, Vol. 38, pp. 323–351.

Lienert, B. R, E. Berg and L. N. Frazer, 1986, “Hypocenter: An Earthquake Location Method Using Centered, Scaled, and Adaptively Damped Least Squares”, *Bulletin of the Seismological Society of America*, Vol. 76, pp. 771–783.

Love, A. E. H., A Treatise on the Theory of Elasticity, 4th ed., pp. 643, 1927, Cambridge University Press.

Marone F. and B. Romanowicz, 2007, “On the Depth Distribution of Azimuthal Anisotropy in the Continental Upper Mantle", *Nature*, Vol. 447, pp. 198-201.

McClusky, S. *et al*., 2000, “Global Positioning System Constraints on Plate Kinematics and Dynamics in the Eastern Mediterranean and Caucasus”, *Journal of Geophysical Research*, Vol. 105, pp. 5695– 5719.

McKenzie, D., 1972, “Active Tectonics of Alpine-Himalayan Belt: The Aegean Sea and Surrounding Regions”, *Geophysical Journal of the Royal Astronomical Society*, Vol. 30, pp.109-185.

McKenzie, D., 1978, “Active Tectonics of the Alpine-Himalayan Belt: the Aegean Sea and Surrounding Regions”, *Geophysical Journal of the Royal Astronomical Society*, Vol. 55, pp. 217–254.

Menke W. and V. Levin, 2003, “A Waveform-Based Method for Interpreting SKS Splitting Observations, With Application to One and Two Layer Anisotropic Earth Models”, *Geophysical Journal International*, Vol. 154, 379-392.

Molnar P. and J. Stock, 1987, “Relative Motions of Hotspots in the Pacific, Atlantic and Indian Ocean Since Late Cretaceous Time”, *Nature*, Vol. 132, pp. 587–591.

Molnar P., 1988, “Continental Tectonics in the Aftermath of Plate Tectonics”, *Nature,* Vol. 335, pp. 131-137.

Montagner J. P., 1998, “Where Can Seismic Anisotropy be Detected in the Earth’s Mantle? In Boundary Layers”, *Pure and Applied Geophysics*, Vol. 151, pp. 223-256.

Montagner, J. P., 2002, “Seismic Anisotropy Tomography”, Workshop on Imaging of Complex Media with Acoustic and Seismic Waves, Carg_ese, (eds.) M. Fink, W. Kuperman, J. P. Montagner, Topics Applied Physics, Vol. 84, pp. 191-231.

Morgan M. J., 1972, “Deep Mantle Convection Plumes and Plate Motions”, *The American Association of Petroleum Geologists Bulletin”,* Vol. 56, pp. 203-216.

Nicolas, A., and N. I. Christensen, “Formation of Anisotropy in Upper Mantle Peridotites: A Review”, in *Composition, Structure and Dynamics of the Lithosphere-Asthenosphere System, Geodyn. Ser.*, Vol. 16, edited by K. Fuchs and C. Froidevaux, pp. 111–123, AGU, Washington, D. C., 1987.

Nyst M. and W. Thatcher, 2004, “New Constraints on the Active Tectonic Deformation of the Aegean”, *Journal of Geophysical Research,* Vol. 109.

Okay, A.I. and O. Tüysüz, 1999, “Tethyan Sutures of Northern Turkey”, in B. Durand, L. Jolivet, F. Horváth and M. Séranne, (eds.), The Mediterranean Basins: Tertiary Extension Within the Alpine orogen, *Geological Society, London,* Vol. 156, pp. 475-515.

Okay, A.I., 2008, “Geology of Turkey: A synopsis”, *Anschnitt*, Vol. 21, pp. 19-42.

Özacar, G. Zandt, H. Gilbert, and S. L. Beck, 2010, “Seismic Images of Crustal Variations Beneath the East Anatolian Plateau (Turkey) from Teleseismic Receiver Functions”, *Sedimentary basin tectonics from the Black Sea and Caucasus to the Arabian Platform,* Vol. 340, pp. 485-496, 2010.

Özener, M.S. and W. Bolt, 2010, “The Dynamics of the Eastern Mediterranean and Eastern Turkey”, *Geophysical Journal International*, Vol. 183, pp. 1165–1184.

Papazachos, C. B., P. M. Hatzidimitriou, D. G. Panagiotopoulos and G. N. Tsokas, 1995, "Tomography of the Crust and Upper Mantle in Southeast Europe*", Journal of Geophysical Research,* Vol. 100(B7), pp. 148-227.

Pasquare, G., S. Poli, L. Venzolli, and A. Zanchi, 1988, "Continental Arc Volcanism and Tectonic Setting in Central Anatolia", *Tectonophysics*, Vol. 146, pp. 217-230.

Pasyanos, M., E., 2005, "A Variable Resolution Surface Wave Dispersion Study of Eurasia, North Africa, and Surrounding Regions", *Journal of Geophysical Research,* Vol. 110.

Paul, A., D. Hatzfeld, A. Kaviani, M. Tatar and C. Péquegnat, "Seismic Imaging of the Lithospheric Structure of the Zagros Mountain Belt (Iran)", Tectonic and Stratigraphic Evolution of Zagros and Makran During the Meso-Cenozoic, P. Leturmy & C. Robin (eds), Geological Society London Special Publications, Vol. 330, pp. 5-18, 2010.

Paul, A., D. Hatzfeld, H. Karabulut, P. Hatzidimitriou, D. M. Childs, S. Nikolova, "The Simbaad Experiment in W-Turkey and Greece: A Dense Seismic Network to Study the Crustal and Mantle Structures", AGU Fall Meeeting, San Francisco, 15-19 December 2008 (abstract).

Pe-Piper, G. and D.J.W. Piper, 2007, "Neogene Back-Arc Volcanism of the Aegean: New Insights into the Relationship Between Magmatism and Tectonics", *Geological Society of America,* Special Paper 418, pp. 17-31.

Piromallo, C., and A. Morelli, 2003, "P Wave Tomography of the Mantle Under the Alpine-Mediterranean Area", *Journal of Geophysical Research,* Vol. 108(B2), pp. 2065.

Plesinger, A., M., Hellweg and D., Seidel, 1986, "Interactive High Resolution Polarization Analysis of Broadband Seismograms", *Journal of Geophysics*, Vol. 59, pp. 129-139.

Polet, J. and H. Kanamori, 2002, “Anisotropy Beneath California: SKS splitting Measurements Using a Dense, Broadband Array”, *Geophysical Journal International*, Vol. 149, pp. 313-327.

Reilinger, R., *et al*., 2006, “GPS Constraints on Continental Deformation in the Africa-Arabia-Eurasia Continental Collision Zone and Implications for the Dynamics of Plate Interactions”, *Journal of Geophysical Research,* Vol. 111.

Reilinger, R., S. C. McClusky, M. B. Oral, W. King and M. N. Toksöz, 1997, “Global Positioning System Measurements of Present-Day Crustal Movements in the Arabia–Africa-Eurasia Plate Collision Zone”, *Journal of Geophysical Research*, Vol. 102, pp. 9983–9999.

Reitter L., 1970, “An Investigation into the Time Term Method in Refraction Seismology”, *Bulletin of the Seismological* Society *of America,* Vol. 60(1), pp. 1-13.

Ribe, N.M., 1992, “The Dynamics of Thin Shells with Variable Viscosity and the Origin of Toroidal Flow in the Mantle”, *Geophysical Journal International*, Vol. 110, pp. 537–552.

Ringwood, A.E., “Origin of the Earth and Moon”, 295 p. Springer-Verlag, New York, 1979.

Rossi, G., and G. A. Abers, 2006, “Unusual Mantle Poisson’s Ratio, Subduction, and Crustal Structure in Central Alaska”, *Journal of Geophysical Research*, Vol. 111.

Sandvol, E., N. Turkelli and M. Barazangi, 2003, “The Eastern Turkey Seismic Experiment: The Study of a Young Continent-Continent Collision”, *Geophysical Research Letters,* Vol. 30, No. 24, pp. 8038.

Sandvol, E., N. Turkelli, E. Zor, R. Gok, T. Bekler, C. Gurbuz, D. Seber, and M. Barazangi, 2003, “Shear Wave Splitting in a Young Continent-Continent Collision: An Example from Eastern Turkey”, *Geophysical Research Letters*, Vol. 30(24), pp. 8041.

Şapaş, A. and A. Boztepe-Güney, “The Analysis of SKS Splitting in Western Turkey, International Earth Sciences, Colloquium on the Aegean Region”, IESCA-2005, Abstracts Book, p 262, M.E. Nakoman, N. Türk, H. İnaner, E. Koralay, S. Aloğlu (eds.), Dokuz Eylül University, Engineering Faculty, Department of Geology, İzmir Turkey, 4-7 October 2005.

Şapaş, A. and A. Boztepe-Güney, 2009, “Shear Wave Splitting in the Isparta Angle, Southwestern Turkey: Anisotropic Complexity in the Mantle”, *Journal of Earth System Science*, Vol. 118 (1), pp. 71-80.

Sato, H., I. S. Sacks and T. Murase, 1989, “The Use of Laboratory Velocity Data for Estimating Temperature and Partial Melt Fraction in the Low-Velocity Zone: Comparison With Heat Flow and Electrical Conductivity Studies”, *Journal of Geophysical Research*, Vol. 94(B5), pp. 5689–5704.

Saunders, P., K. Priestly, T. Taymaz, 1998, “Variations in the Crustal Structure Beneath Western Turkey”, *Geophysical Journal International*, Vol. 134, pp. 373-389.

Savage, M. K, 1999, “Seismic Anisotropy and Mantle Deformation: What Have We Learned from Shear-Wave Splitting?” *Reviews of Geophysics*, Vol. 37, pp. 65–106.

Scheidegger A. E. and P. L. Willmore, 1957, “The Use of A Least Squares Method for the Interpretation of Data from Seismic Surveys”, *Geophysic*s, Vol. 22, pp. 9-22.

Şengör, A. M. C. and Y. Yılmaz, 1981, “Tethyan Evolution of Turkey, a Plate Tectonic Approach”, *Tectonophysics*, 75, pp. 181-241.

Şengör, A. M. C., 2003, “The Repeated Rediscovery of Melanges and its Implications for the Possibility and the Role of Objective Evidence in the Scientific Enterprise”, *Geological Society of America*, Special Paper 373, pp. 385-445.

Şengör, A.M.C, 1993, “Some Current Problems on the Tectonic Evolution of the Mediterranean During the Cainozoic”, in Boschi, E. *et al.*, (eds,) Recent Evolution and Seismicity of the Mediterranean Region, pp 1-51, 1993, Kluwer Academic Publishers.

Şengör, A.M.C., M. Satır and R. Akkok, 1984, “Timing of Tectonic Events in the Menderes Massif, Western Turkey: Implications for Tectonic Evolution and Evidence for Pan-African Basement in Turkey”, *Tectonics*, Vol. 3, pp. 693–707.

Şengör, A.M.C., O. Tüysüz, C. İmren, M. Sakınç, H. Eyidoğan, N. Görür, X. Le Pichon and C. Claude Rangin, 2005, “The North Anatolian Fault. A New Look”, *Annual Reviews Earth Planet of Sciences*, Vol. 33, pp. 1–75.

Silver, P. G. and M. Savage, 1994, “The Interpretation of Shear-Wave Splitting Parameters in the Presence of Two Anisotropic Layers”, *Geophysical Journal International*, Vol. 119, pp. 949-963.

Silver, P. G. and W. E. Holt, 2002, “The Mantle Flow Field Beneath Western North America”, *Science*, Vol. 295, pp. 1054-1057.

Silver, P. G. and W. W. Chan, 1991, “Shear-Wave Splitting and Sub-continental Mantle Deformation”, *Journal of Geophysical Research*, Vol. 96, pp. 16,429-16,454.

Silver, P.G., 1996, “Seismic Anisotropy Beneath the Continents: Probing the Depths of Geology”, *Annual Reviews Earth Planet of Sciences*, Vol. 24, pp. 385-432.

Sodoudi, F., R. Kind, D. Hatzfeld, K. Priestley, W. Hanka, K. Wylegalla, G. Stavrakakis, A. Vafidis, H. P. Harjes and M. Bohnhoff , 2006, “Lithospheric Structure of the Aegean Obtained from P and S Receiver Functions”, *Journal of Geophysical Research*, Vol. 111.

Solomon, S. C., Sleep, N. H. and Richardson, R. M., 1975, “On the Forces Driving Plate Tectonics: Inferences from Absolute Plate Velocities and Intraplate Stress”, *Geophysical Journal of the Royal Astronomical Society,* Vol. 42, pp. 769–801.

Stampfli G. M., 2000, “Tethyan Oceans”, *Tectonic and Magmatism in Turkey and the Surrounding Area,* From: Bozkurt E., Winchester, J. A. and Piper, J. D.A. (eds.), Vol. 173, pp. 1-23, Geological Society, London, Special Publications.

Tatar O., J. D. Piper, H. Gürsoy, 2000, “Paleomagnetic study of the Erciyes Sector of the Ecemiş Fault Zone: Neotectonic Deformation in the Southeastern Part of the

Anatolian Block." in Bozkurt, E., Winchester, J. A. and Piper, J. D. A. (eds.) *Tectonics and Magmatism in Turkey and the Surrounding Area.*, 173, pp. 423-440, Geological Society, London.

Taymaz, T., Jackson, J., and Mckenzie, D.P. 1991, "Active Tectonics of the North and Central Aegean Sea", *Journal of Geophysical Research*, 106, 433-490.

Taymaz, T., Yılmaz, Y. and Dilek, Y., 2007, "The Geodynamics of the Aegean and Anatolia: Introduction". In: *The Geodynamics of the Aegean and Anatolia* (eds.) Tuncay Taymaz, Yücel Yılmaz & Yıldırım Dilek), Vol. 29, pp. 1-16, Geological Society, London, Special Publications.

Van Hinsbergen, D. J. J., M. J. Dekkers, E. Bozkurt, and M. Koopman, 2010, "Exhumation with A Twist: Paleomagnetic Constraints on the Evolution of the Menderes Metamorphic Core Complex (Western Turkey)", *Tectonics*, Vol. 29.

Vinnik, L., V. Farra and B. Romanowicz, 1989, "Observational Evidence for Diffracted SV in the Shadow of the Earth's Core", *Geophysical Research Letters,* Vol. 16.

Wagner, L. S., Anderson, M. L., Jackson, J., Beck, S. L. and Zandt, G., 2008, "Seismic Evidence for Orthopyroxene Enrichment in the Continental Lithosphere", *Geology*, Vol. 36, pp. 935-938.

Watanabe, T., 1993, "Effects of Water and Melt on Seismic Velocities and Their Application to Characterization of Seismic Reflectors", *Geophysical Research Letters,* Vol. 20(24), 2933–2936.

Wessel, P. and Smith, W. H. F., 1998, "New, Improved Version of Generic Mapping Tools Released", EOS, *Trans. American Geophysical Union,* Vol. 79, pp. 579.

Willmore P. L. and Bancroft, A. M., 1960, "The Time Term Approach to Refraction Seismology", *Geophysical Journal of the Royal Astronomical Society,* Vol. 3, pp. 419-432.

Wolfe, C. J. and P. G. Silver, 1998, “Seismic Anisotropy of Oceanic Upper Mantle: Shear-Wave Splitting Observations and Methodologies”, *Journal of Geophysical Research,* Vol. 103, pp. 749-771.

Woodhouse, J. H., and A. M. Dziewonski, 1984, “Mapping the Upper Mantle: Three-Dimensional Modeling of Earth Structure by Inversion of Seismic Waveforms”, *Journal of Geophysical Research,* Vol. 89(B7), pp. 5953–5986.

Wortel, R. and Spakman, W., 2000, “Subduction and Slab Detachment in the Mediterranean-Carpathian Region”, *Science*, 290, pp. 1910-1917.

Wüstefeld, A. and G. Bokelmann, 2007, “Null Detection in Shear-Wave Splitting Measurements”, *Bulletin of the Seismological* Society *of America,* Vol. 97.

Wüstefeld, A., 2007, *Methods and Applications of Shear Wave Splitting: The East European Craton,* PhD Thesis, University of Montpellier (France).

Wüstefeld, A., G. Bokelmann, C. Zaroli and G. Barruol, 2008, “SplitLab: A Shear-Wave Splitting Environment in Matlab”, *Computers & Geosciences,* Vol. *34,* pp. 515-528.

Yılmaz, Y., 1997, “Geology of western Anatolia”. E.T.H. Univ. Press, Zurich. In: Schidler, C., Fister, M.P. (eds.), *Active Tectonics of Northwestern Anatolia – The Marmara Poly-Project*. Vdf Hochshulverlag A G an der ETH, Zurich, pp. 31-53.

Yılmaz, Y., 1993, “New Evidence and Model on the Evolution of the Southeast Anatolian Orogen”, *Geological Society of America Bulletin,* Vol. 105, pp. 251–271.

Yılmaz, Y., E. Yiğitbaş, M. Yıldırım, 1987, “Güneydoğu Anadolu’da Triyas Sonu Tektonizması ve Bunun Jeolojik Anlamı”, *Türkiye 7. Petrol Kongresi Bildiriler Kitabı,* pp. 65-77, Ankara.

Yılmaz, Y., O. Tüysüz, E. Yiğitbaş, Ş. C. Genç, A. M. C. Şengör, 1997, “Geology and Tectonics of the Pontides”, in A. G. Robinson (eds.) *Regional and Petroleum Geology of the Black Sea and Surrounding Region,* AAPG Memoir, Vol. 68, pp. 183-226.

Yılmaz, Y., Y. Güner, F. Şaroğlu, 1998, "Geology of the Quaternary Volcanic Centers of the East Anatolia", *Journal of Volcanology and Geothermal Research,* Vol. 85, pp. 173-210.

Zhang, S. and S. Karato, 1995, "Lattice Preferred Orientation in Olivine Due to Shear Deformation", *Nature*, Vol. 375, pp. 774-777.

Zheng, Y., & Lay, T., 2006, "Low Vp /Vs Ratios in the Crust and Upper Mantle Beneath the Sea of Okhotsk Inferred from Teleseismic pmP, smP, and smS Underside Reflections From the Moho", *Journal of Geophysical Research*, Vol. 111.

Zhu, L., B. J. Mitchell, N. Akyol, I. Cemen, K. Kekovali, 2006, "Crustal Thickness Variations in the Aegean Region and Implications for the Extension of Continental Crust", *Journal of Geophysical Research*, Vol. 111.

Zor, E., 2008, "Tomographic Evidence of Slab Detachment Beneath Eastern Turkey and the Caucasus", *Geophysical Journal International*, Vol.175, pp.1273-1282.

Zor, E., E. Sandvol, C. Gurbuz, N. Turkelli, D. Seber, M. Barazangi, 2003, "The Crustal Structure of the East Anatolian Plateau (Turkey) from Receiver Functions.", *Geophysical Research Letters*, Vol. 30 (24).

Zor, E., S. Özalaybey, C. Gürbüz, 2006, "The Crustal Structure of the Eastern Marmara Region (Turkey) by Teleseismic Receiver Functions". *Geophysical Journal International*, 1365- 246X, p.10.1111.

APPENDIX A: LIST OF STATIONS USED IN SKS MEASUREMENTS

Station Name	Latitude	Longitude
ADVT	29.7383	40.4332
AFSR	33.0707	39.4468
AGG	22.3303	39.0222
AGRB	42.9870	39.6088
AHLR	32.7735	40.8867
ALN	26.0457	40.8972
ALT	30.1103	39.0552
ALTB	28.7400	41.0880
ANTB	30.6538	36.8998
ANTO	32.7937	39.8688
AOS	23.8800	39.1703
APE	25.5307	37.0688
ARG	28.1262	36.2162
ARMT	28.8617	40.5657
AYDB	27.8908	37.9465
AYDN	27.8792	37.6608
BALB	27.8800	39.6400
BALY	27.6195	39.7403
BAYT	40.1410	40.3935
BCA	41.6223	41.4450
BCK	30.5890	37.4608
BEL	31.2645	37.9708
BGKT	28.7730	41.1810
BLCB	27.0420	38.3853
BLKV	32.7517	40.8613
BNGB	40.6790	38.9913
BNN	35.8667	38.8462
BODT	27.3103	37.0622
BOLV	30.9502	38.7138
CANB	27.0623	40.0167
CANT	33.6197	40.6062
CDAG	34.3718	39.6237
CEYT	35.7473	37.0107
CHOS	26.0550	38.3868
CLDR	43.9170	39.1432
CORM	34.5467	40.1785
CRLT	27.7360	41.1290
CSS	33.3307	34.9622
CTKS	28.5065	41.2363
CTYL	28.2890	41.4750
CUKT	43.6075	37.2473
DALT	28.6372	36.7692
DALY	28.6532	36.8162
DARE	37.4830	38.5712
DAT	27.5767	36.7307
DIGO	43.3712	40.4088

Station Name	Latitude	Longitude
DIKM	35.2577	41.6495
DYBB	40.1393	37.9531
E08	30.4050	39.8970
E13	30.7140	38.3600
E17	30.7133	37.3208
E18	30.6810	37.1630
E23	30.4300	36.3668
EDC	27.8618	40.3463
EDRB	26.7440	41.8470
EIL	34.9512	29.6698
ELL	29.9085	36.7483
ENEZ	26.1530	40.7362
EPOS	42.7279	41.5035
ERBA	36.7547	40.6813
EREN	34.1700	35.5300
ERIK	26.5132	40.6708
ERMK	32.9128	36.6417
ERZN	39.7220	39.5867
ESPY	38.7272	40.9165
EZN	26.3253	39.8258
FETY	29.0835	36.6353
FNA	21.3762	40.7838
GADA	25.8987	40.1908
GAZ	37.2113	37.1722
GBZX	29.4502	40.7865
GDZ	29.4812	39.0888
GELI	26.4742	40.3980
GEMT	29.1890	40.4350
GEVA	43.0587	38.3122
GLHS	29.4983	37.1560
GONE	27.6860	40.0465
GRG	22.4013	40.9567
GULT	30.5150	40.4323
GVD	24.0873	34.8392
HAKT	43.7072	37.5578
HDMB	32.4860	36.9640
HNZ	29.2696	37.7495
HORT	23.0997	40.5978
HRFI	35.0370	30.0363
HRTX	29.6730	40.8008
IKL	33.6853	36.2387
ILGA	33.7165	41.0522
ILIC	38.5700	39.4540
INL	32.5502	36.1288
ISK	29.0592	41.0657
ISP	30.5222	37.8227

Station Name	Latitude	Longitude
KARA	35.0543	37.2597
KARN	23.9200	35.4000
KARS	43.0788	40.6277
KAVA	24.5137	40.9967
KCTX	28.3353	40.2625
KDZE	31.4428	41.3132
KELT	39.2557	40.1495
KEMA	38.4932	39.2688
KHAL	29.4917	38.3703
KLYT	29.0420	41.2530
KMRS	36.9000	37.5087
KNT	22.8982	41.1618
KONT	32.3605	37.9453
KOZT	35.8263	37.4795
KRBG	27.2977	40.3932
KRNZ	32.7847	40.9093
KRTS	35.3748	36.5730
KTUT	39.7665	40.9893
KVT	36.0463	41.0807
LADK	32.3648	38.2000
LAP	26.7602	40.3727
LAST	25.4787	35.1612
LEF	32.8903	35.1193
LFK	33.5325	35.2792
LIT	22.4900	40.1008
LKD	20.6507	38.7072
LOD	32.7497	39.9195
LTK	22.9673	38.0228
MALT	38.4273	38.3133
MAN	31.7250	36.7820
MATE	16.7040	40.6490
MAZI	40.4465	37.4593
MDNY	28.8845	40.3708
MDU	31.1975	40.4712
MERS	34.5217	36.8665
MFTX	27.2977	40.7867
MLR	25.9450	45.4908
MLSB	27.7765	37.2953
MORC	17.5425	49.7768
MRMT	27.5957	40.6032
MRMX	27.5830	40.6088
OUR	23.9818	40.3343
PAIG	23.6797	39.9272
PASA	32.6240	40.8693
PHSR	27.5237	41.6308
PLD	24.7032	42.1048
PSZ	19.8943	47.9183
PTK	39.3920	38.8920
PZAR	40.8987	41.1777
RDO	25.5375	41.1462
RKY	27.1777	40.6875
RSDY	37.3273	40.3972
SANT	25.4590	36.3710
SARI	36.4182	38.4072
SERE	33.5600	38.9500
SHUT	30.5510	38.5530
SIGR	25.8553	39.2113
SILT	29.6430	41.1530
SIVA	24.8100	35.0175
SLVT	28.2100	41.2300
SOH	23.3538	40.8217
SPNC	30.3073	40.6840
SRS	23.5922	41.1172
SULT	33.5157	38.1988
SUTC	30.9975	37.4755
SVAN	41.1985	38.1511
SVRC	39.3058	38.3775
SVRH	31.5230	39.4468
SVSK	36.9980	39.9170
TAHT	36.1855	36.3753
THE	22.9650	40.6322
THL	22.0145	39.5647
TIR	19.8650	41.3477
TIRR	28.4128	44.4582
TKMK	32.7730	40.9298
TKR	27.5357	40.9902
TRIZ	22.0150	38.3700
TROY	26.4183	40.1097
TVSB	29.4615	39.4497
URFA	38.8213	37.4410
VANB	43.3890	38.5950
VRTB	41.4560	39.1602
W07	27.9208	39.2958
W14	28.0492	38.3005
XOR	23.1918	39.3662
YAYL	36.1070	36.0343
YER	28.2828	37.1347
YLVX	29.3727	40.5667
ZKR	26.2170	35.1147